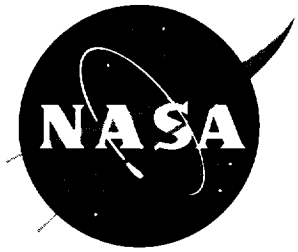

NASA Reference Publication 1341

A Shadowgraph Study of Space Transportation System (STS): The Space Shuttle Launch Vehicle (SSLV)

A.M. Springer
Marshall Space Flight Center • MSFC, Alabama

National Aeronautics and Space Administration
Marshall Space Flight Center • MSFC, Alabama 35812

June 1994

TABLE OF CONTENTS

LIST OF ILLUSTRATIONS

LIST OF ILLUSTRATIONS (Continued)

LIST OF ILLUSTRATIONS (Continued)

LIST OF ILLUSTRATIONS (Continued)

REFERENCE PUBLICATION

A SHADOWGRAPH STUDY OF SPACE TRANSPORTATION SYSTEM (STS): THE SPACE SHUTTLE LAUNCH VEHICLE (SSLV)

INTRODUCTION

This report, the second in a series of shadowgraph studies of various launch vehicle configurations, presents shadowgraphs of the space transportation system (STS), the space shuttle launch vehicle (SSLV), for the trisonic Mach range of 0.6 to 5.0. The first report[1] presented shadowgraphs of two proposed Shuttle-C configurations. Shadowgraphs of the SSLV at angles-of-attack of 0° and –4° and roll angles of 90° are shown for the majority of the Mach range. The enclosed shadowgraphs present a pictorial view of the flow fields over the STS configuration. Marshall Space Flight Center's (MSFC's) 14-×14-inch trisonic wind tunnel has been used throughout the development of the space shuttle program. These shadowgraphs are a compilation of shadowgraphs taken at MSFC over the past 15 years.[2–7]

This report presents shadowgraphs for the space shuttle launch vehicle in a concise format, offers a means of easy transfer of the data to interested parties, and documents the results for future study.

MODEL AND FACILITY DESCRIPTION

Facility Description

The MSFC 14-×14-inch trisonic wind tunnel is an intermittent blowdown tunnel which operates by high pressure air flowing from storage to either vacuum or atmosphere conditions. The transonic test section, with variable porous walls, provides a Mach number range from 0.2 to 2.0. A solid-wall supersonic test section provides the entire range from 2.74 to 5.0 with one set of automatically actuated contour blocks. Downstream of the test section is a hydraulically controlled pitch sector that provides the capability of testing up to 20 angles-of-attack from –10° to +10° during each run. Sting offsets are available for obtaining various maximum angles-of-attack up to 90°. This is further detailed in reference 8. The MSFC 14-×14-inch trisonic wind tunnel facility is shown in figure 1.

Model Description

The model is a 0.004 scale replica of the space shuttle launch vehicle consisting of the orbiter (ORB), external tank (ET), and two solid rocket boosters (SRB's) as shown in figures 2 through 4. The vehicle is described by the space shuttle level II interface control document, ICD Number 2-0001, Revision F, dated January 31, 1980. The space shuttle integrated vehicle is shown in figure 2.

Two ORB models were used throughout the program. One configuration was fabricated to the OV101 outer mold lines, while the other model was fabricated to the OV102 outer mold lines. The mold lines of the two configurations do not vary significantly. Figure 3 shows the general ORB geometry. All of the major aerodynamic surfaces were modeled, including the wing, inboard and outboard elevons,

body flap, and vertical tail. The orbital maneuvering system (OMS) pods and nozzles were also simulated; however, the main propulsion system (MPS) nozzles could not be simulated because of the model sting arrangement. The elevon deflections were set manually by use of interchangeable elevon brackets. The difference in ORB models and elevon settings had no noticeable effect discernible from shadowgraphs. This is seen in the comparison of figures 5 and 6. The enclosed shadowgraphs are a compilation of shadowgraphs from many tests of the two ORB configurations with various elevon settings.

The ET model was built in accordance with Rockwell International interface control drawing ICD2-0001, Rev. F. Figure 4*a* shows the full-scale ET geometry. The ET is of a cylindrical cross-section with a nominal diameter of 333 inches and a maximum diameter of 336.2 inches. The forward portion of the ET has a tangent ogive nose which terminates in a biconic nose cap over the liquid oxygen (lox) vent valve. Structural stiffeners on the intertank between the lox and liquid hydrogen (LH_2) tanks result in an area with a slightly larger than nominal diameter, which is simulated on the test model. The aft end of the tank was basically an ellipsoid of revolution. The entire ET is covered with spray-on thermal protection system (TPS), foam-type insulation of varying thickness. Approximate thicknesses are 2.5 inches on the tangent ogive nose, 1.0 inch on the cylindrical sections, and 2.0 inches on the aft dome. Model dimensions include this TPS layer. The ET flight configuration includes a number of protuberances which consist of electrical trays, propellant feedlines, and attach hardware. Electrical trays which run parallel to the ET centerline were simulated; some of those adjacent to the aft ORB/ET attach hardware were not. The lox and LH_2 feedlines were simulated. The attach hardware between the ORB/ET and ET/SRB's were also simulated. The forward ET/ORB attach strut was not scaled in the x-direction along the vehicle. This was due to the loads the ORB model would see in the mated vehicle configuration.

The SRB models were built to the same interface control drawing (ICD2-0001, Rev. F) as the ET. Figure 4*b* shows the SRB geometry. The two SRB's are 146-inch diameter cylinders, each with an 18° semivertex angle nose cone terminated by a 13.27-inch diameter spherical cap. An 18° flared skirt, 208.20 inches in diameter at the trailing edge, was simulated. The rocket nozzle and base thermal shield were not simulated on the model. SRB protuberances consist of a forward attach lug, front and rear separation motors, an aft attach ring, various stiffener rings, integrated electronics assembly (IEA) box, and a full-length electrical systems tunnel. All of these protuberances were simulated on the model.

Figure 7 shows the 0.004-scale space shuttle launch vehicle model mounted in the trisonic wind tunnel.

Shadowgraph System

The 14-×14-inch wind tunnel's shadowgraph system consists of a spark source, multiple film holders, and a mounting bracket for the holders. The spark source is mounted on one side with the mounting bracket/film holder on the other side of the test section. Glass wall inserts are installed in the transonic test section, while the supersonic test section has conventional windows. The spark source is fired, exposing the film, thus producing a shadowgraph. Figure 8 shows a sketch of the shadowgraph setup.

Without flow, the spark source shines through the test section containing stagnant air and illuminates the film with uniform intensity. When the tunnel is started and flow passes through the test section, the light beam will be refracted wherever there is a density gradient. A constant gradient, an empty test section, or no flow in the test section will result in every light ray being refracted evenly, producing no change on the film (figs. 9 and 10). Only if there is a variation in the density gradient will the light from

the spark source converge or diverge. A picture of the instantaneous density gradients will be shown on the film when the spark source is fired (figs. 11 and 12). The shadowgraph easily allows shock waves to be seen. The second derivative of density is positive in the forward region of the shock and negative in the aft region. A shock wave is not infinitely thin. The shadowgraph film will show the shock wave as a dark line followed by a white line.

The shadowgraph system used for the 14-×14-inch wind tunnel is explained in detail in reference 9. Reference 9 also explains the theory behind the system and the supporting tests done to initially verify the system. This reference also explains the effects of the glass walls on the shadowgraph. This appears on the shadowgraph to look something like cross hatching in the subsonic and sonic Mach range. Currently, only the single film method, not the multiple exposure roll which is also shown in reference 9, is used. Kodak™ Tri-X pan, 8- by 20-inch black and white professional film is used for the shadowgraphs.

SHADOWGRAPH DESCRIPTION

The shadowgraph is a flow visualization technique that shows the second spatial derivative of the density field or the gradient of the density gradient. The shadowgraph is used to show boundary layers, flow separation, and shock wave formations. All flow visualization techniques are dependent on variation in the flow fields density. An interferometer measures the density level with regard to a reference. The fringe shifts are counted to obtain the density variations. A Schlieren system shows the gradient in density or the first x-derivative. The shadowgraph system is easy to use, and the relative shock strengths are easily seen, but the actual density levels cannot be obtained.

Boundary layers and separated regions are easily seen in shadowgraphs if the flow field density is not too low. The density changes across shocks, and expansions waves are functions of Mach number and are configuration dependent. The density gradients of the flow are dependent on the ratios of upstream and downstream flow fields. Low-density flow fields are not as discernible as high-density flow in the shadowgraphs. The shadowgraph system and its relation to other optical flow methods are discussed in reference 10. Further details concerning shadowgraphs and their application to launch vehicle aerodynamic study are found in reference 11.

SHADOWGRAPH ENGINEERING INTERPRETATIONS

These visual representations of the flow have been used in conjunction with launch vehicle aerodynamic analyses to gain a better understanding of the aerothermodynamic environments.

Shadowgraphs are presented for the trisonic range of Mach numbers for the space shuttle. The effects of Mach number, angle-of-attack, and angle-of-sideslip are shown. The shadowgraphs presented are of great use in the analysis of the aerodynamic characteristics of the SSLV. A greater understanding of the pressure distributions for the SSLV can be gained from these shadowgraphs.

The SSLV is a multibody configuration which inherently results in significant flow interactions between each of its primary elements: the ORB, ET, and SRB's. Part of this interaction is due to the intersection of the bow shock waves off each of the elements. This can be seen in figures 11 and 12, top and side views. Notice the region of high interactions at the forward attach structure between the ORB

and the ET. Also note the area between the ORB and the ET contains a large variation in flow field characteristics discernible by the patterns on the shadowgraphs.

Because of the bluntness of the space shuttle vehicle, the primary bow shocks at low supersonic Mach numbers are detached and appear as vertical lines forward of the vehicle. As Mach number increases, the angle of the shock wave increases, changing from the appearance of a vertical line, a normal shock, to that of an oblique line, an oblique shock. At approximately Mach 1.96, the bow shock off the ET becomes attached.

At the higher Mach numbers, the shadowgraphs appear to be clearer and shock waves more pronounced. This is due to the larger density variation fore and aft of the shock.

Compare the mated vehicle shadowgraphs to those in appendix A and appendix B. Appendix A contains shadowgraphs of the ORB alone at angles-of-attack of $-2°$, $0°$, and $2°$ at Mach numbers of 1.25, 1.46, and 1.96. Appendix B contains shadowgraphs of the SSLV lower stack only, the ET with the two SRB's attached, at the corresponding angles of attack and Mach numbers as those of the ORB in appendix A. The shadowgraphs in these two appendices show the shock waves and flow fields around the individual elements. When the individual elements are compared to the mated vehicle, the large interactions between elements are evident.

Appendix C contains a study[6] done during the intermediate stages of STS development concerning the ET nose geometry. This study is presented to show how the geometry of the ET's nose affects the bow shock off the ET and the subsequent interactions between the SSLV flow fields. Figure C1 is a photograph of the ORB and the five nose geometries tested. Notice the ORB geometry, the spine down the back of the ORB. This was an intermediate ORB configuration. A photograph of each mated vehicle configuration is presented followed by the corresponding shadowgraph in this appendix. These shadowgraphs were taken at a Mach number of 3.48. No attach structure was present for these shadowgraphs, since no attach structure had been determined at the time of this test. Therefore, the attach structure interactions with the SSLV flow fields disrupting the ET nose geometry's effects cannot be seen. The elements were mounted in proximity using individual stings for the ORB and the lower stack. Notice how the shock wave contour changes with the different ET's noses. This is due to the change in pressure fields about the ET's nose resultant from the nose geometry.

The shock wave off the nose of the ORB and the shock from the transition of the nose to cockpit interact at supersonic Mach numbers. The strong shock off the cockpit at these supersonic Mach numbers causes the nose shock and ET bow shock to diminish. The angle of these shocks is also affected by their encounter with the shock wave off the cockpit. These effects are easily seen when comparing figures 11 and 38.

The oblique shock seen at transonic speeds at the nose/cockpit junction (fig. 11) is resultant from the large turning angle the flow encounters at the cockpit.

The shock off the ORB tail is also readily visible. A region of separated flow occurs at the forward base of the tail due to the tail not being faired into the body. The flow encounters a step at the base of the tail (fig. 11). The OMS pods located on the boattail, port, and starboard of the vertical tail form shocks. The OMS pod's shocks are blocked from view by the ORB's tail and are not pronounced enough to be discernible at the base of the vehicle.

The SRB stiffener rings near the base of the booster form some noticeable disturbances in the flow. These disturbances are not strong shocks, but rather weaker Mach waves resulting from disturbances within the boundary layer.

The shadowgraphs taken with the STS at a roll angle of 90°, providing a top view of the vehicle, show the shock waves off the leading edge of the ORB's wings, the ET's bow shock, and the SRB's bow shocks. Notice the SRB's shocks impinge on the ET in the ET's intertank region. These shocks cause a large pressure gradient on the intertank region. The shock off the nose of the ORB is discernible as the two light lines come together between the bow shocks of the ET and the ORB wings leading edge (fig. 12).

The flow phenomena around the SSLV configuration, as seen in a typical shadowgraph, is shown in figure 13. This figure is the same shadowgraph as figure 11 but with the major points of the flow field highlighted.

It should be noted that boundary layer effects cannot accurately be determined from a scale model of a vehicle, since boundary layers do not scale as the aerodynamic characteristics do.

Due to the complex nature of the base region of the vehicle, as can be seen in the shadowgraphs, the flow fields interact and a clear picture of the causes of the flow field disturbances become difficult to discern. A description/interpretation of the flow fields in this region would be of question because of the interaction of the stings with the base of the model.

CONCLUSIONS

A compilation of shadowgraphs taken at the NASA MSFC's 14-×14-inch trisonic wind tunnel over the past 15 years is presented. The enclosed shadowgraphs present a pictorial view of the flow fields over the STS configuration. They have been used throughout the development of the space shuttle program in conjunction with launch vehicle aerodynamic analyses to gain a better understanding of the aerothermodynamic environments.

This report presents the shadowgraphs in a concise format, offers a means of easy transfer of the data to interested parties, and documents the results for future study.

REFERENCES

1. Springer, A.M., and Pokora, D.C.: "A Shadowgraph Study of Two Proposed Shuttle-C Configurations." NASA RP-1303, 1993.

2. Frost, A.L.: "Results of the SSLV Plume Simulation Test – TWT 675 in the MSFC 14-Inch Trisonic Wind Tunnel." ED32-82-32, November 1, 1982.

3. Frost, A.L.: "Results of the STS-51L Wind Tunnel Investigation (TWT-704)." ED32-30-86, August 11, 1986.

4. Rawlinson, E.G.: "Pretest Information for a Space Shuttle Launch Vehicle Test in the MSFC 14×14 Inch Trisonic Wind Tunnel (TWT 655, 656 and 657)." LMSC-HREC TM D568893, February 1979.

5. TWT 705, MSFC, 1985.

6. Davis, T.: "Pretest Information for a Multiple Balance Force Test of a 0.004 Scale Model of the NA MCR 0074 Baseline Space Shuttle Launch Configuration (TWT-570)." Northrup Services, Inc., M-9230-73-152, March 20, 1973.

7. Garton, W.P.: "Pretest Report for an Investigation in the MSFC TWT of the Influence of the Orbiter Vehicle and Solid Rocket Booster on the Pressure Filed About the Nose of the External Tank in the Transonic Range Utilizing the 0.004-Scale Model (74-OTS) of the Shuttle Vehicle 5 Configuration (IA181)." Rockwell International Space Division SD77-SH-0269, November 1977, TWT 649.

8. Simon, E.H.: "The George C. Marshall Space Flight Center's 14×14 Inch Trisonic Wind Tunnel Technical Handbook." NASA TMX-64624, November 5, 1971.

9. Clark, J., Heaman, J.P., and Stewart, D.L.: "14-Inch Wind Tunnel Spark Shadowgraph System." NASA TM X-53195, January 22, 1965.

10. Shapiro, A.H.: "The Dynamics and Thermodynamics of Compressible Fluid Flow Volume I." "Chapter 3.7. Optical Methods of Investigation," John Wiley and Sons, Inc., 1953, pp. 59–68.

11. Andrews, C.D., and Carlson, D.R.: "Shadowgraph Study of the Upper Stage Flow Fields of Some Saturn V Study Configurations in the Transonic Mach Number Range." NASA TN D-2755, April 1965.

ORIGINAL PAGE
BLACK AND WHITE PHOTOGRAPH

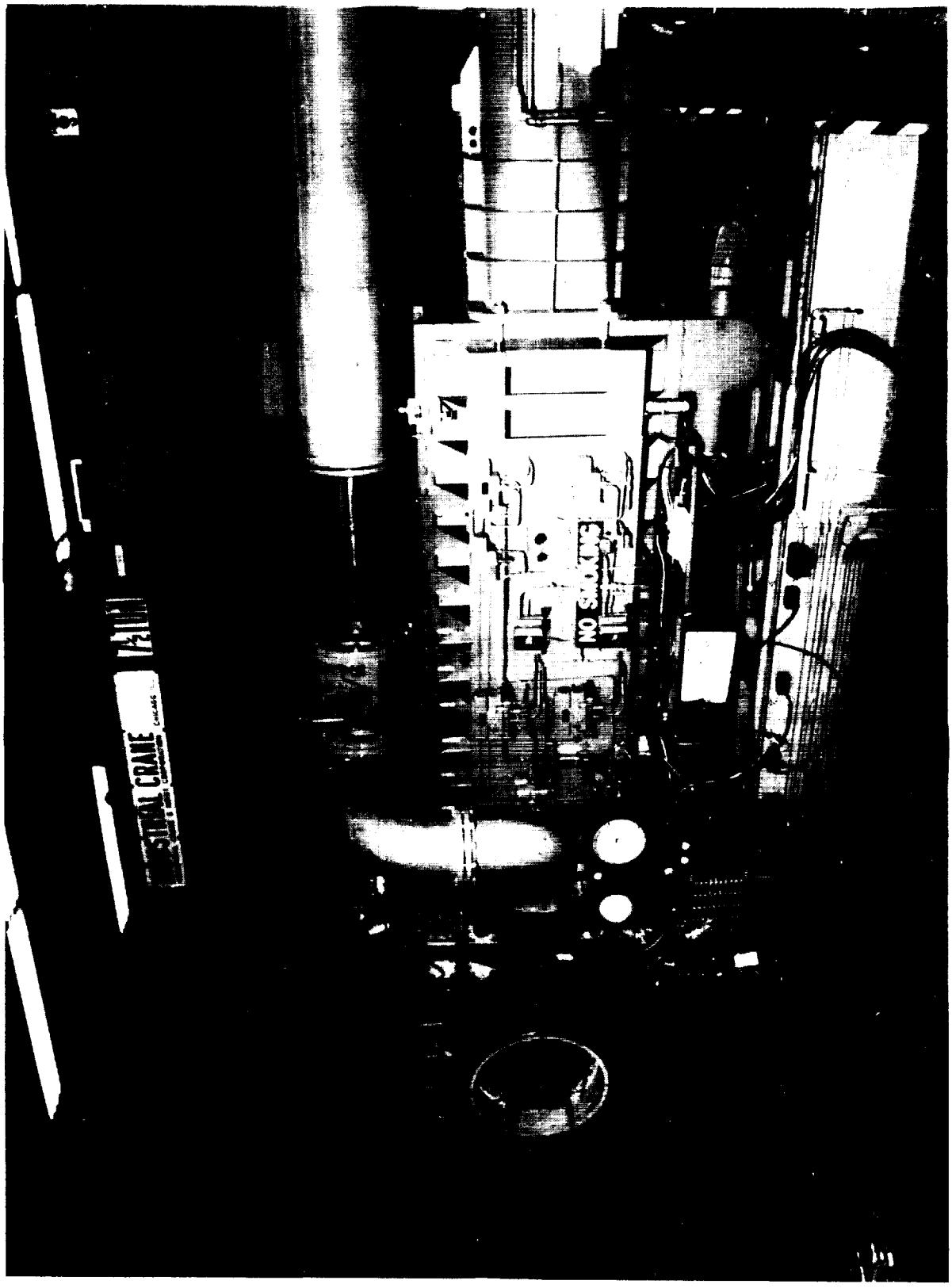

Figure 1. MSFC's 14×14-inch trisonic wind tunnel facility.

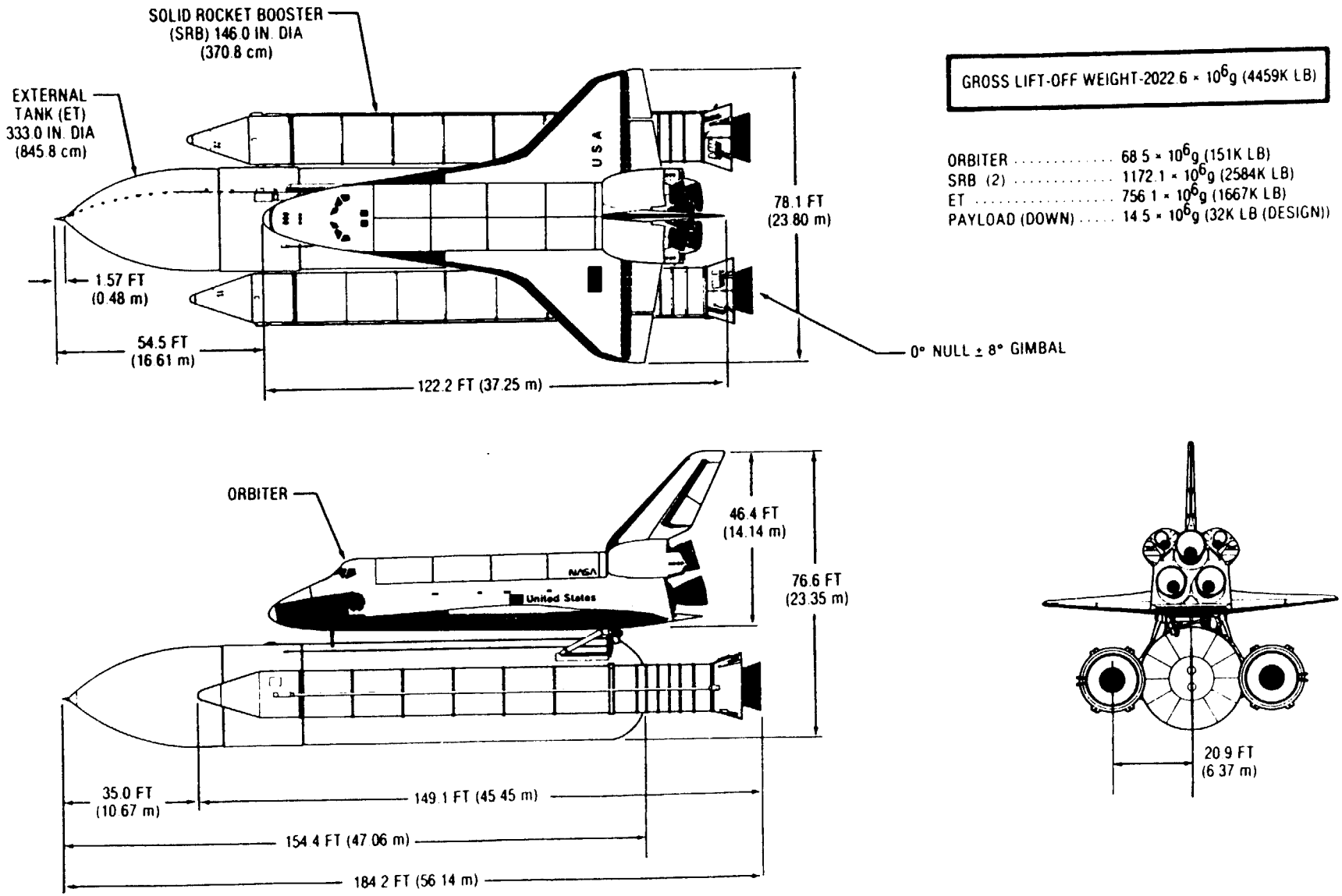

Figure 2. STS integrated vehicle geometry.

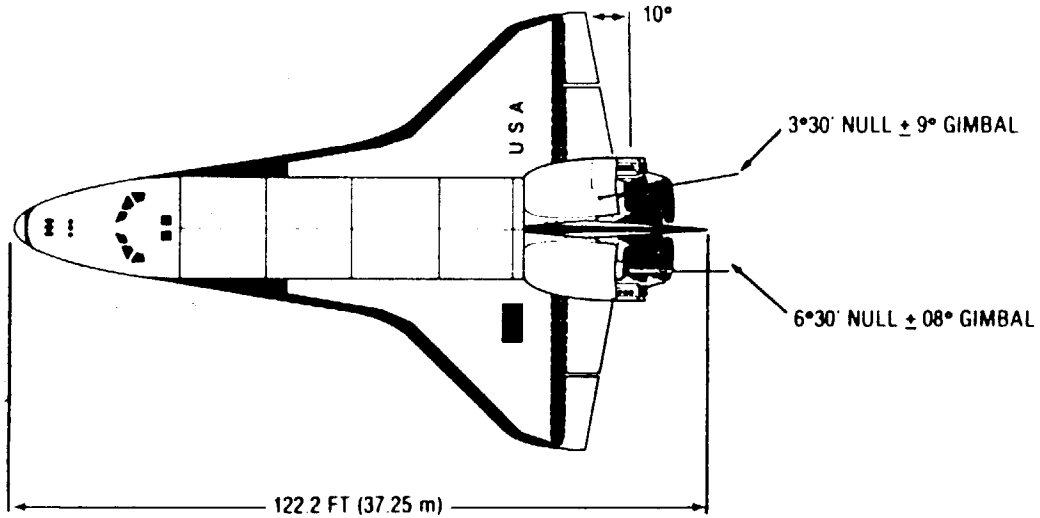

	WING	VERTICAL STAB
AREA	2690 FT^2 (249.90 m^2)	413.25 FT^2 (38.39 m^2)
ASPECT RATIO	2.265	1.675
SWEEP (L.E.)	45°	45°
M.A.C.	474.81 IN.(1206.0 cm)	199.81 IN.(507.52 cm)
DIHEDRAL (T.E.)	3°30'	—

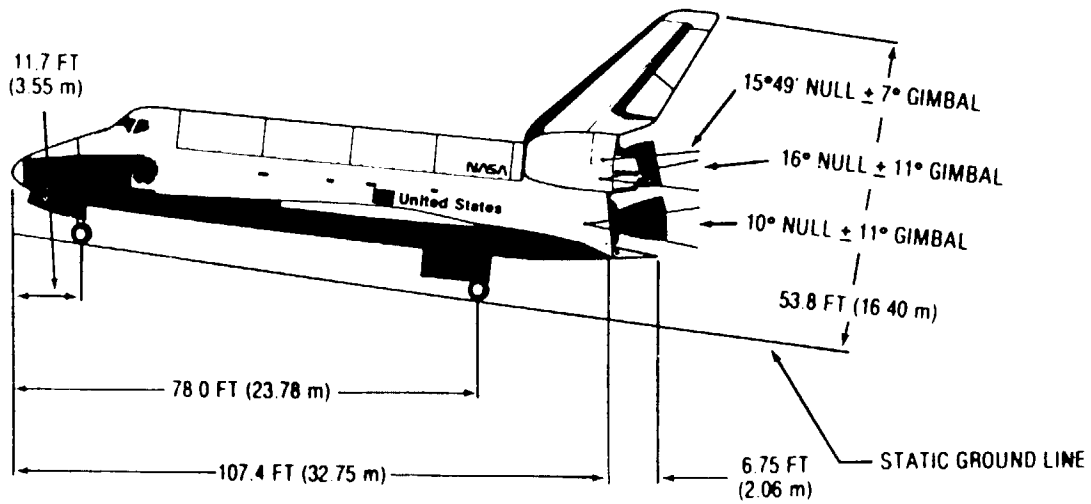

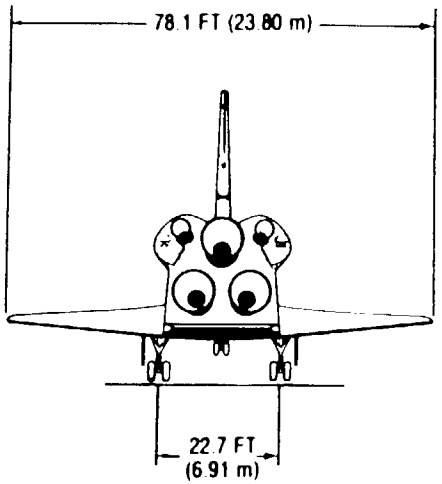

Figure 3. STS ORB geometry.

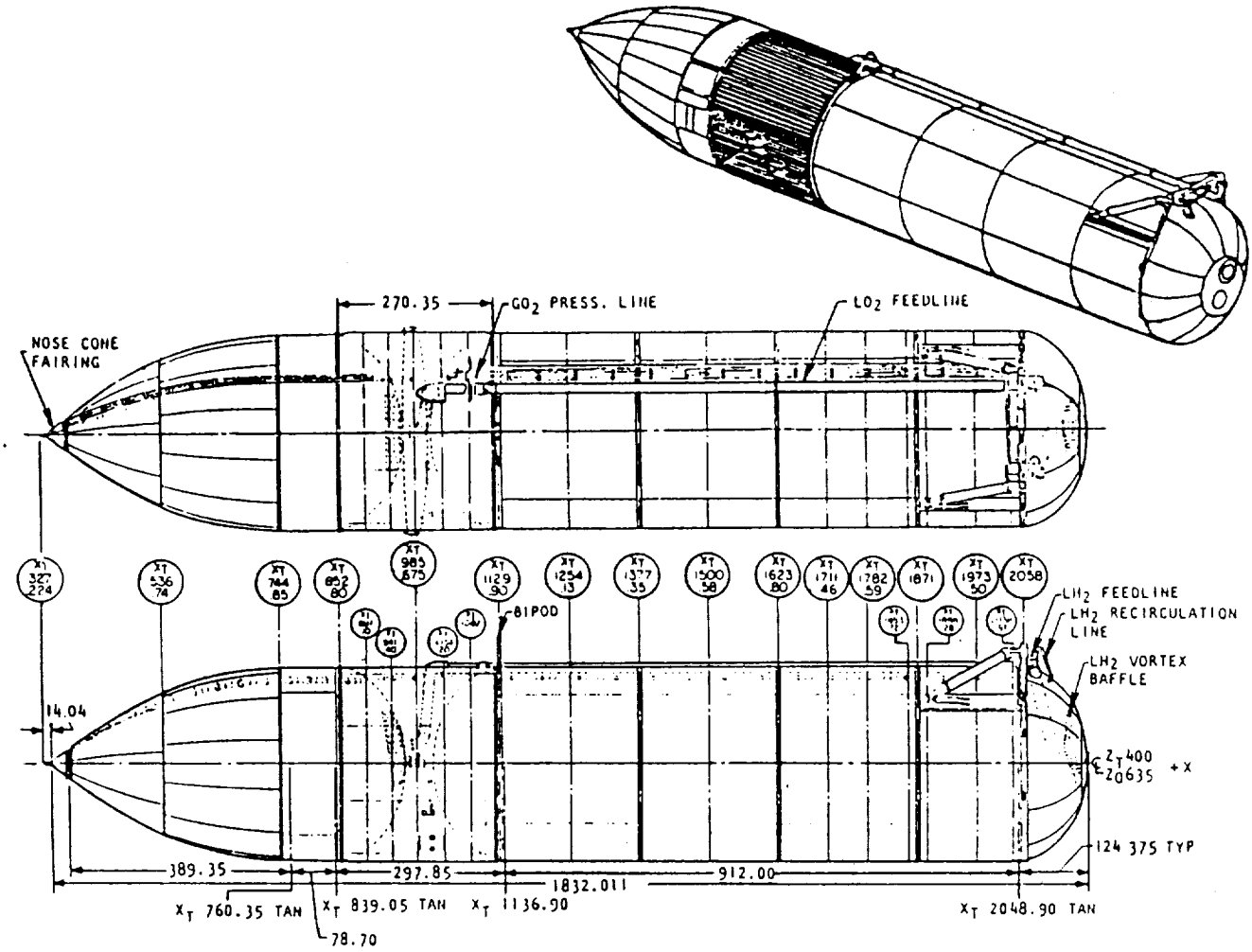

Figure 4*a*. STS ET geometry.

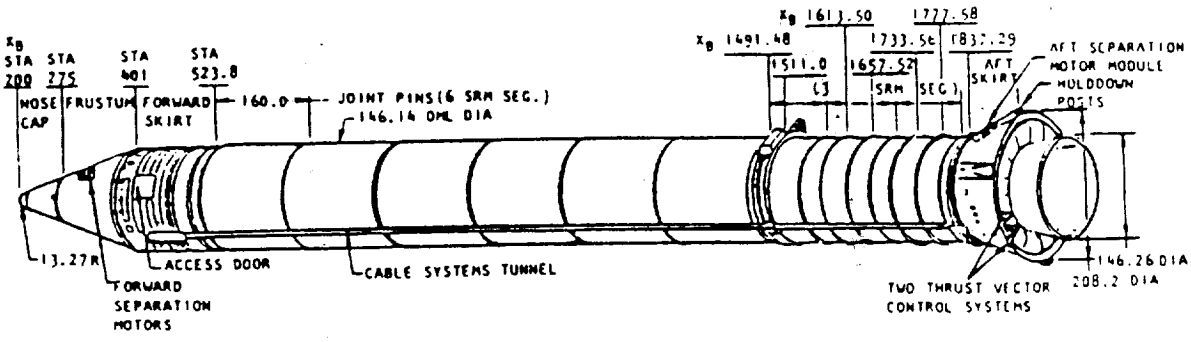

Figure 4*b*. STS SRB geometry.

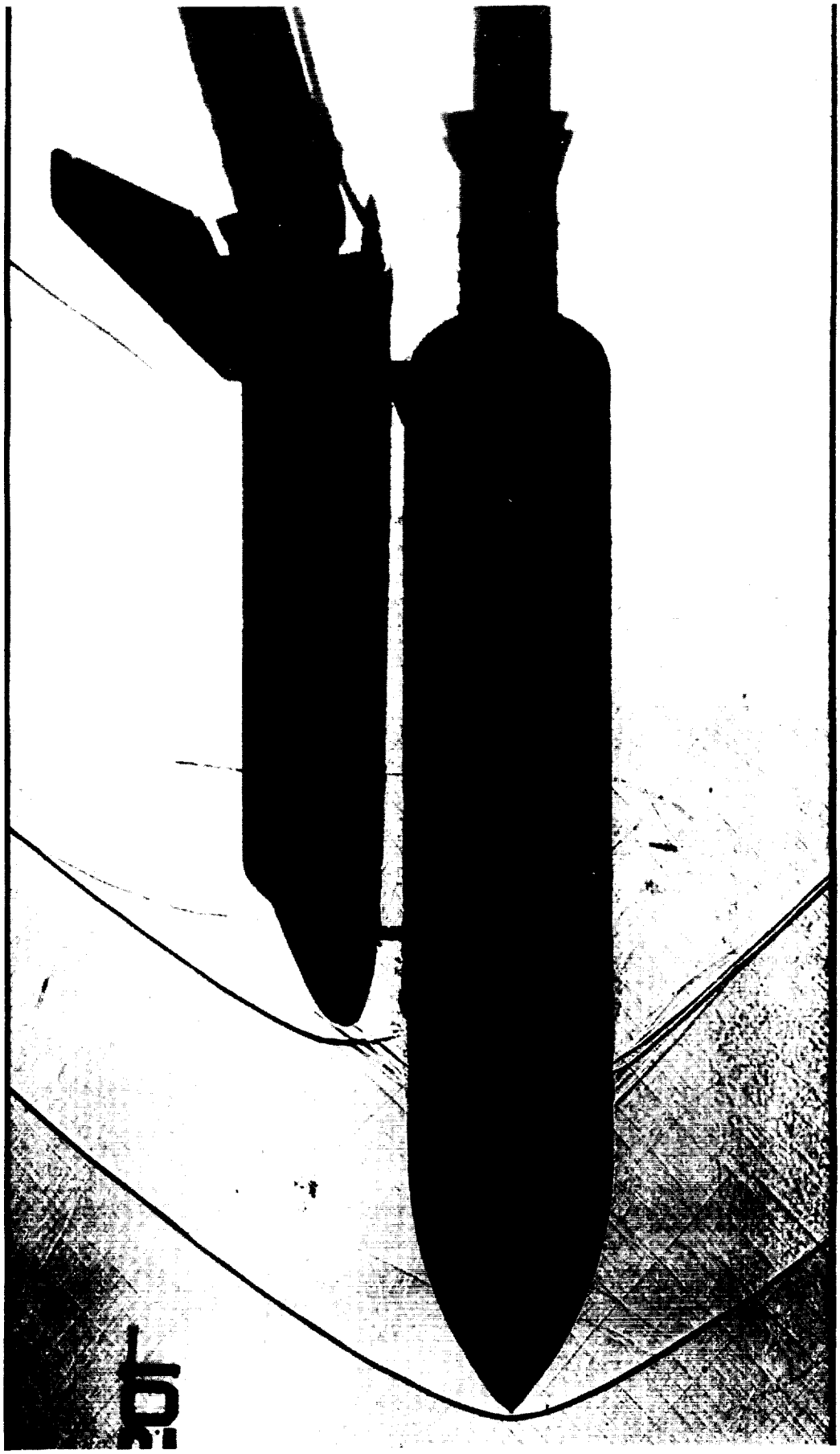

Figure 5. Shadowgraph of SSLV at Mach 1.46 with an OV101 ORB.

ORIGINAL PAGE
BLACK AND WHITE PHOTOGRAPH

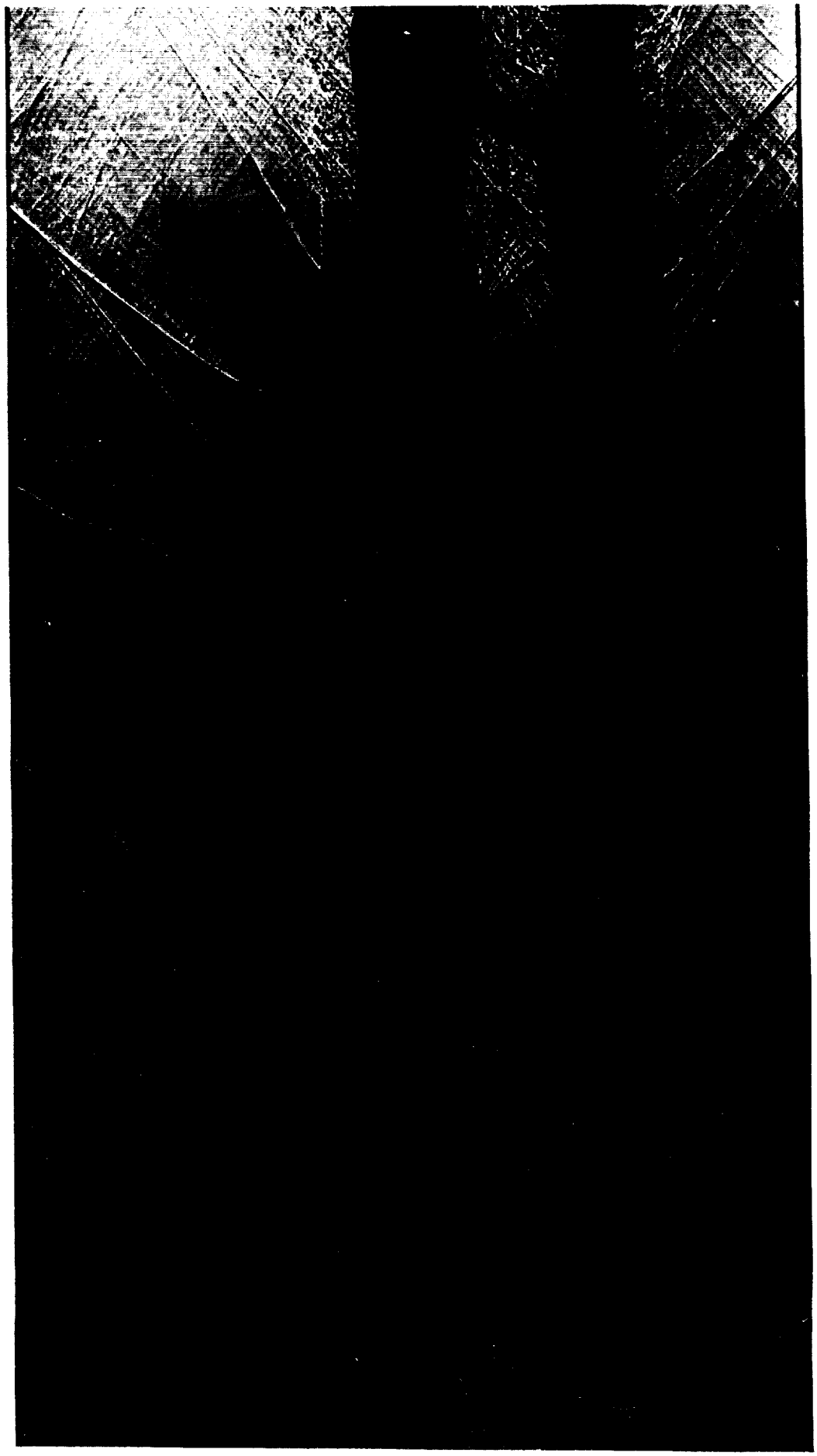

Figure 6. Shadowgraph of SSLV at Mach 1.46 with an OV102 ORB.

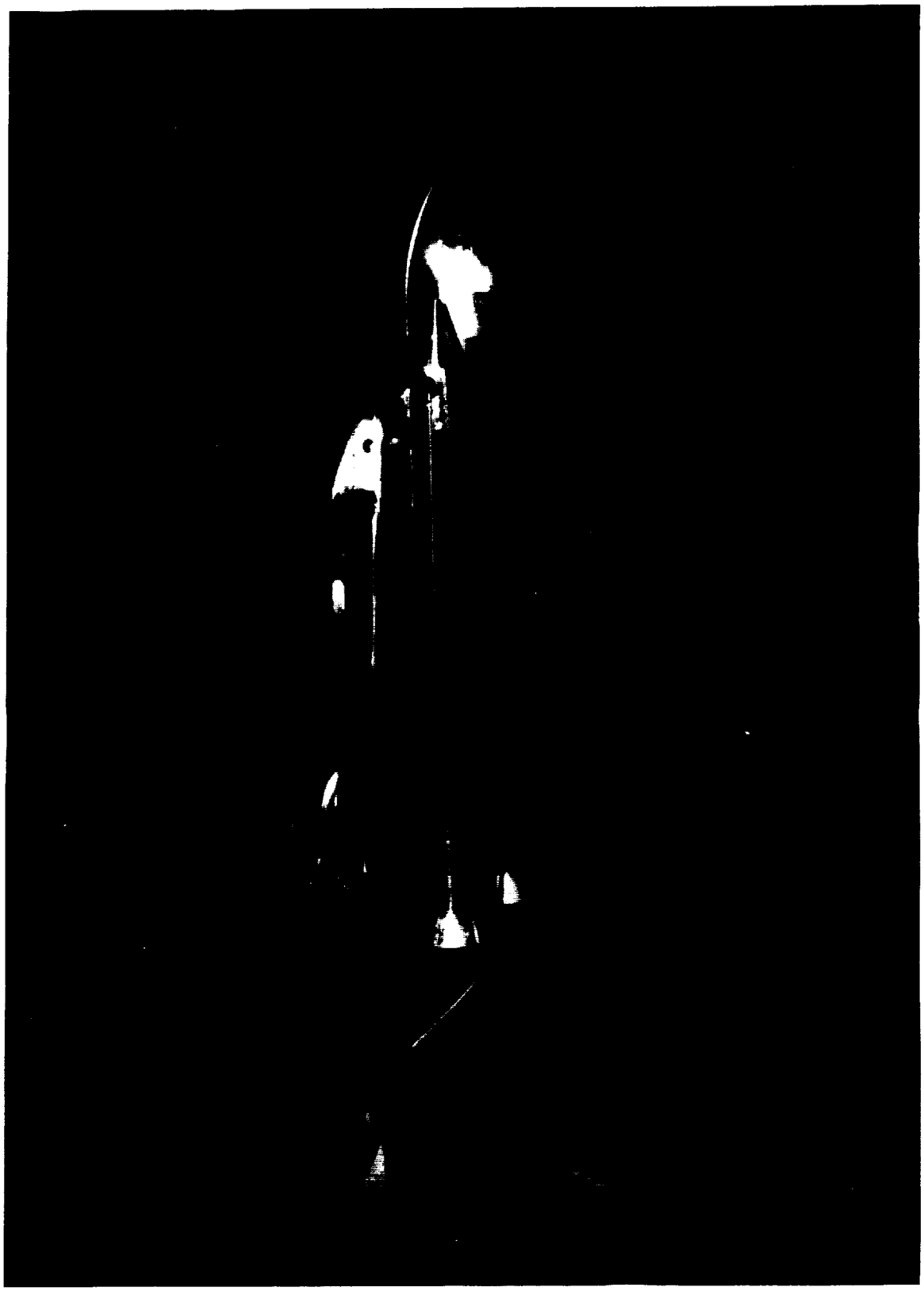

Figure 7. SSLV mounted in MSFC's 14-×14-inch trisonic wind tunnel.

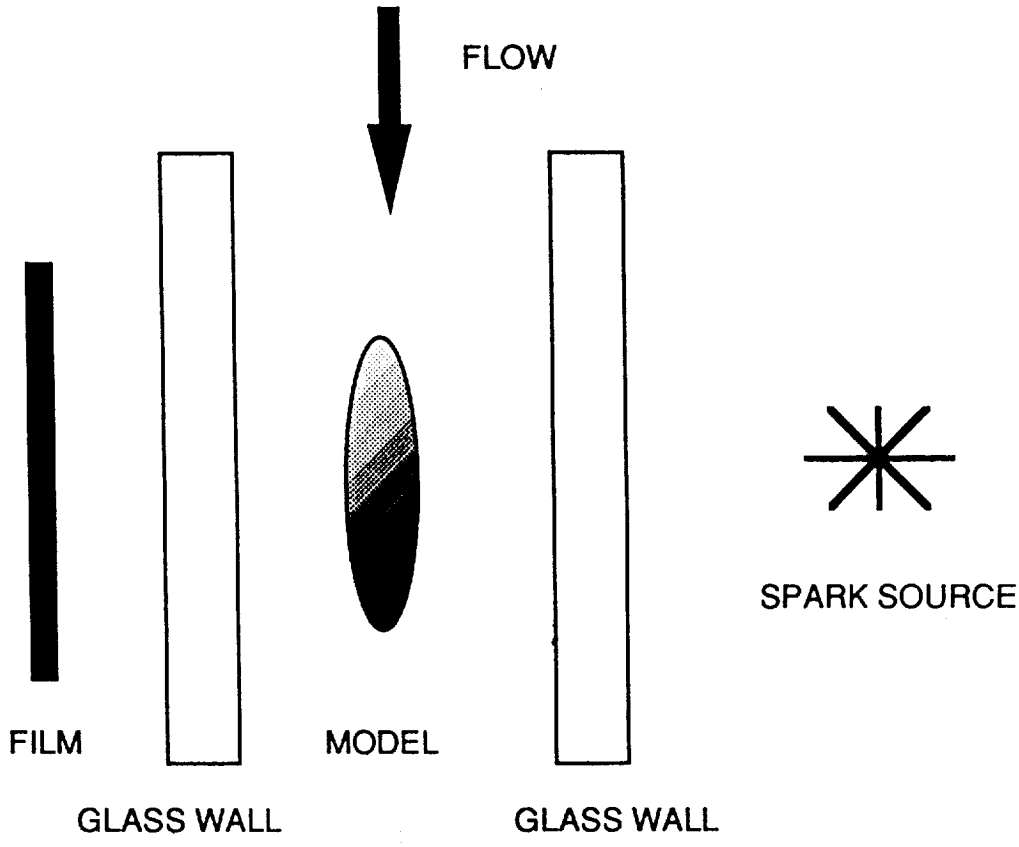

Figure 8. Sketch of the spark shadowgraph setup.

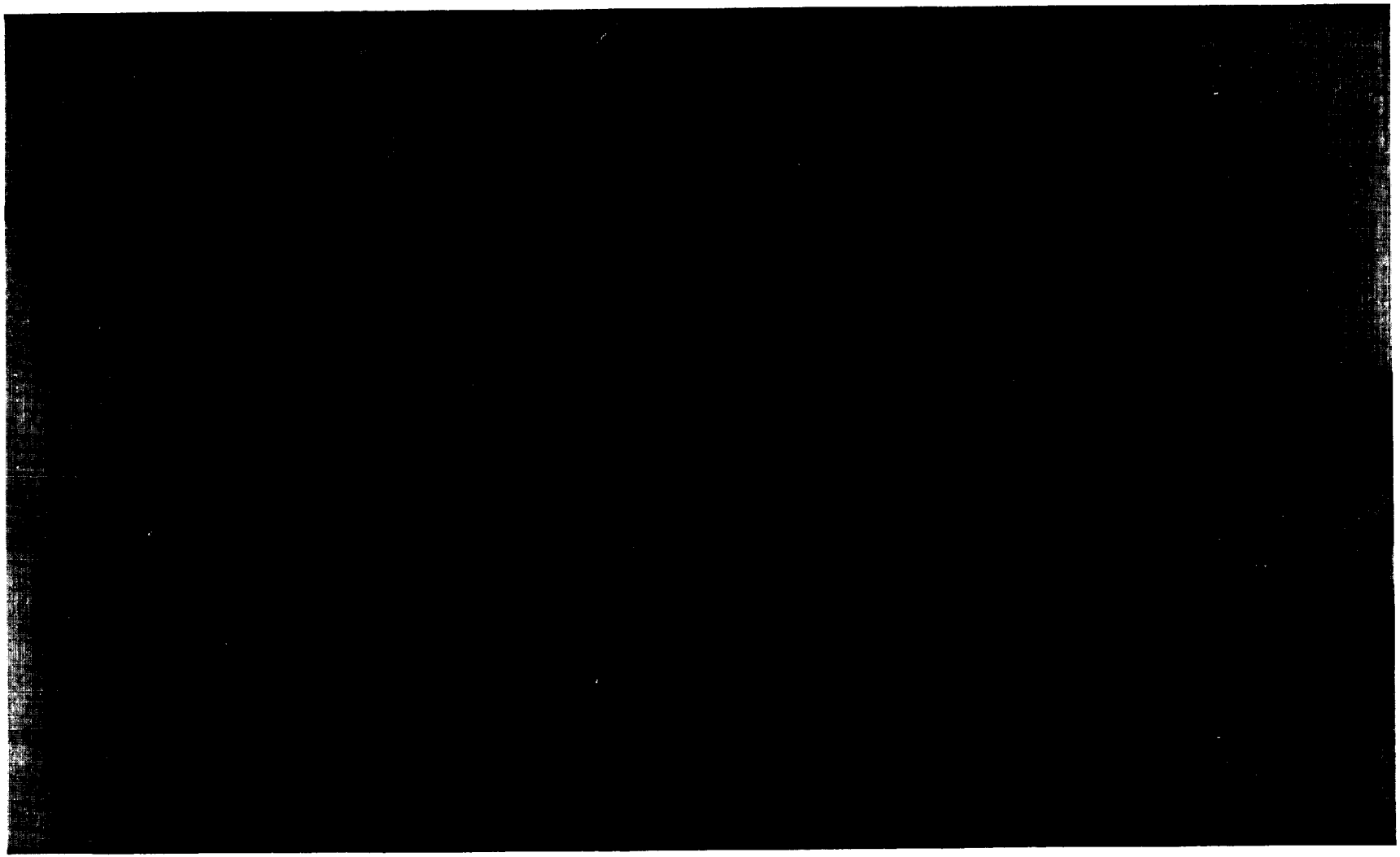

Figure 9. Shadowgraph of SSLV with no flow (Mach 0).

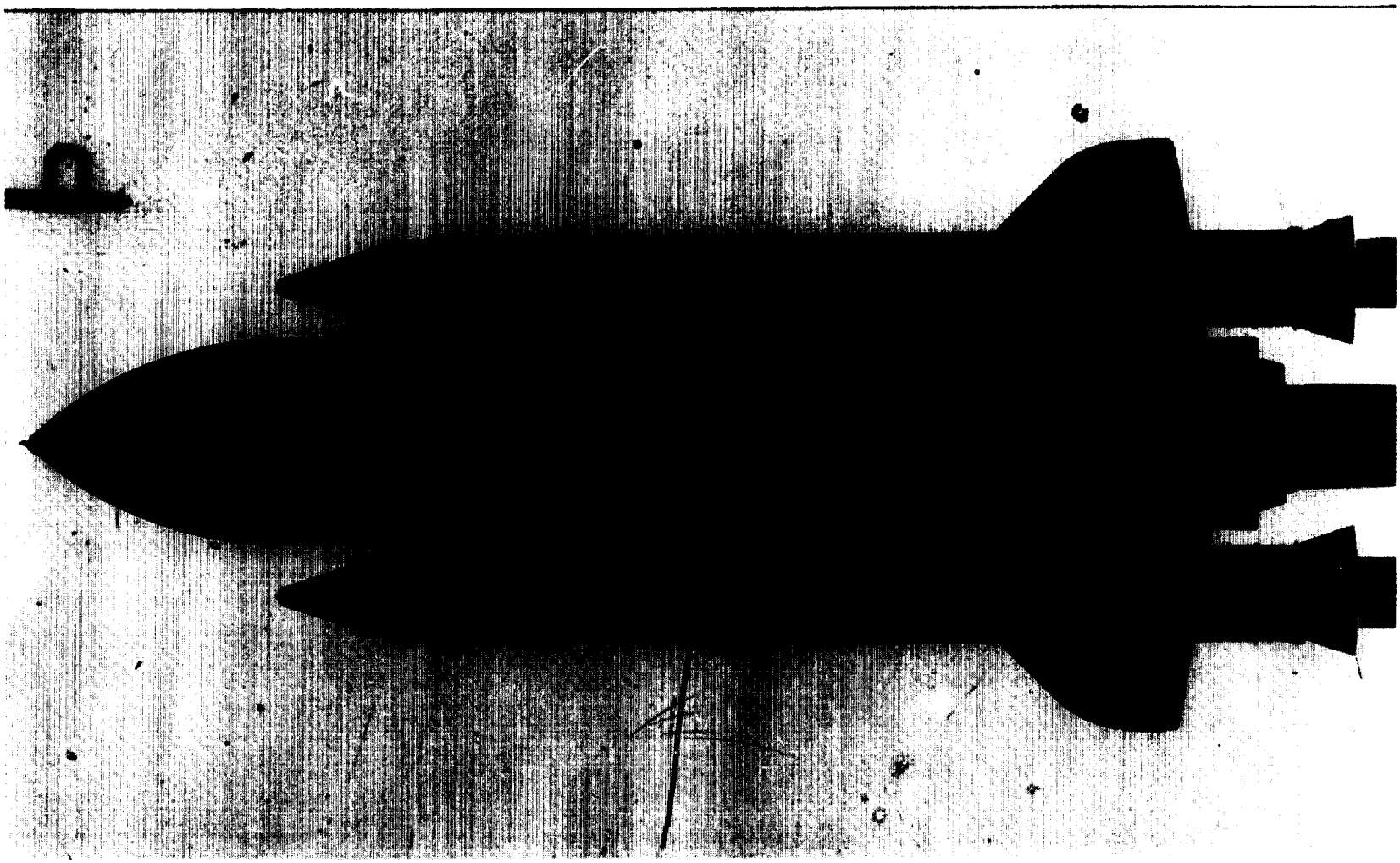

Figure 10. Shadowgraph of SSLV at a roll angle of 90° with no flow (Mach 0).

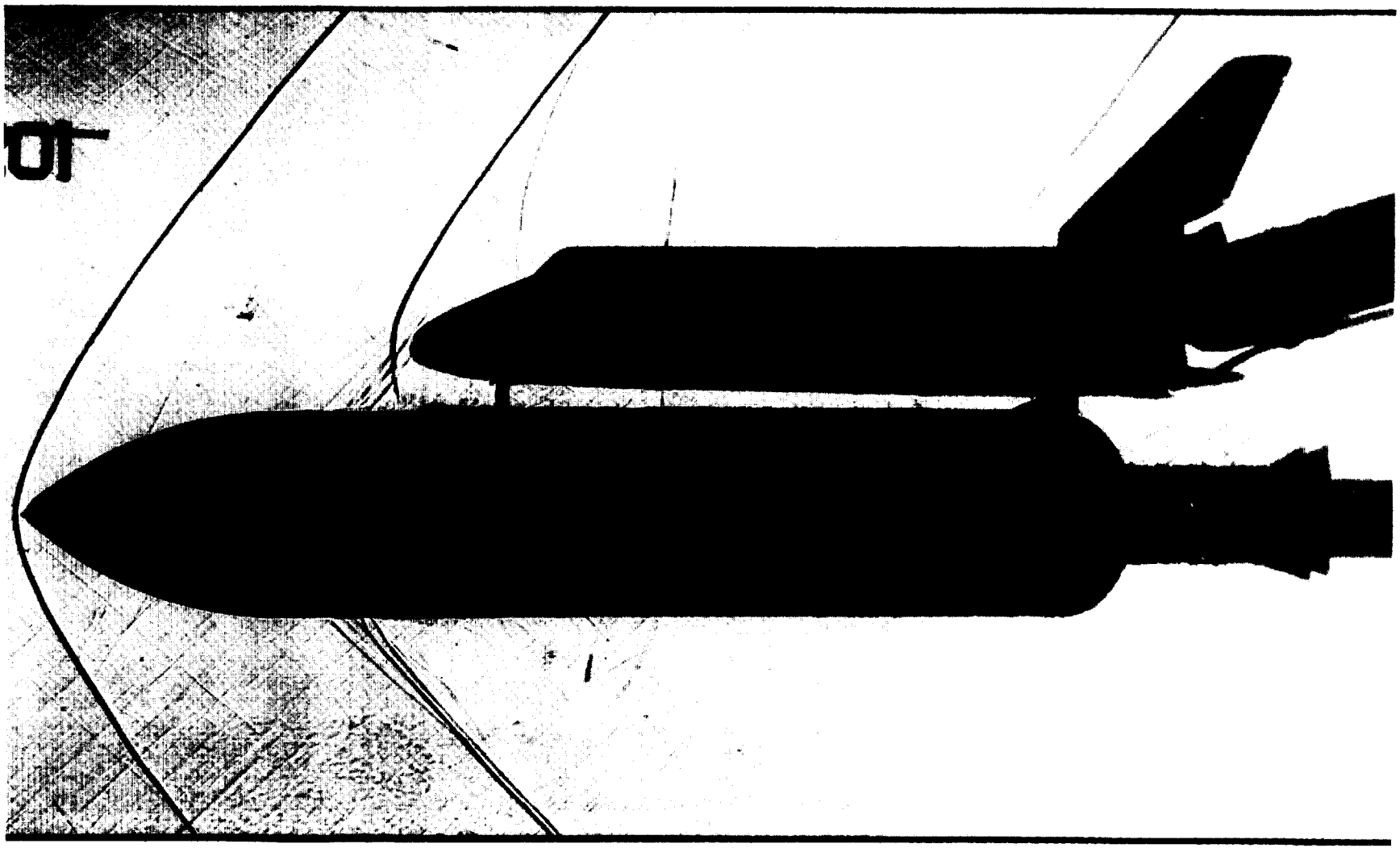

Figure 11. SSLV Mach 1.46, alpha = 0, beta = 0, roll = 0.

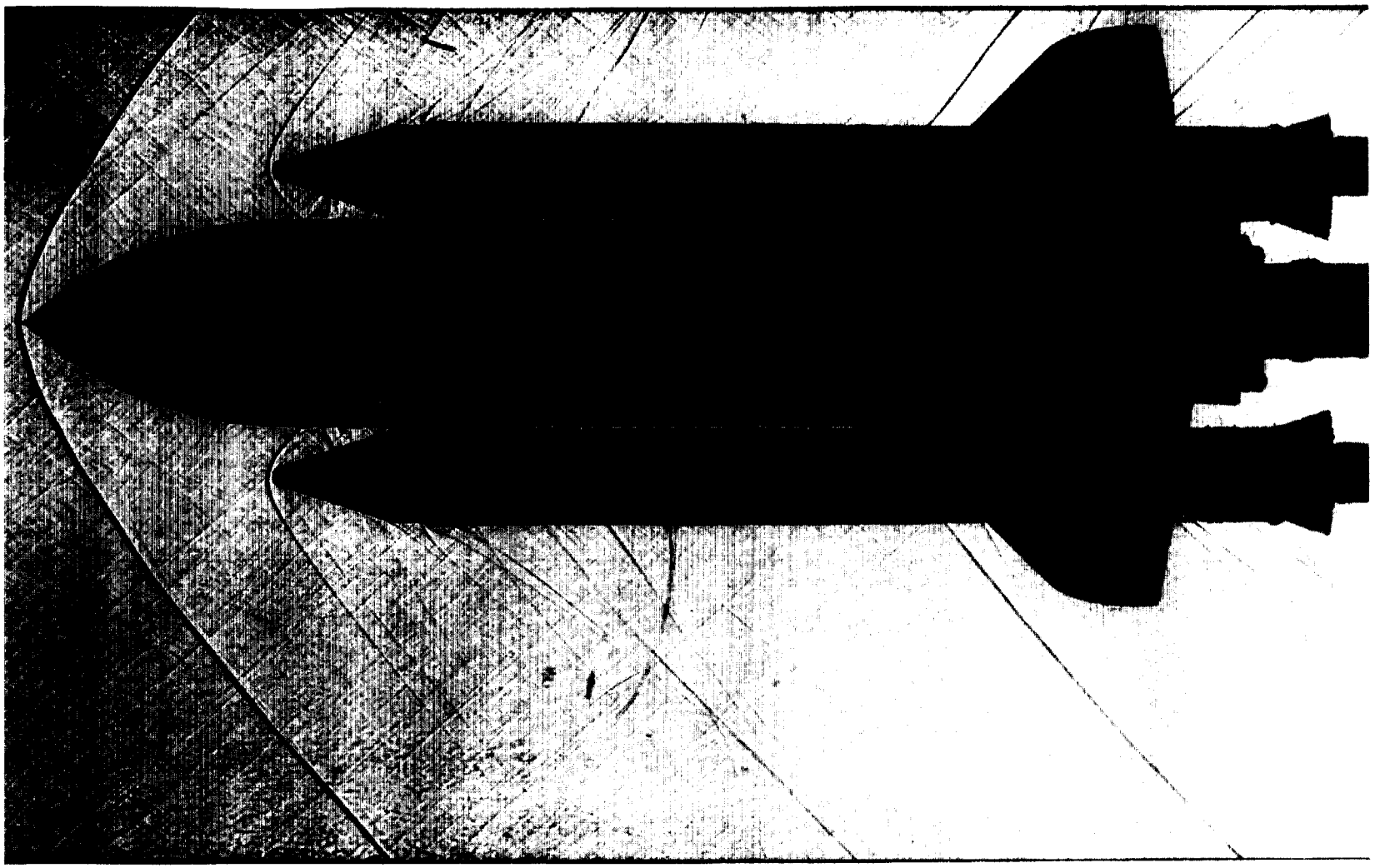

Figure 12. SSLV Mach 1.46, alpha = 0, beta = 0, roll = 90.

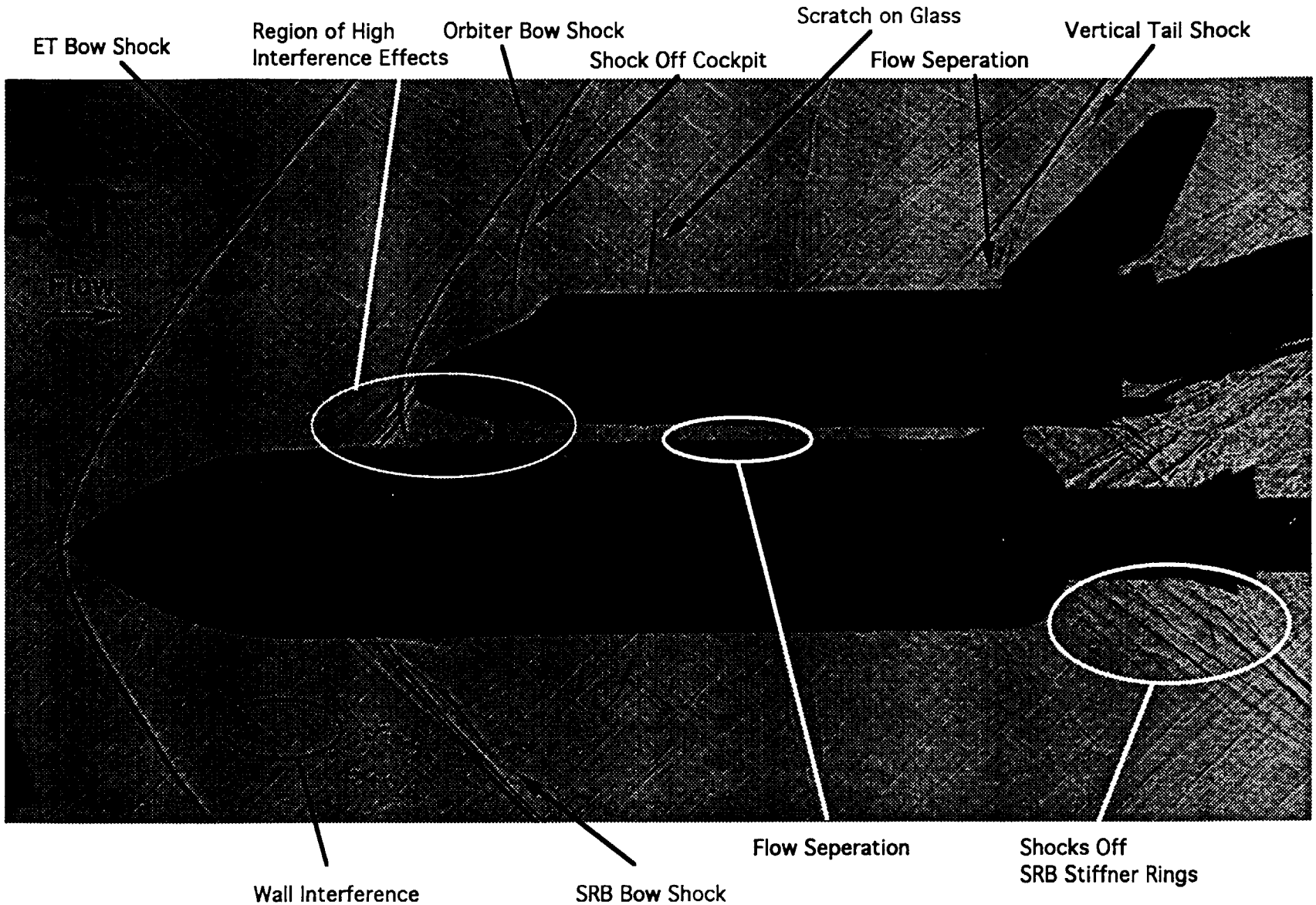

Figure 13. Description of flow phenomena over the SSLV Mach 1.46, alpha = 0, beta = 0.

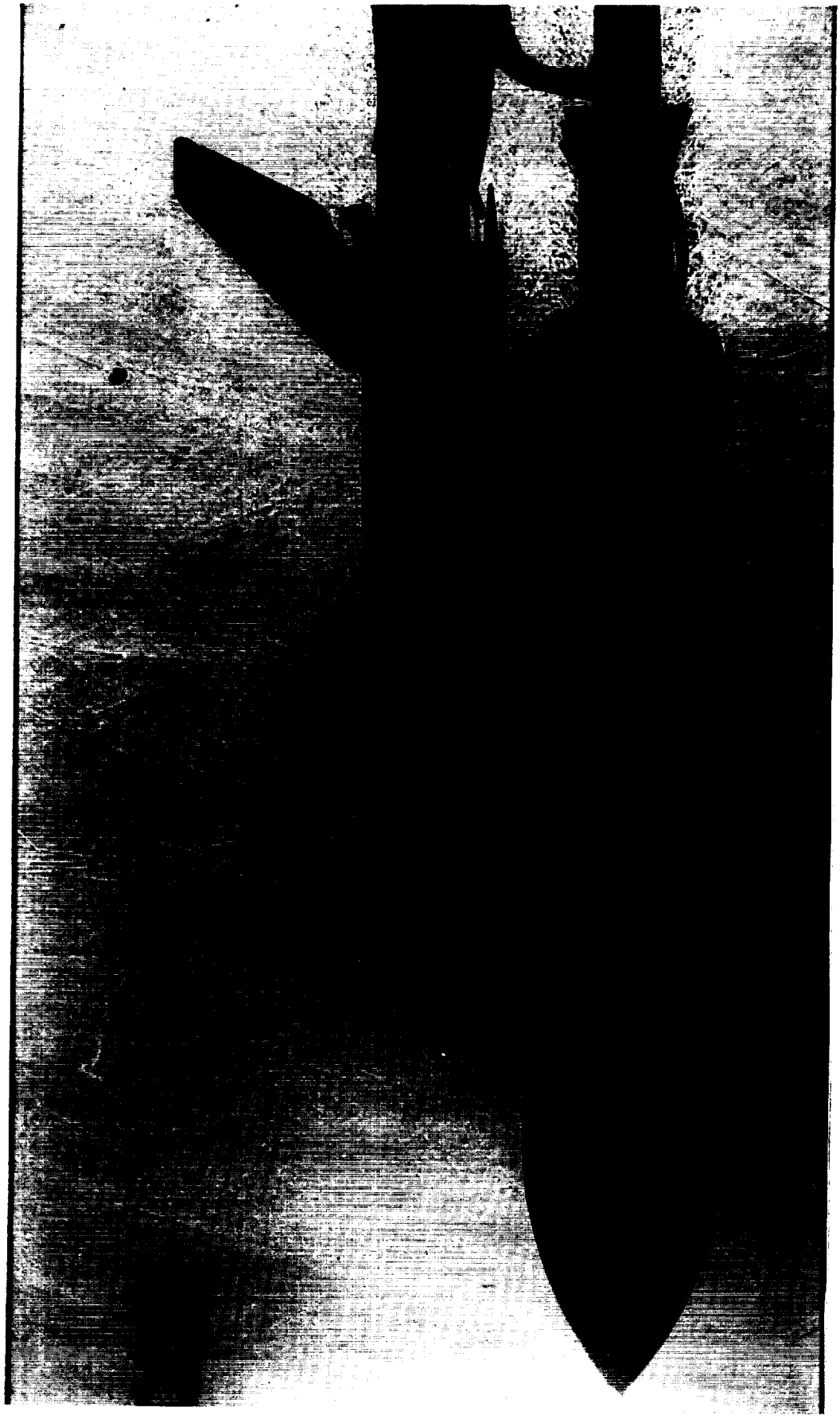

Figure 14. SSLV Mach 0.80, alpha = 0, beta = 0, roll = 0.

Figure 15. SSLV Mach 0.80, alpha = –5, beta = 0, roll = 0.

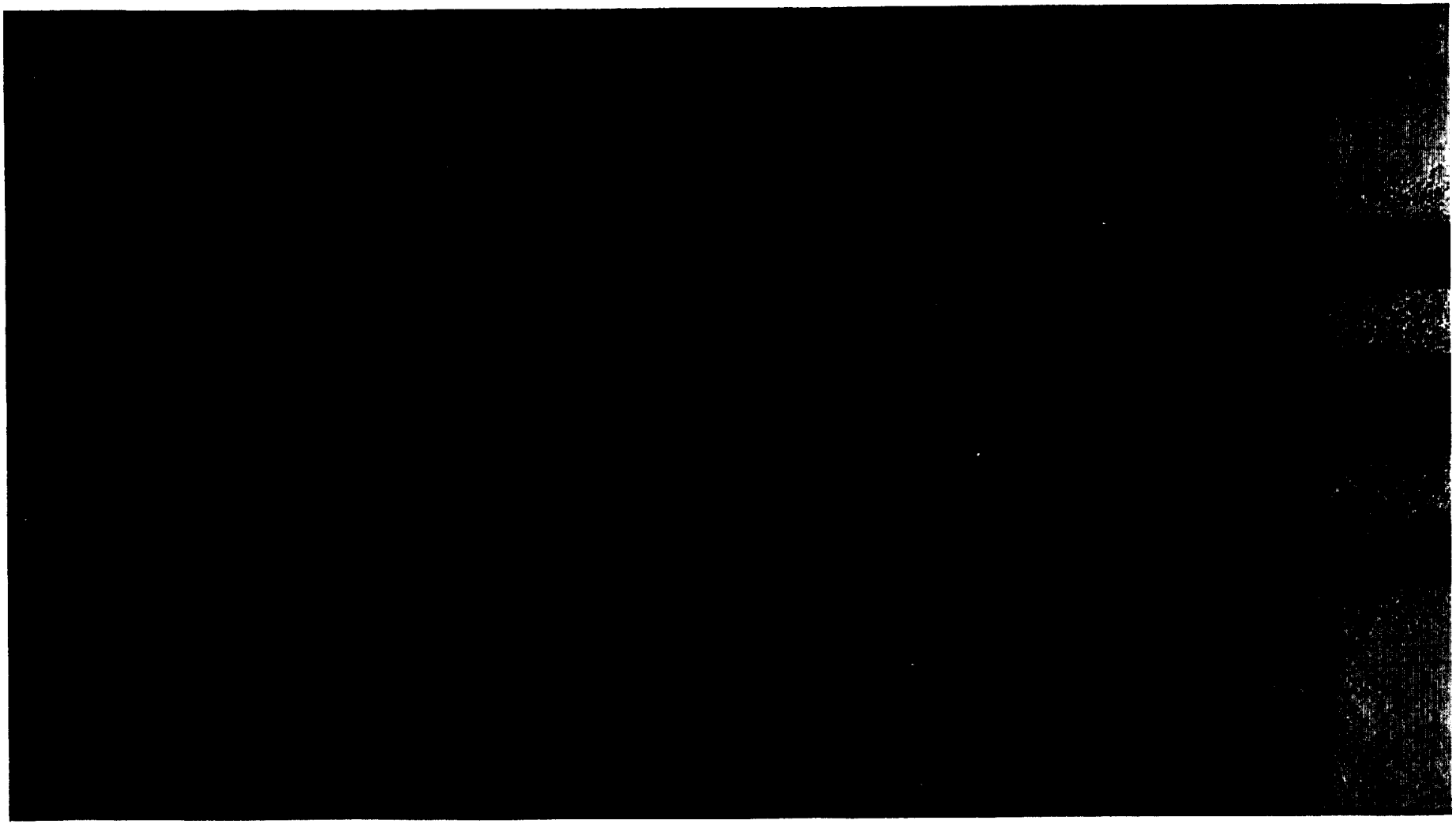

Figure 16. SSLV Mach 0.80, alpha = 0, beta = 0, roll = 90.

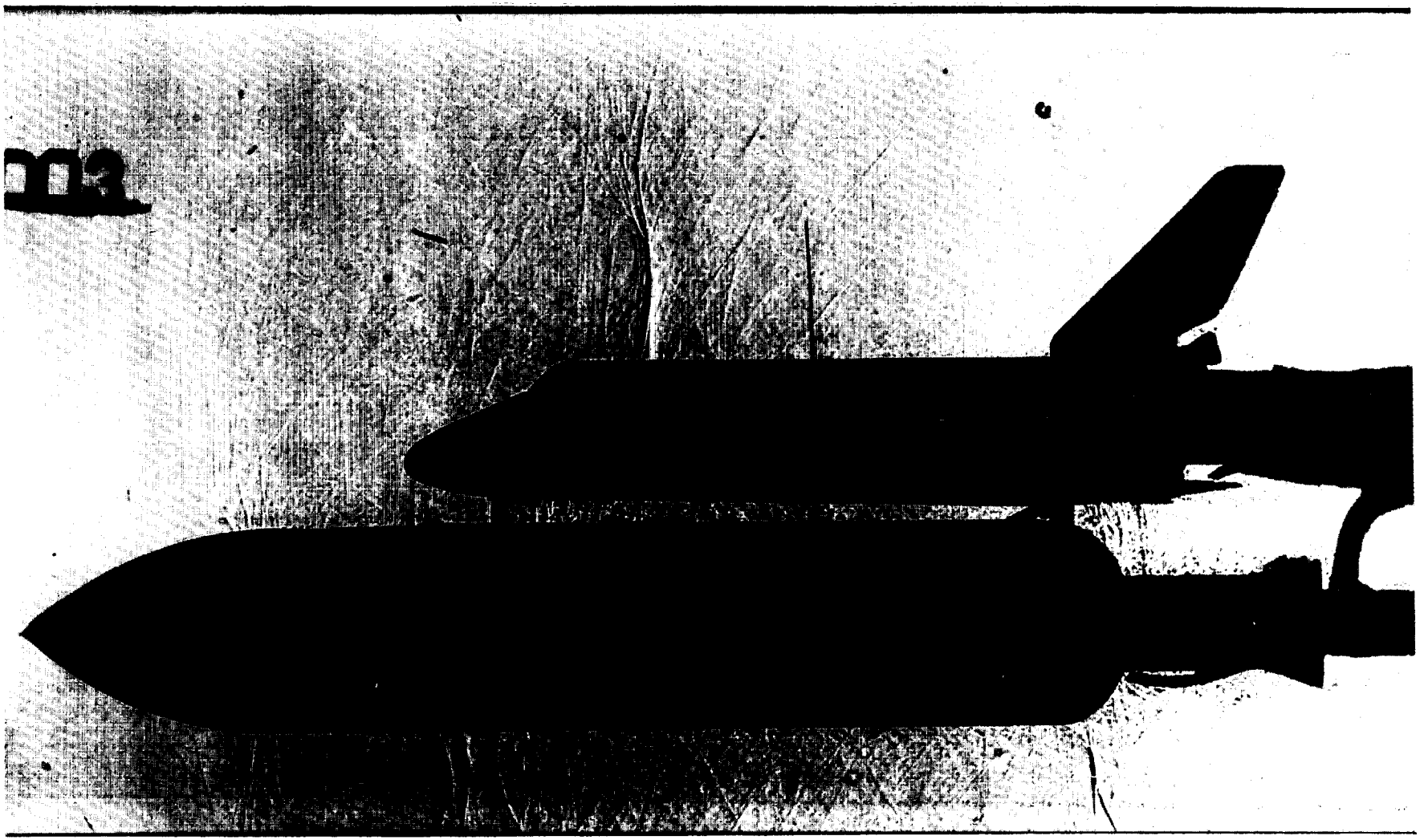

Figure 17. SSLV Mach 0.90, alpha = 0, beta = 0, roll = 0.

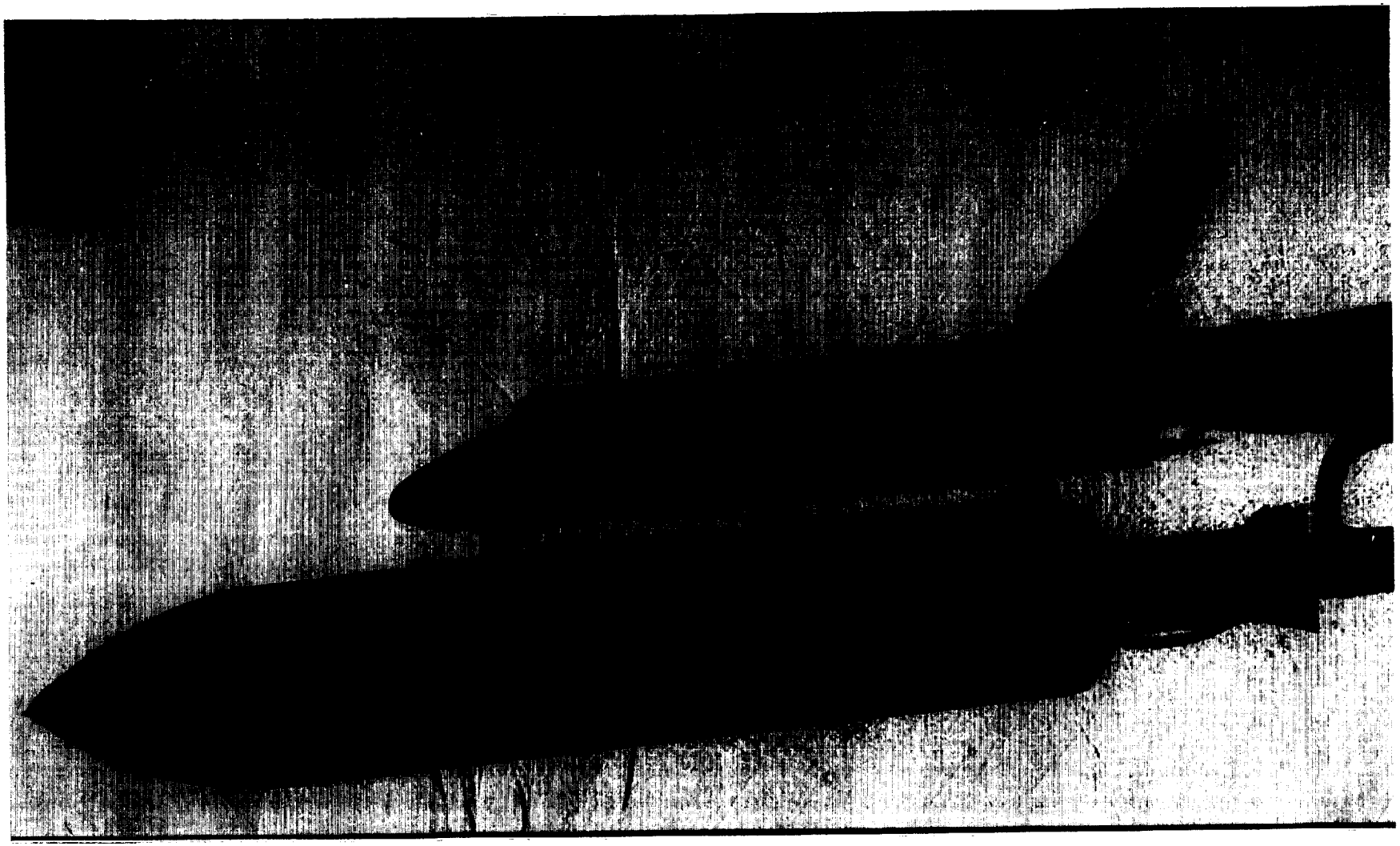

Figure 18. SSLV Mach 0.90, alpha = –5, beta = 0, roll = 0.

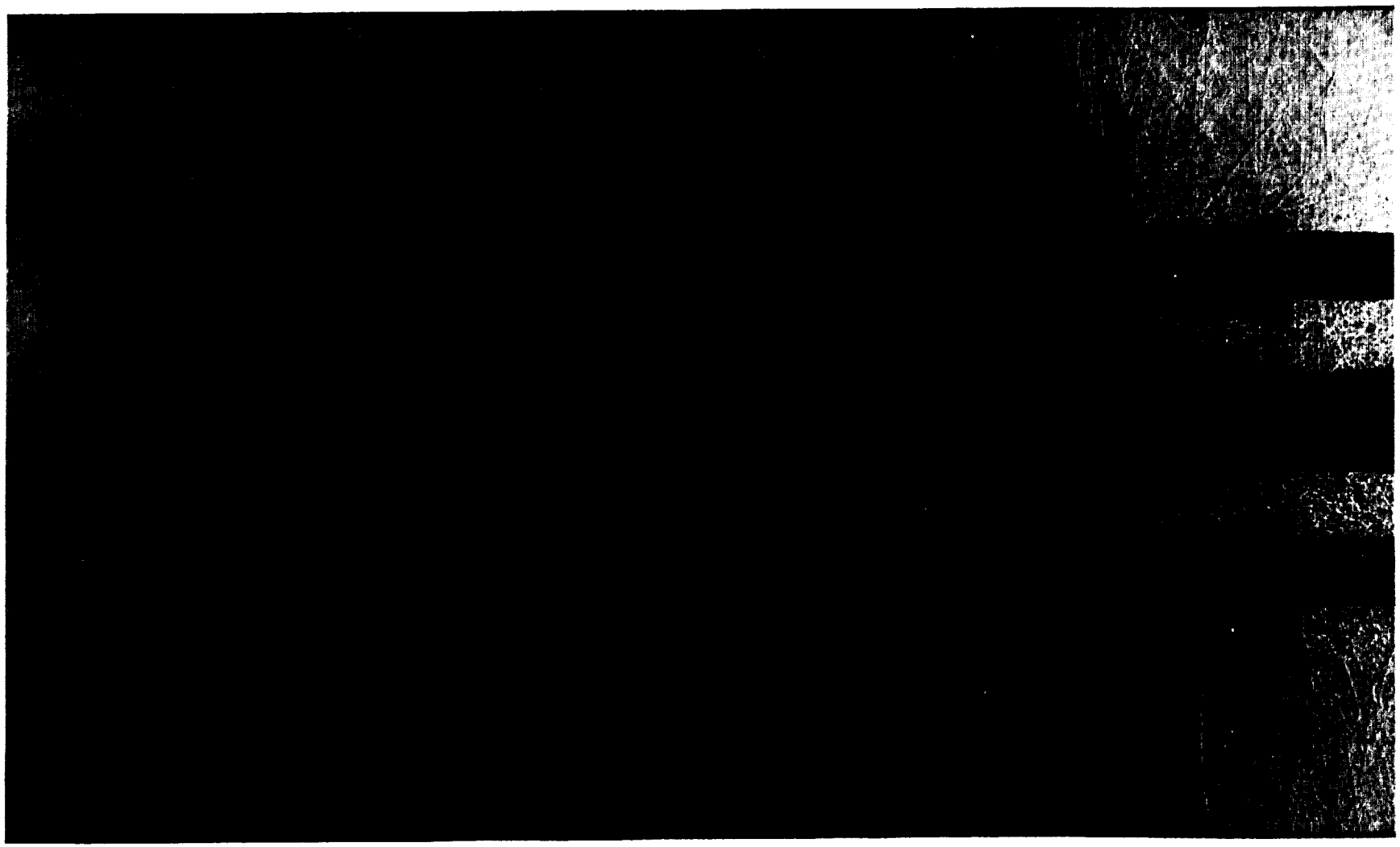

Figure 19. SSLV Mach 0.90, alpha = 0, beta = 0, roll = 90.

Figure 20. SSLV Mach 1.05, alpha = 0, beta = 0, roll = 0.

Figure 21. SSLV Mach 1.05, alpha = –5, beta = 0, roll = 0.

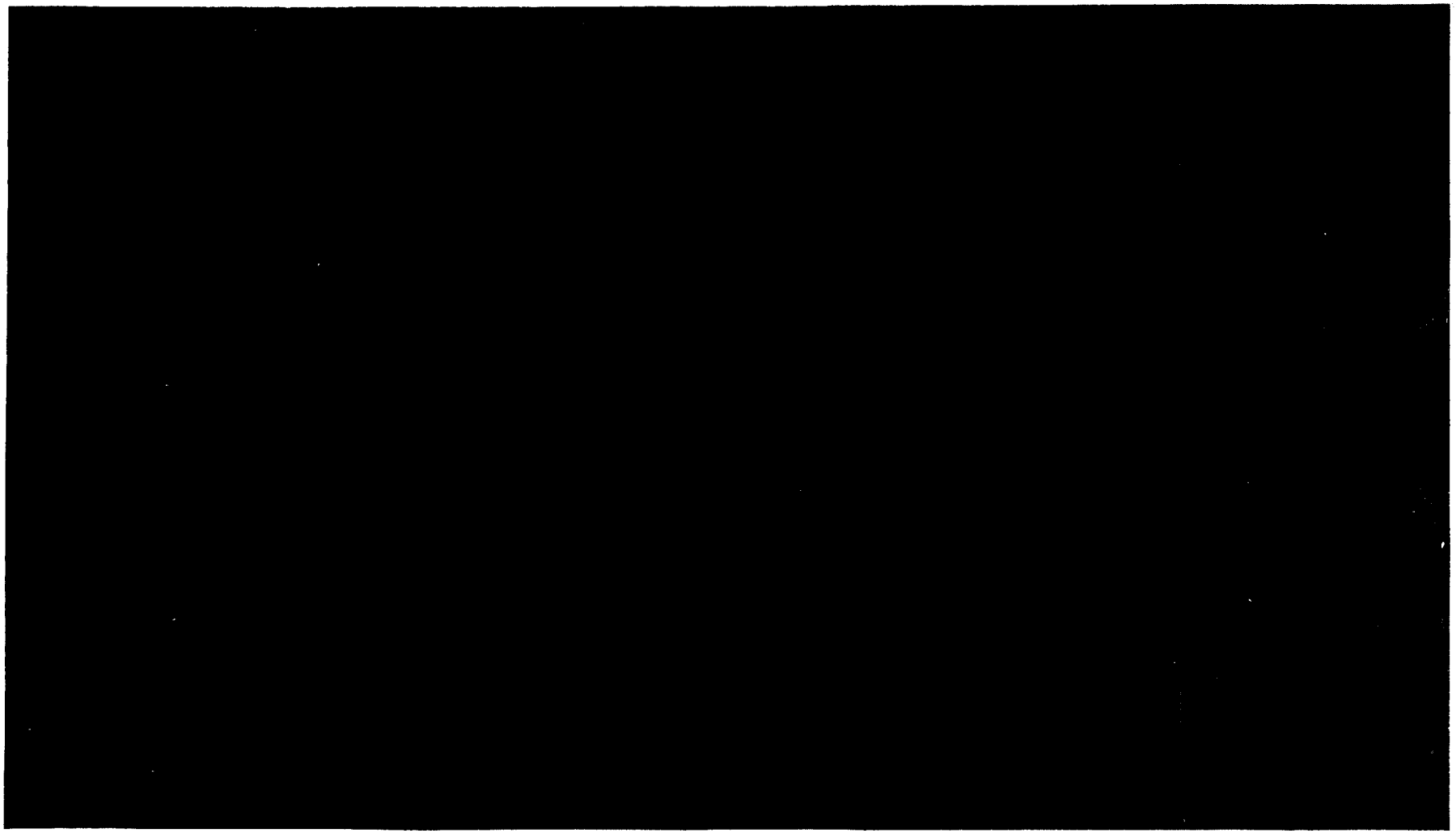

Figure 22. SSLV Mach 1.05, alpha = 0, beta = 0, roll = 90.

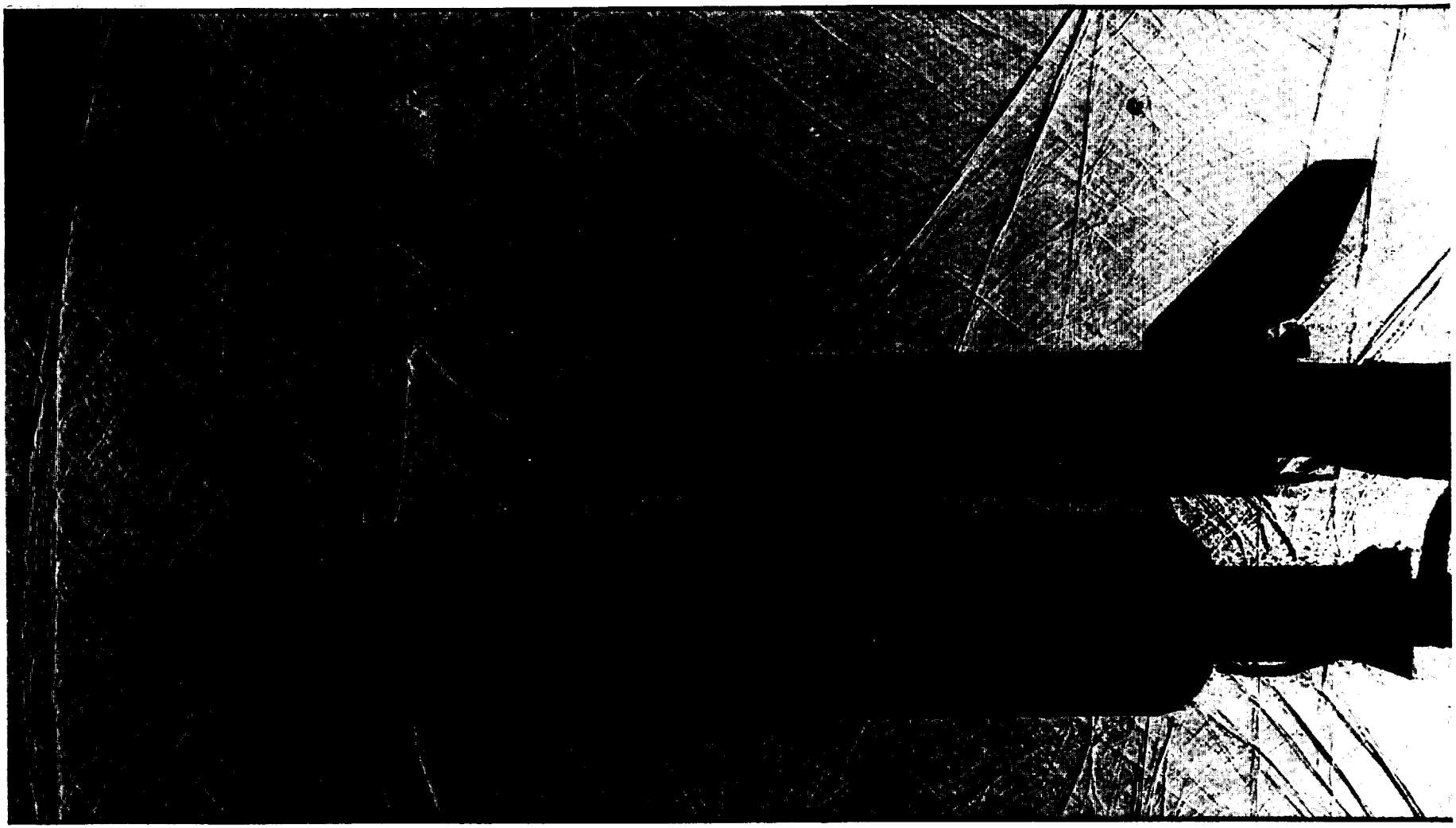

Figure 23. SSLV Mach 1.10, alpha = 0, beta = 0, roll = 0.

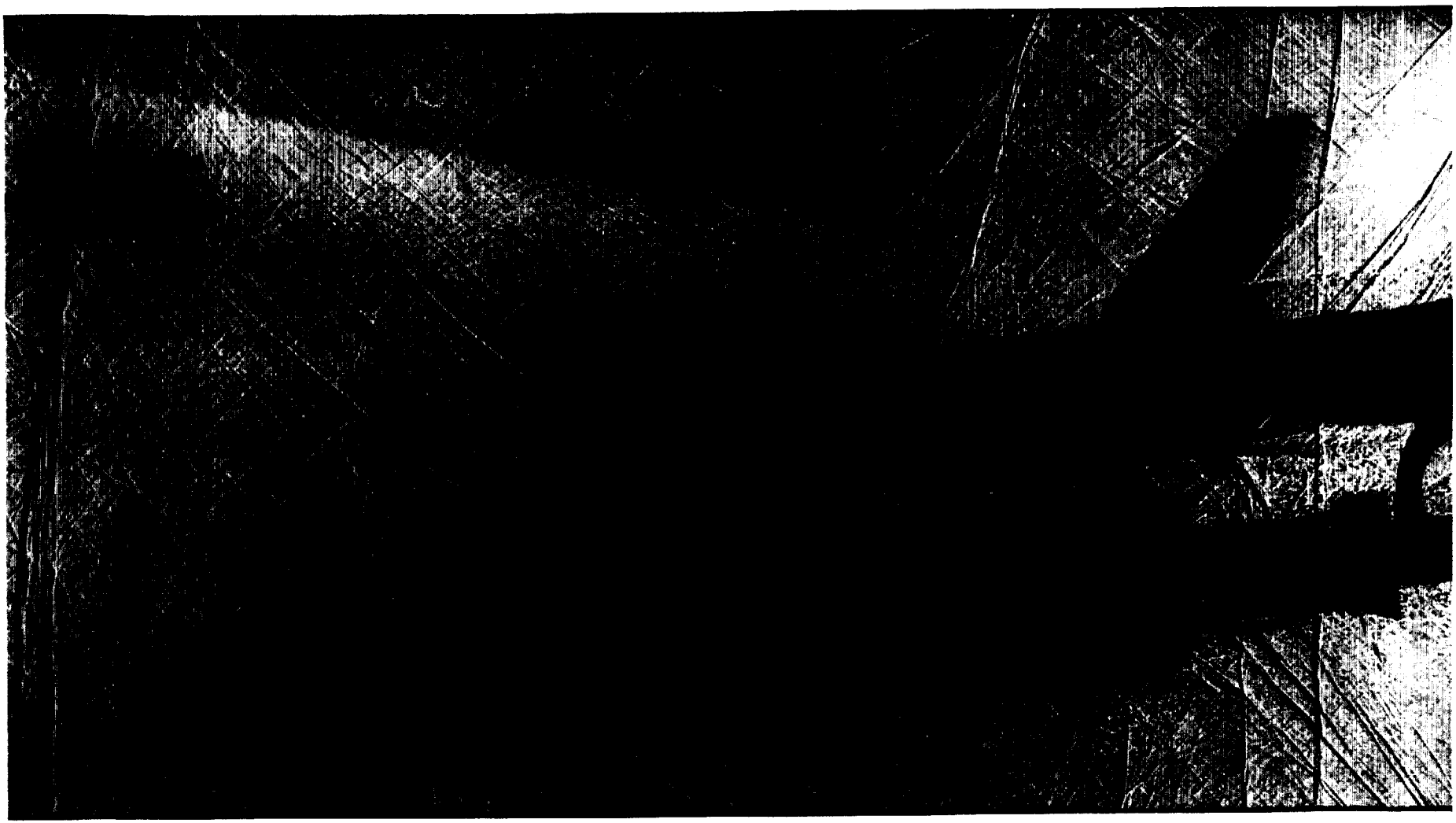

Figure 24. SSLV Mach 1.10, alpha = –5, beta = 0, roll = 0.

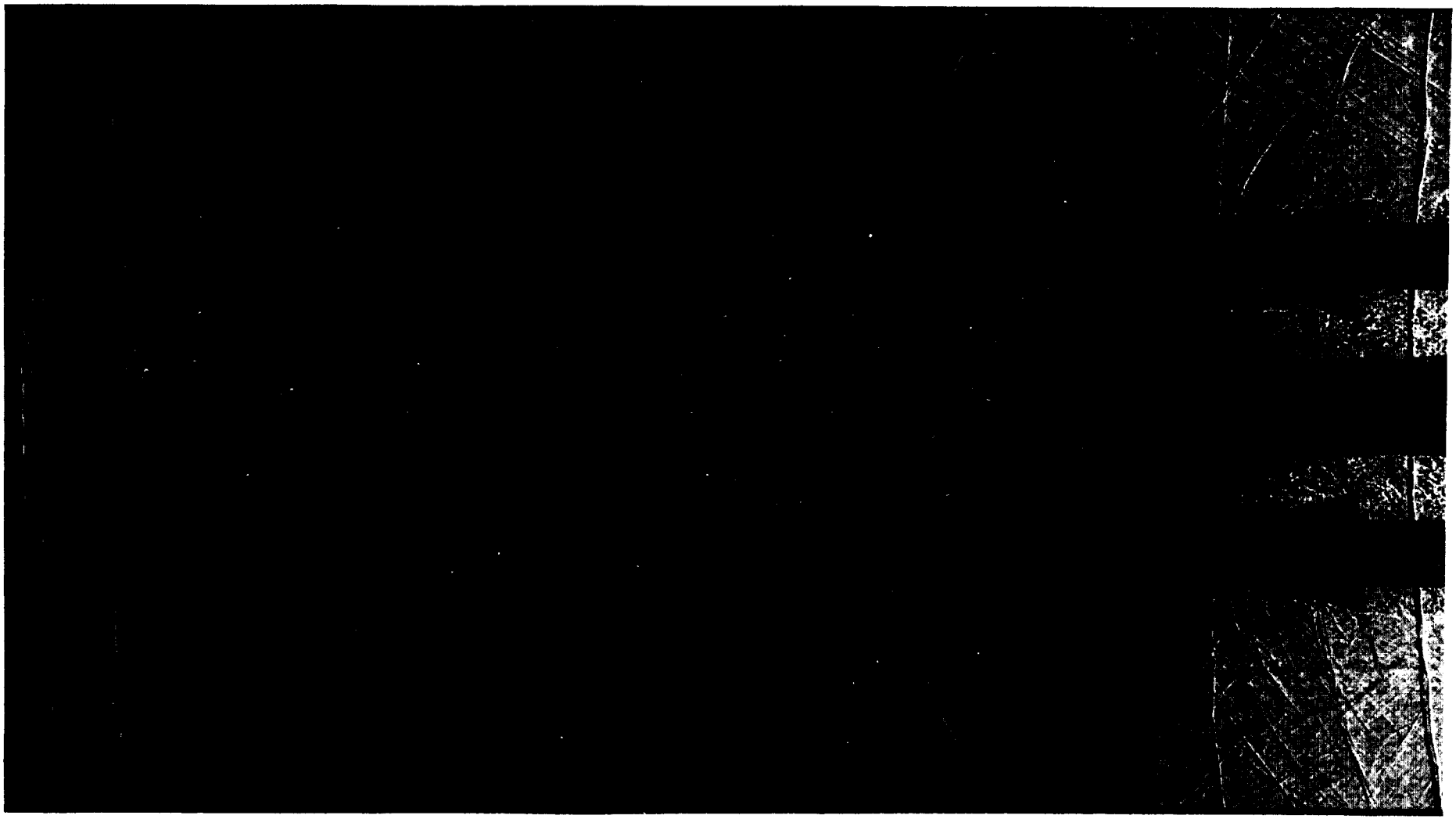

Figure 25. SSLV Mach 1.10, alpha = 0, beta = 0, roll = 90.

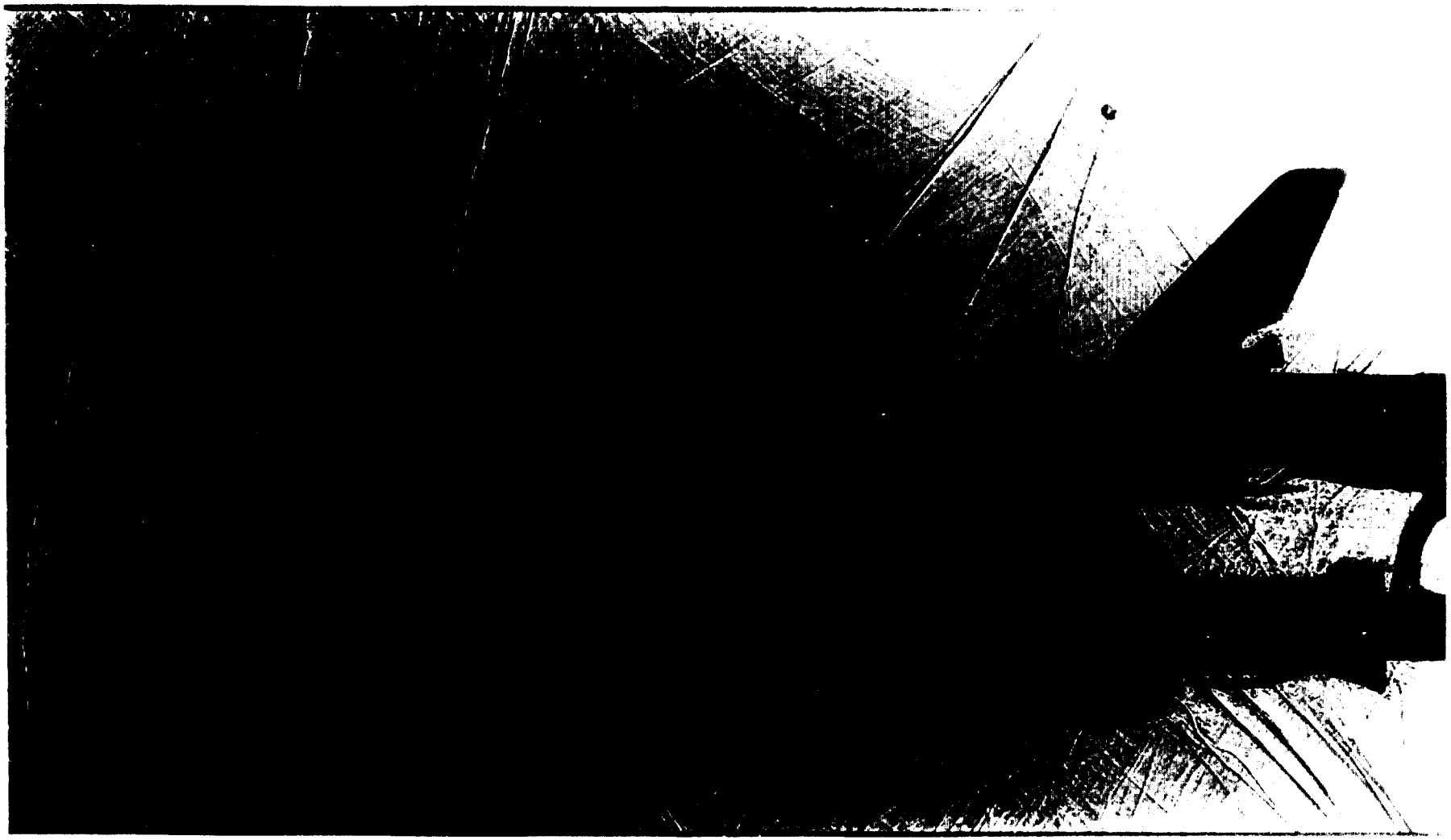

Figure 26. SSLV Mach 1.15, alpha = 0, beta = 0, roll = 0.

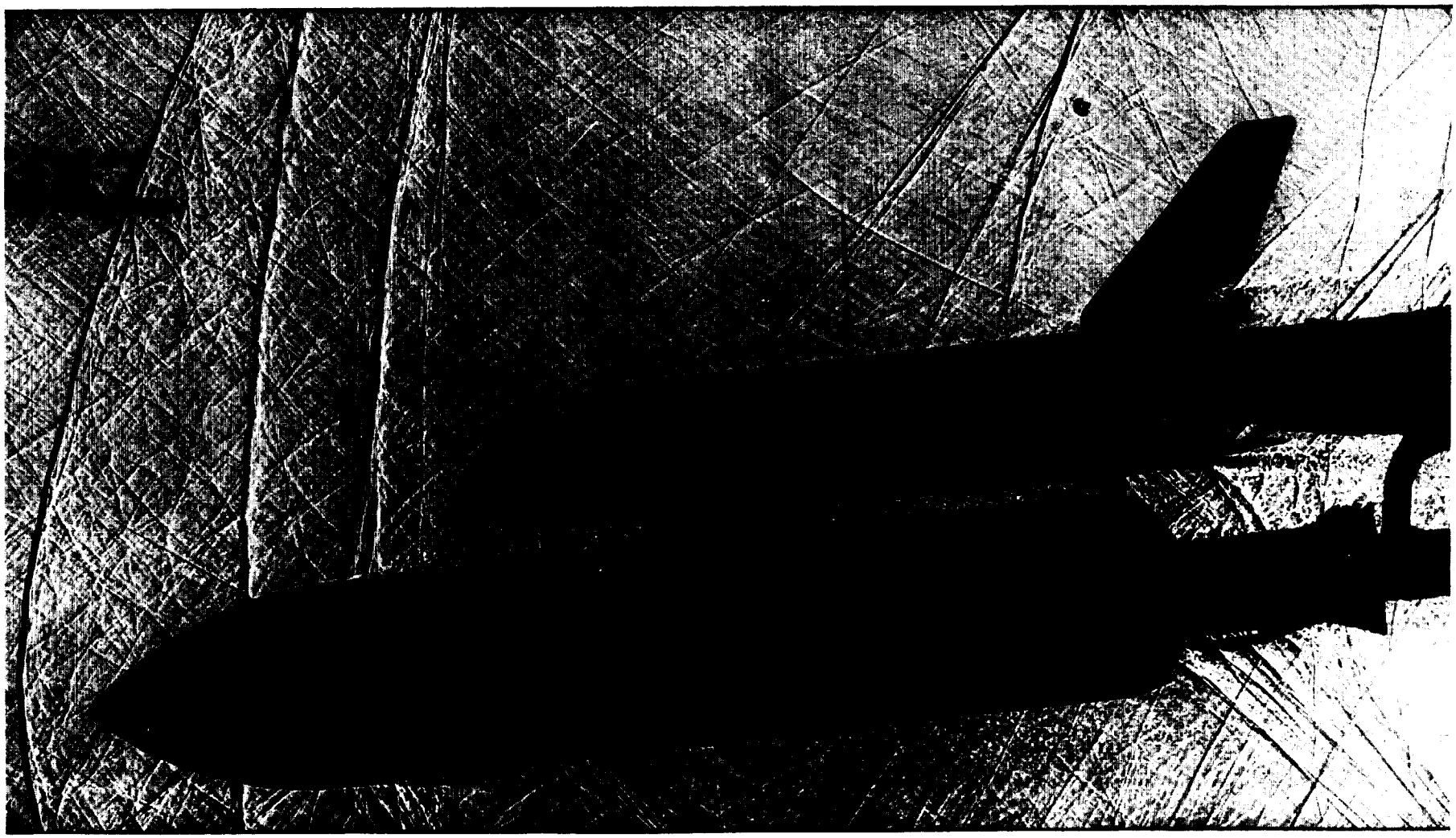

Figure 27. SSLV Mach 1.15, alpha = –5, beta = 0, roll = 0.

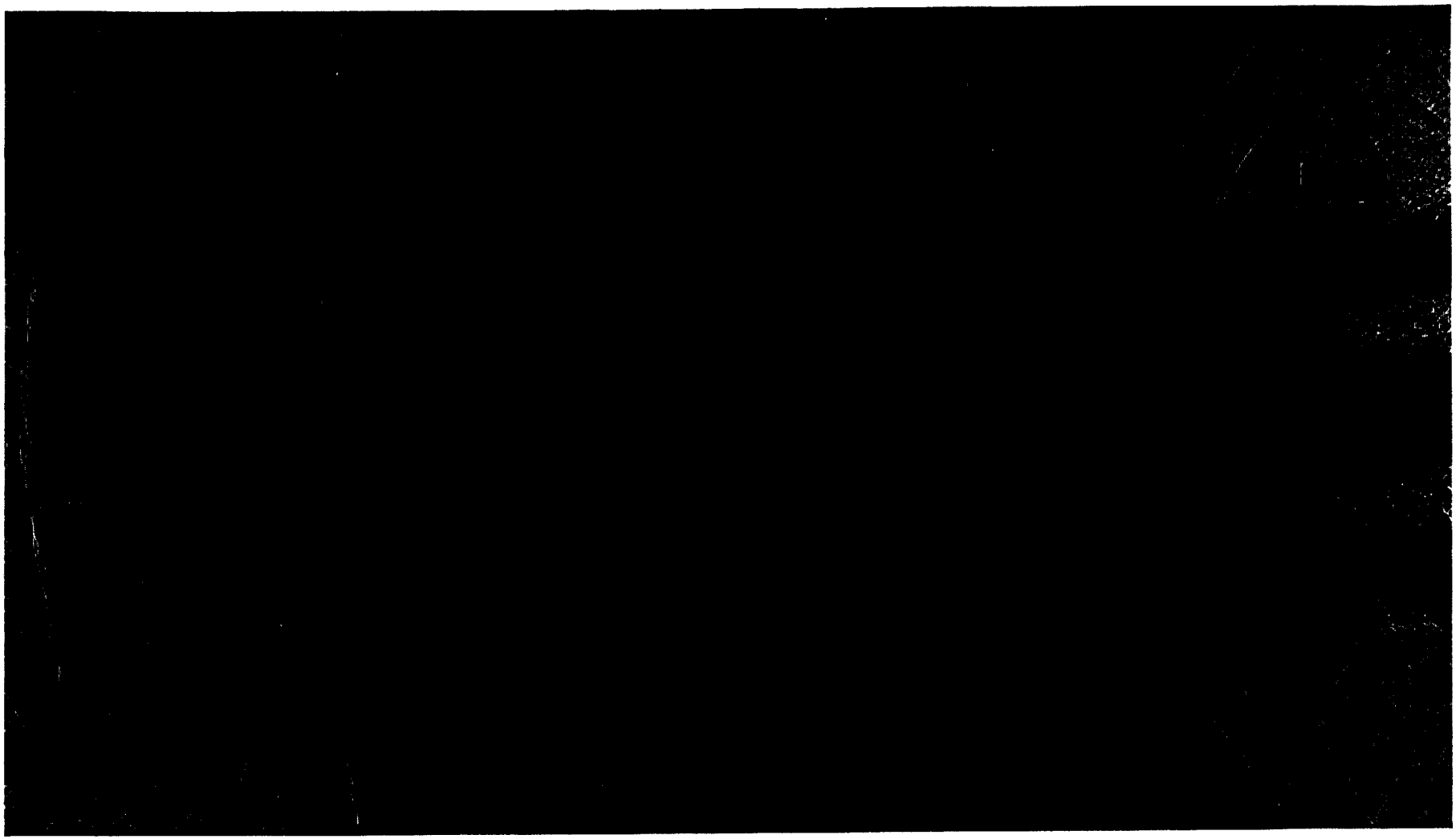

Figure 28. SSLV Mach 1.15, alpha = 0, beta = 0, roll = 90.

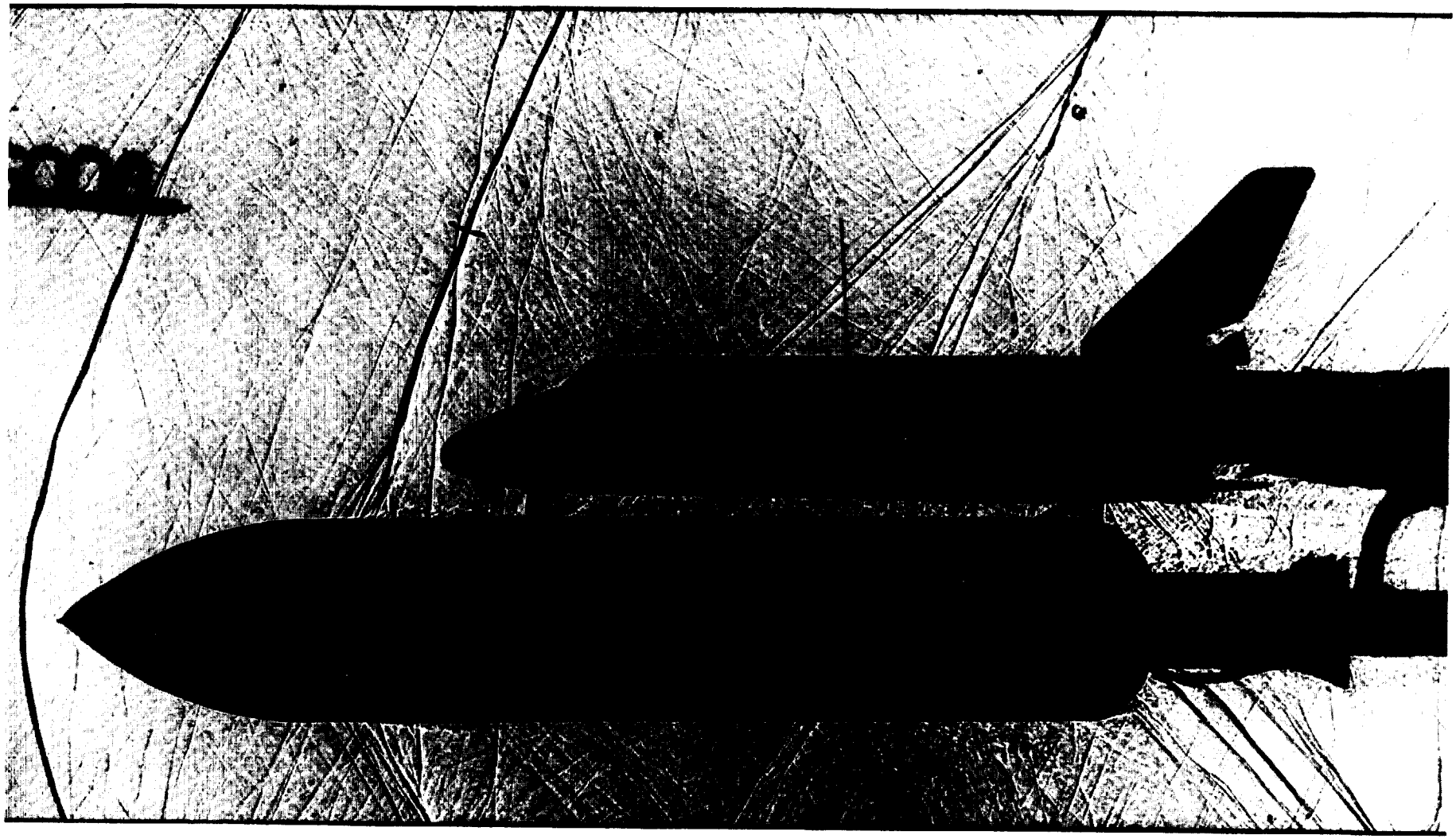

Figure 29. SSLV Mach 1.25, alpha = 0, beta = 0, roll = 0.

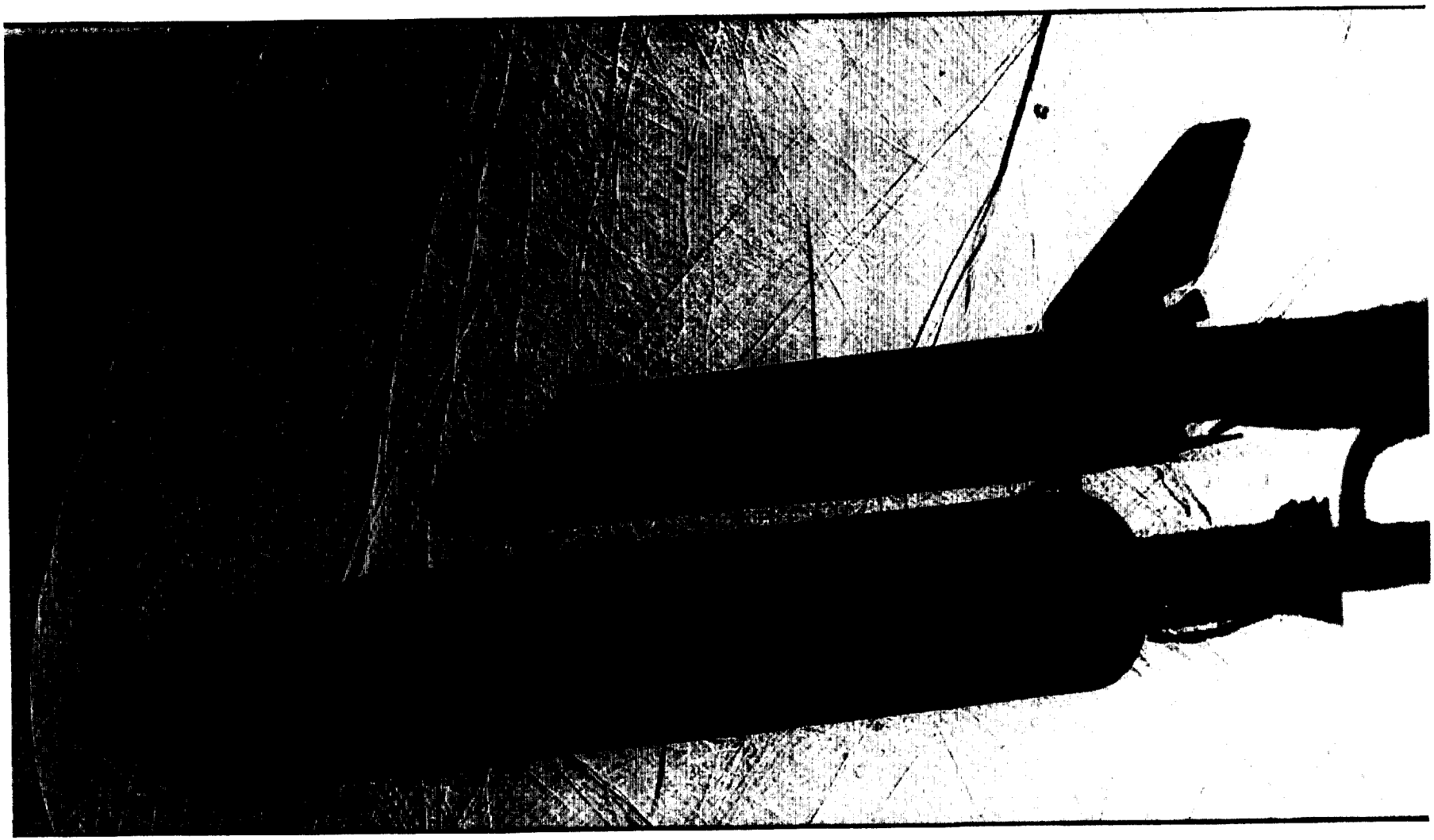

Figure 30. SSLV Mach 1.25, alpha =–5, beta = 0, roll = 0.

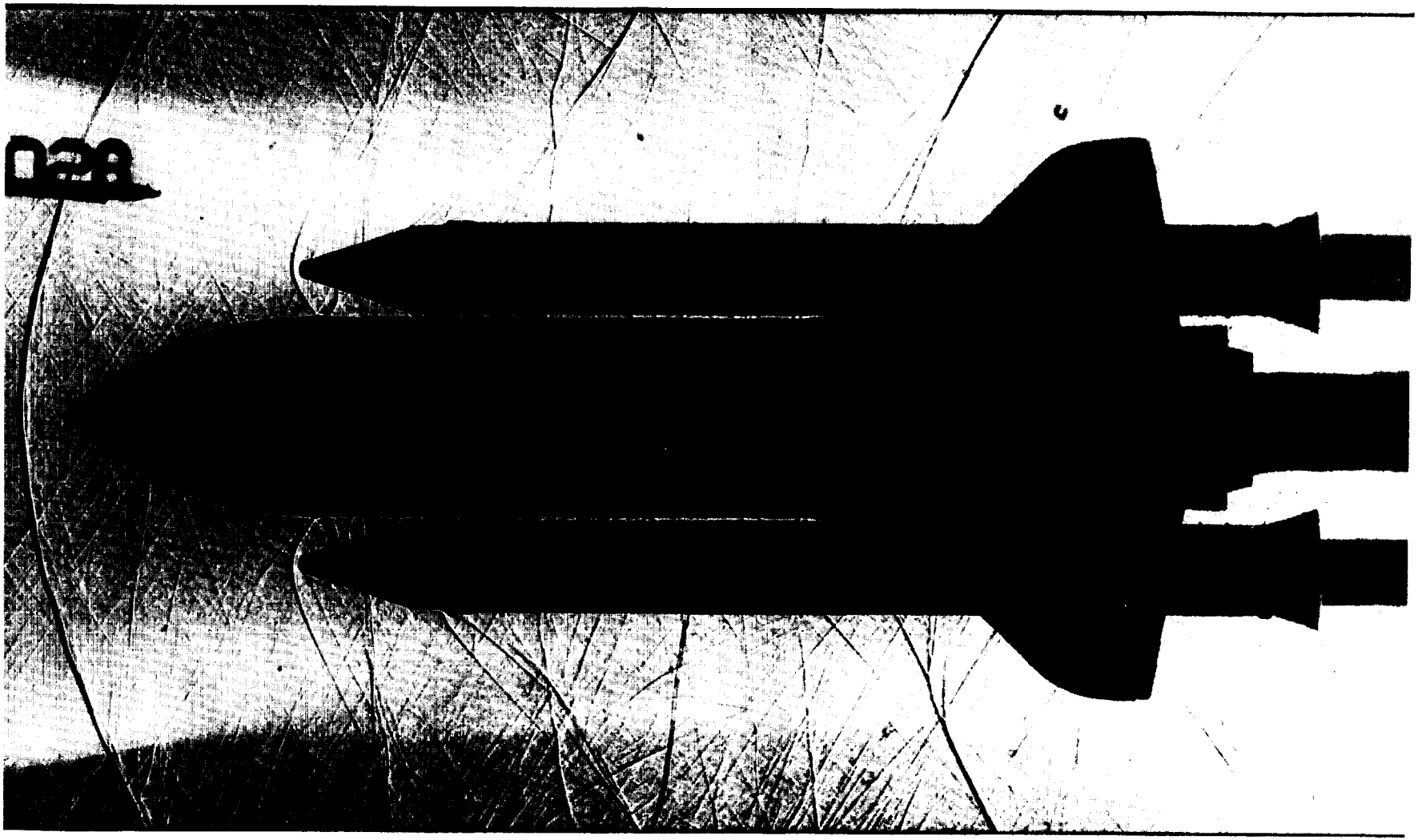

Figure 31. SSLV Mach 1.25, alpha = 0, beta = 0, roll = 90.

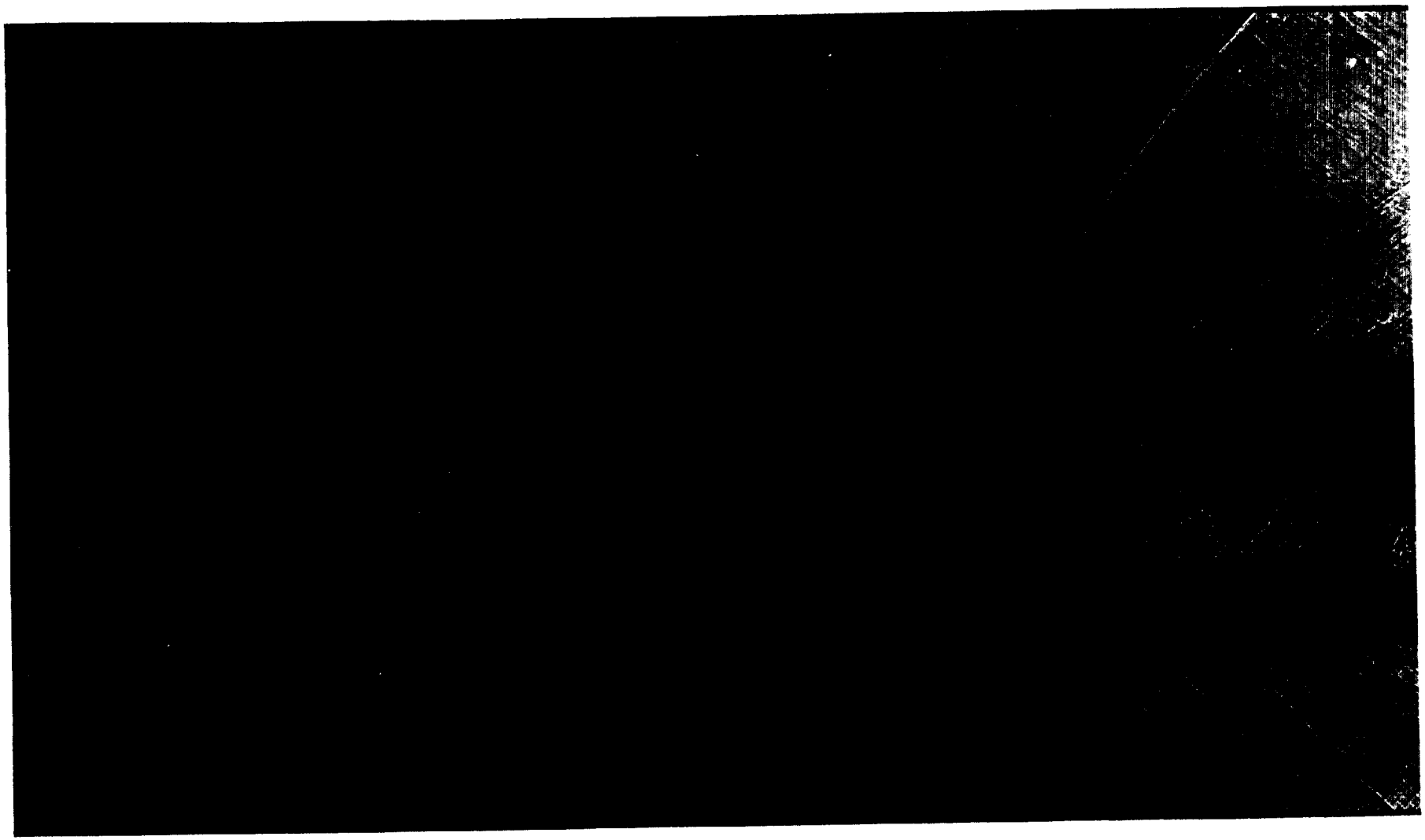

Figure 32. SSLV Mach 1.46, alpha = 0, beta = 0, roll = 0.

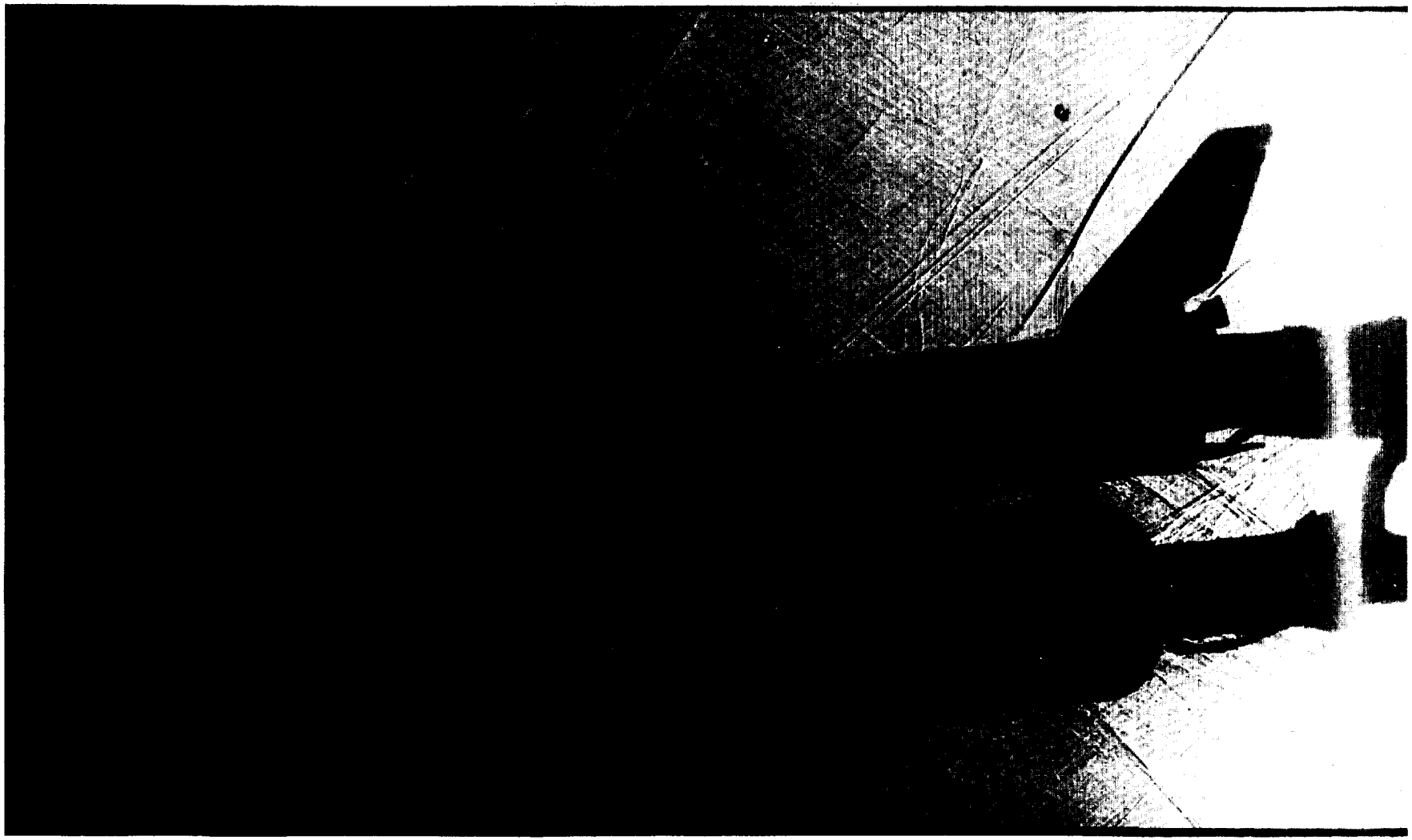

Figure 33. SSLV Mach 1.46, alpha =–5, beta = 0, roll = 0.

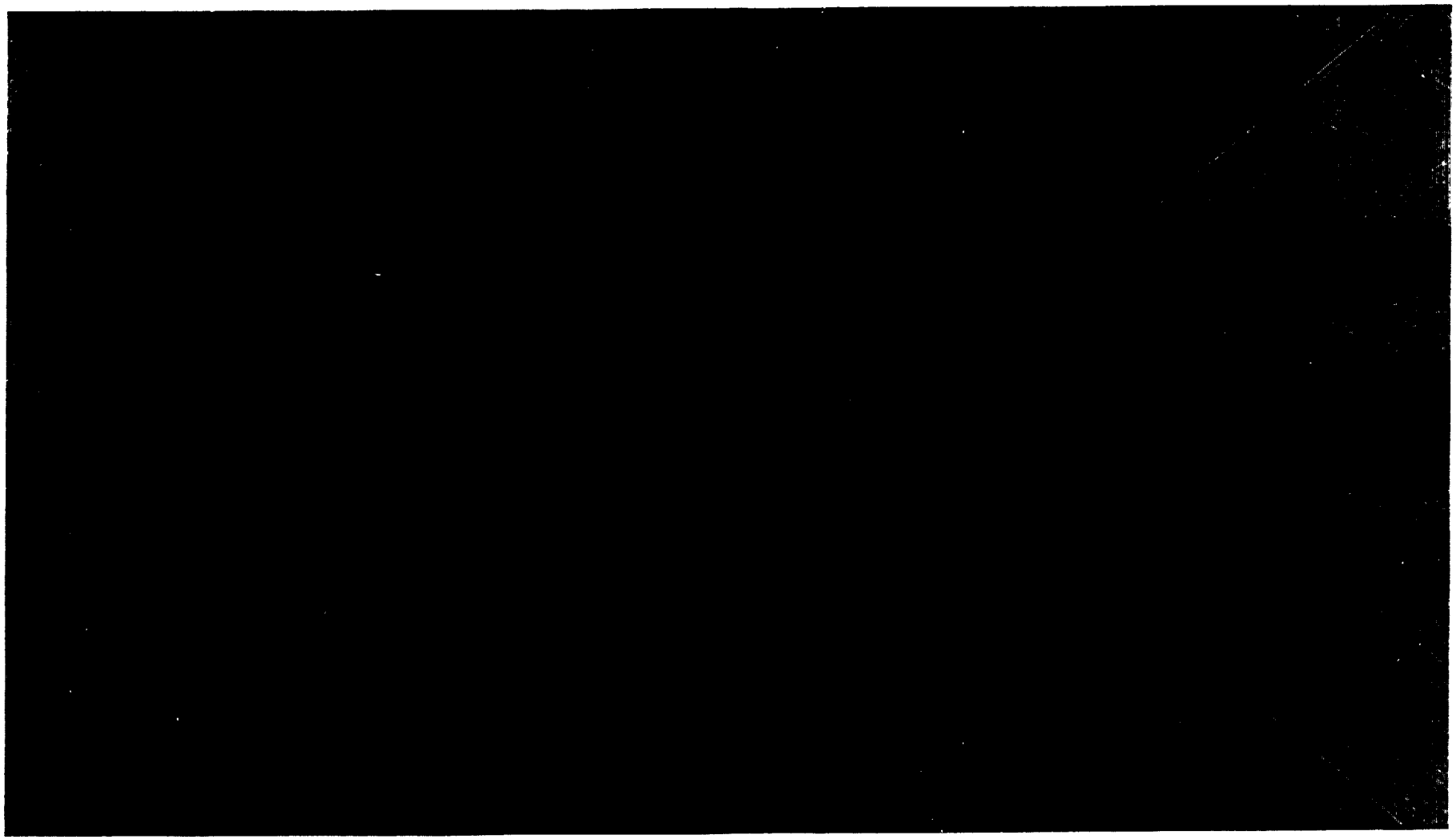

Figure 34. SSLV Mach 1.46, alpha = 0, beta = 0, roll = 90.

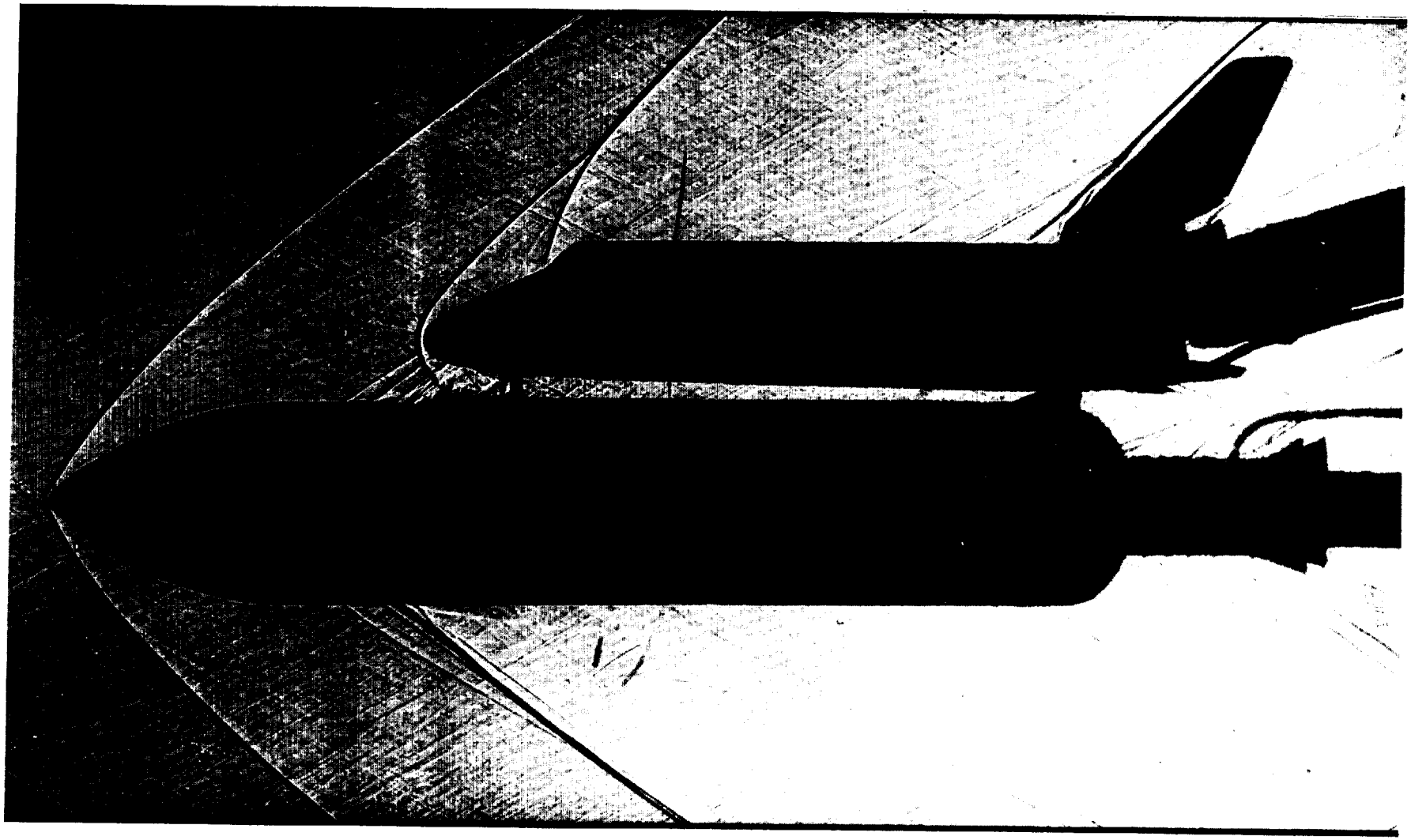

Figure 35. SSLV Mach 1.96, alpha = 0, beta = 0, roll = 0.

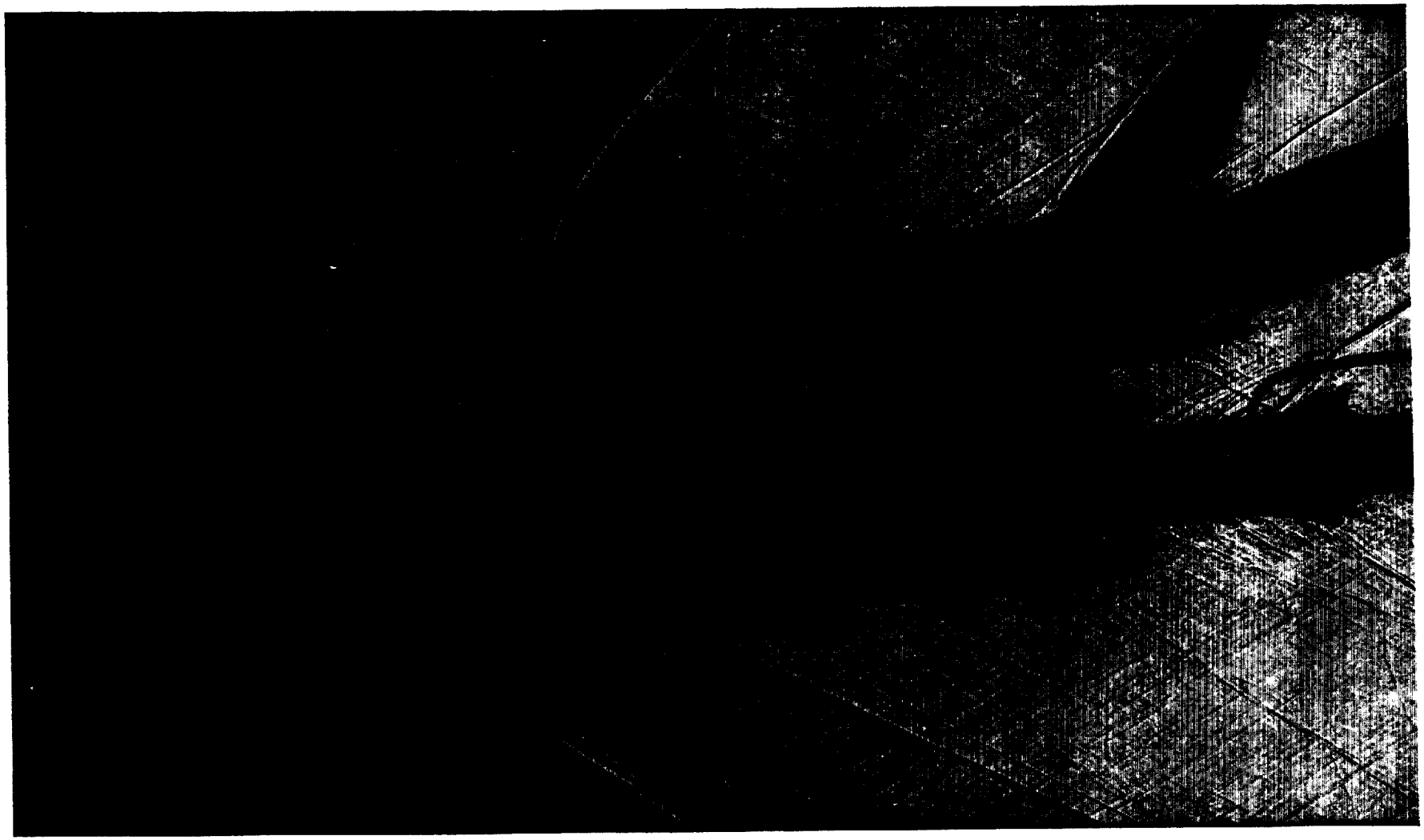

Figure 36. SSLV Mach 1.96, alpha = –4, beta = 0, roll = 0.

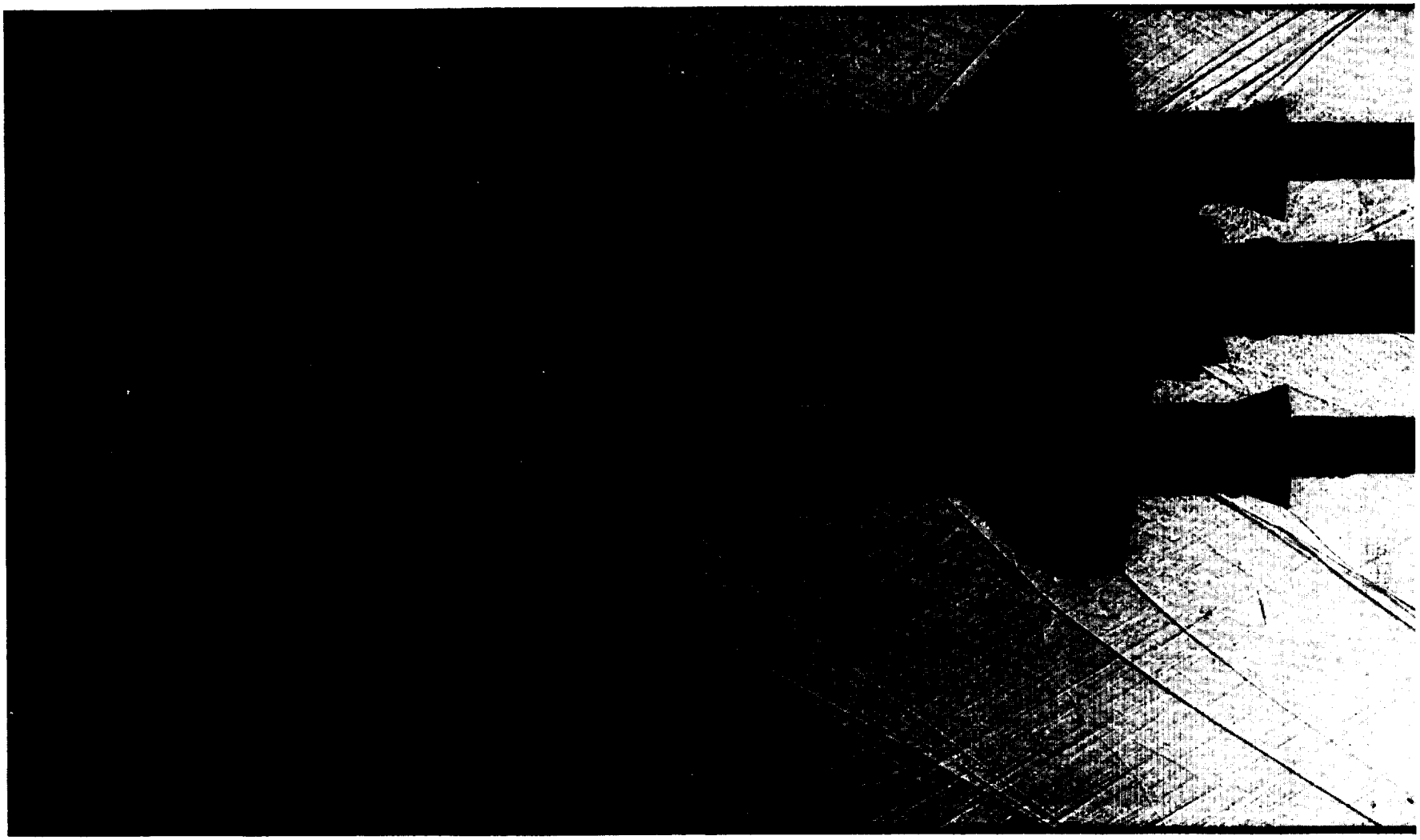

Figure 37. SSLV Mach 1.96, alpha = 0, beta = 0, roll = 90.

Figure 38. SSLV Mach 2.74, alpha = 0, beta = 0, roll = 0.

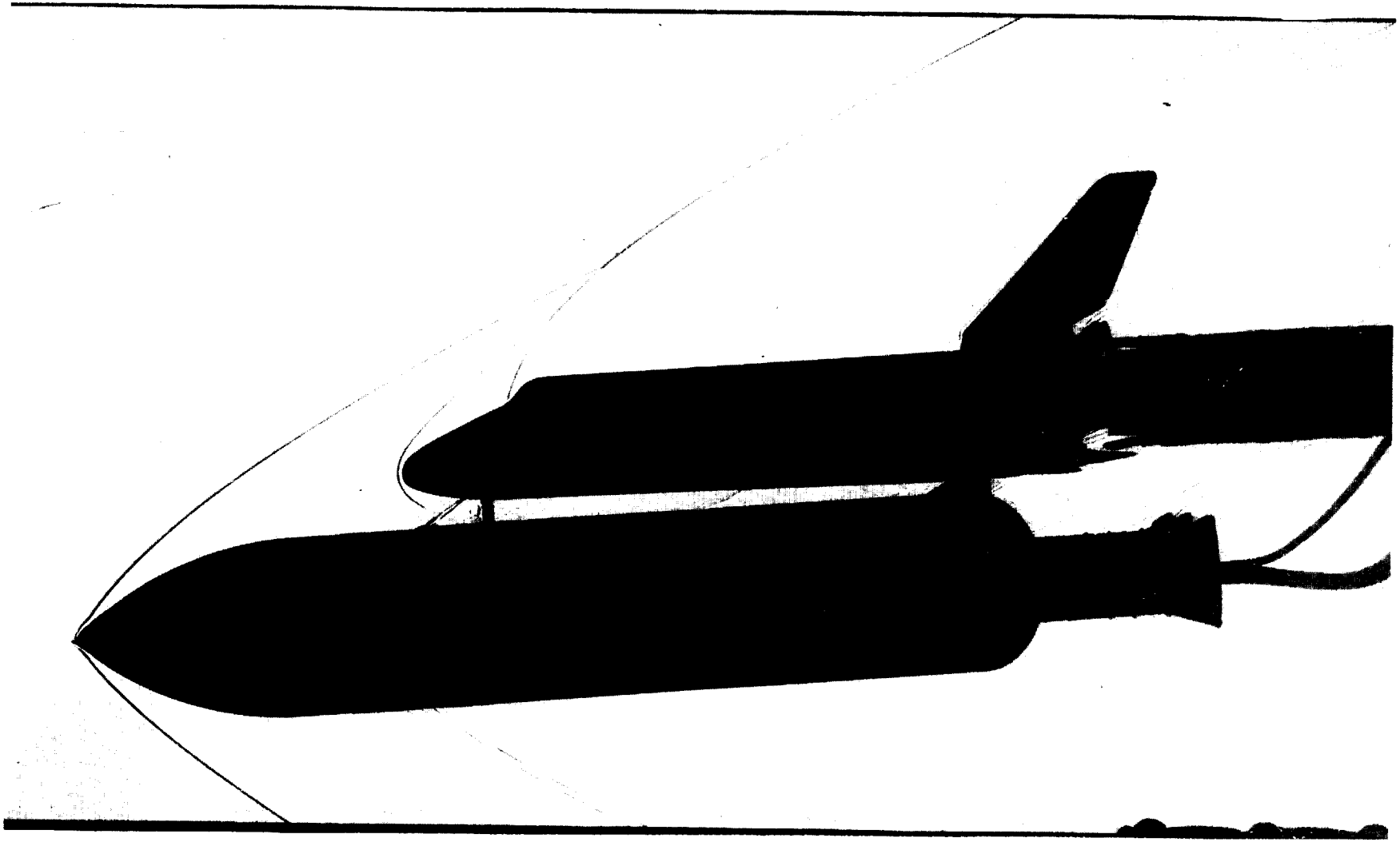

Figure 39. SSLV Mach 2.74, alpha = –4, beta = 0, roll = 0.

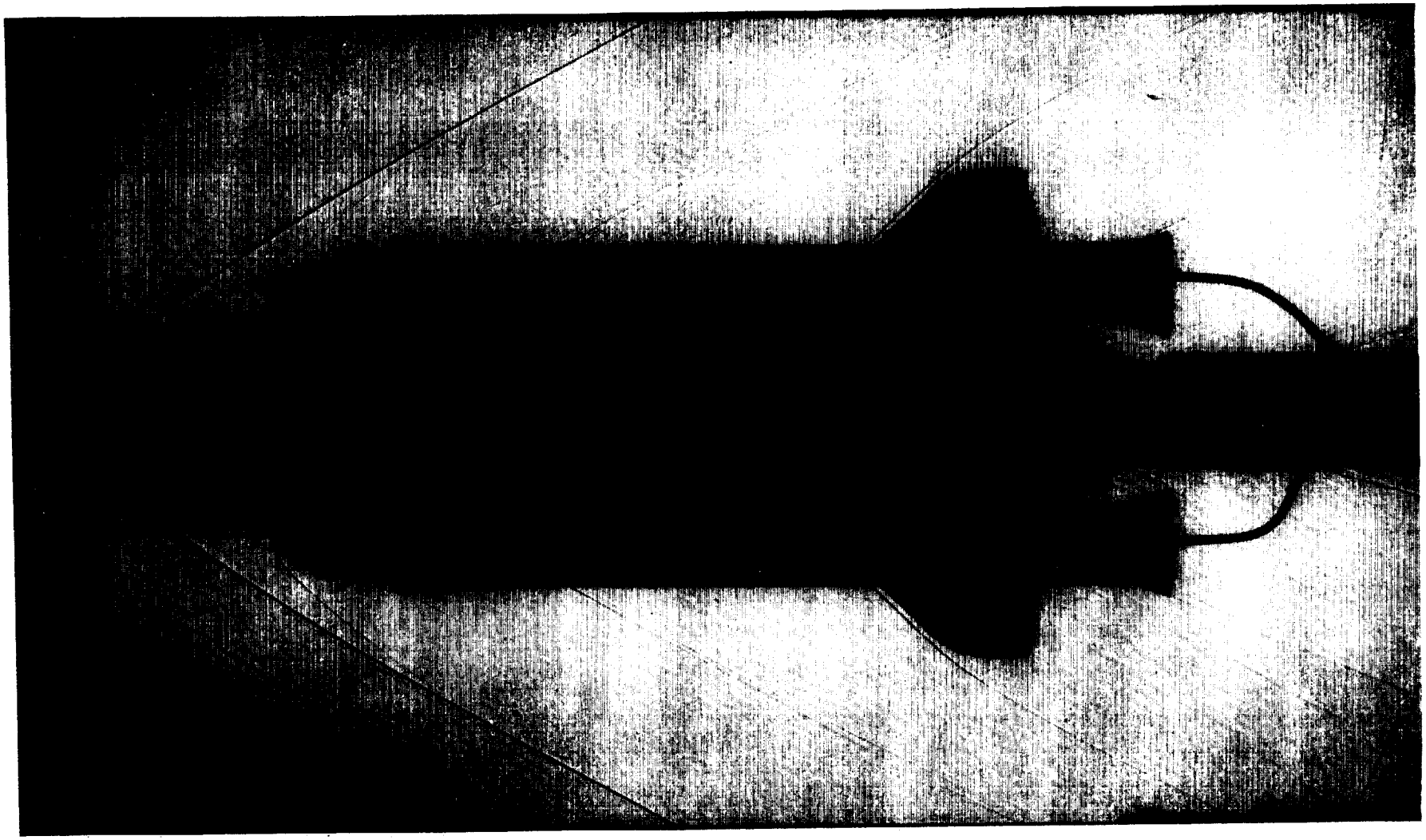

Figure 40. SSLV Mach 2.74, alpha = 0, beta = 0, roll = 90.

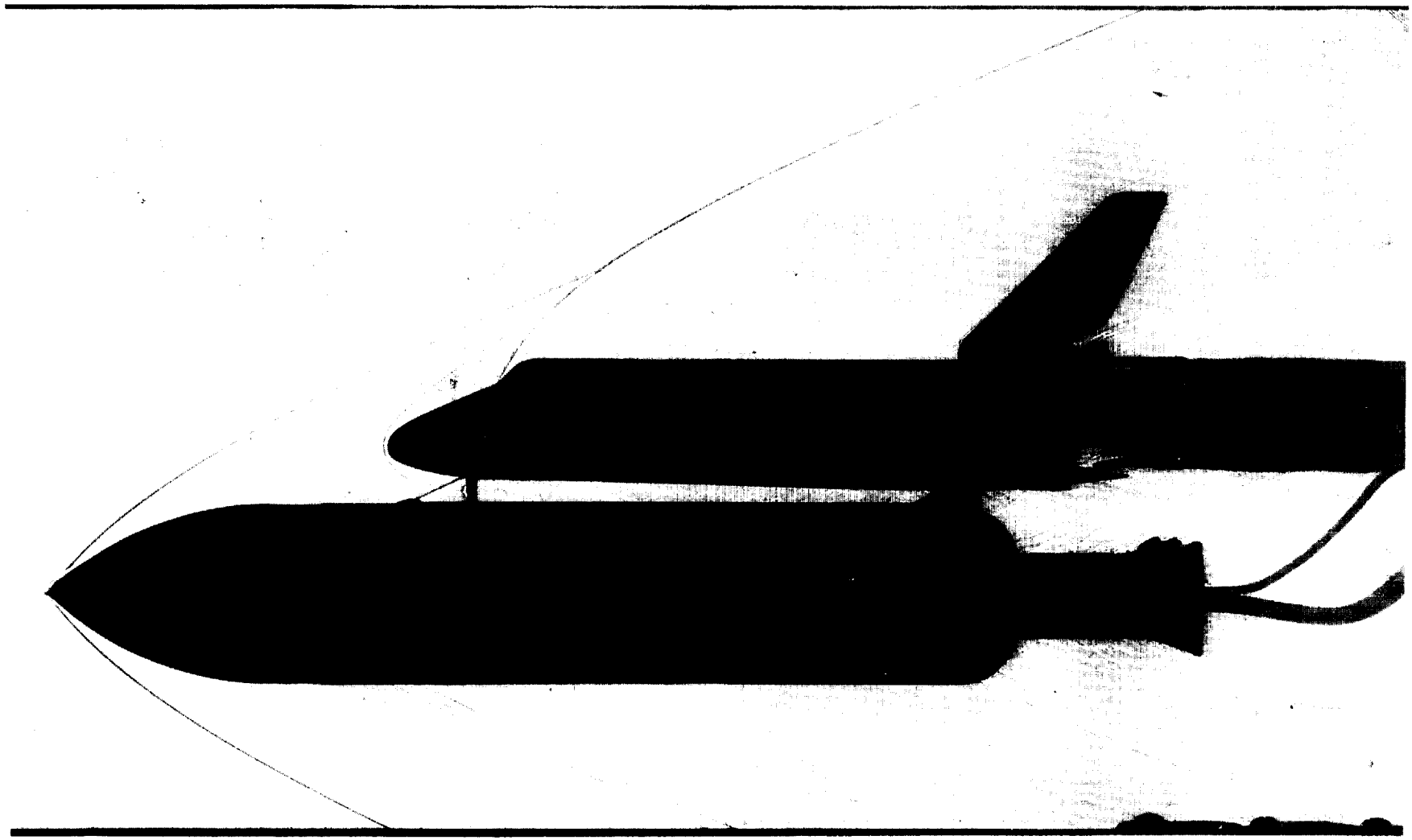

Figure 41. SSLV Mach 3.48, alpha = 0, beta = 0, roll = 0.

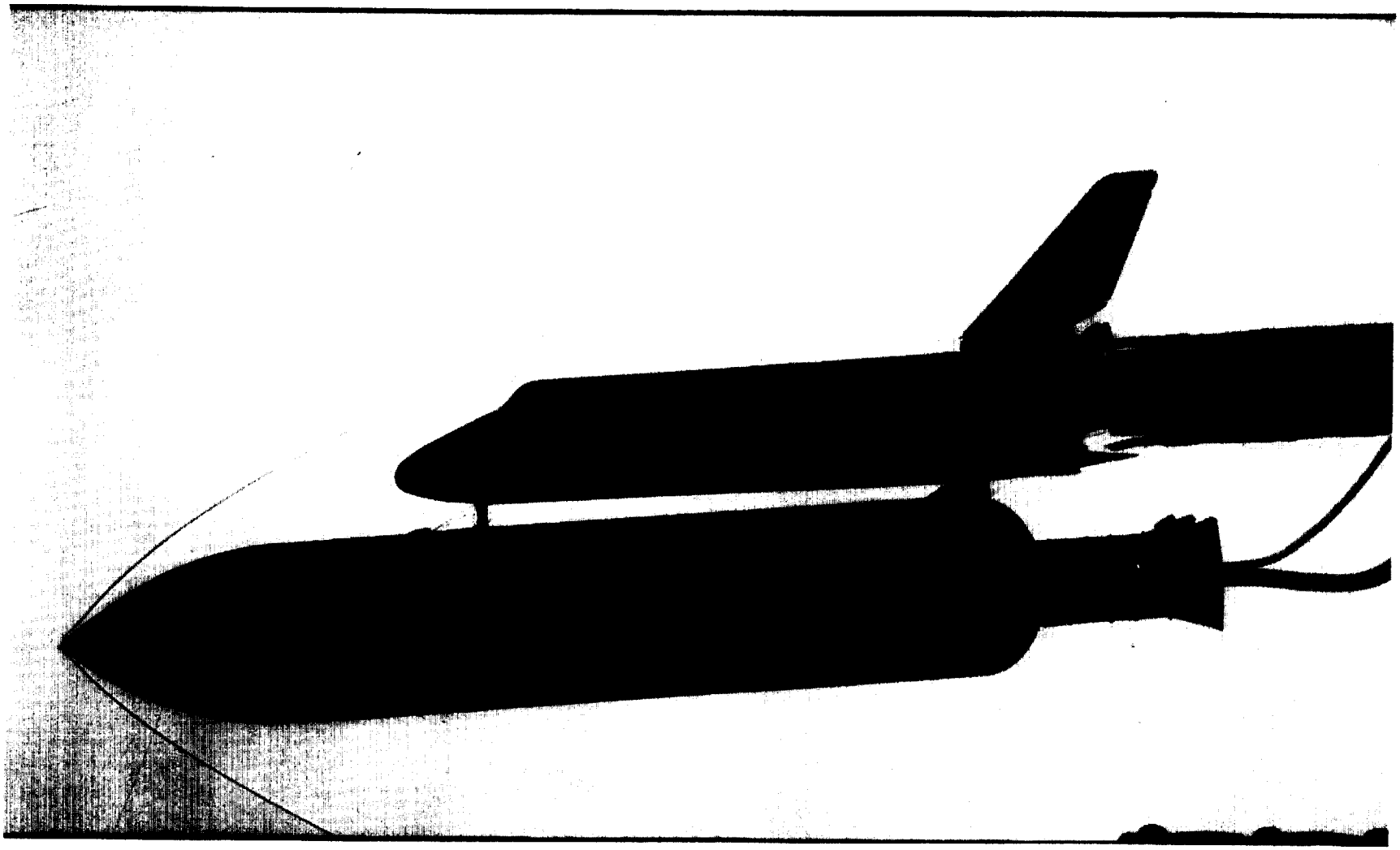

Figure 42. SSLV Mach 3.48, alpha = –4, beta = 0, roll = 0.

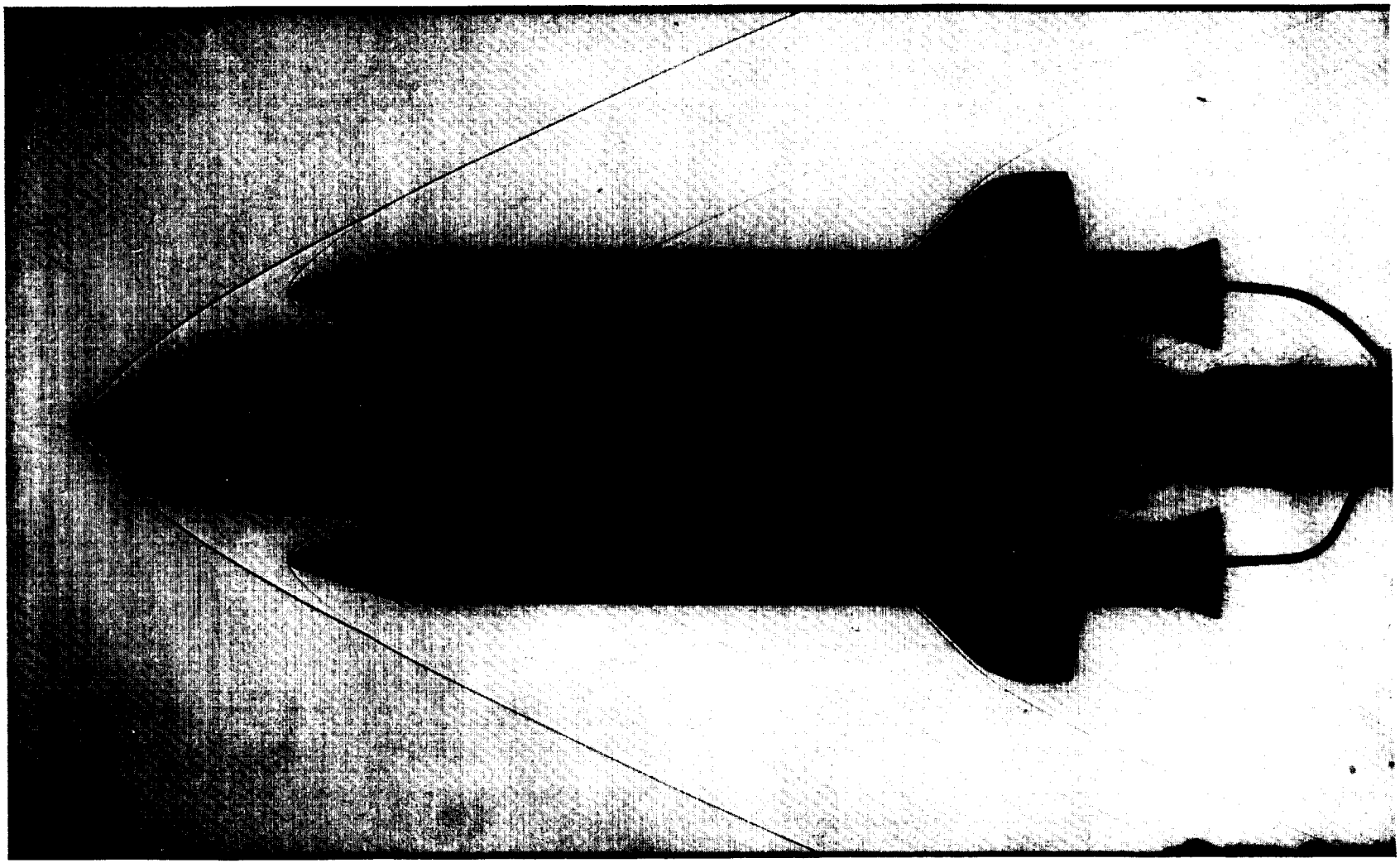

Figure 43. SSLV Mach 3.48, alpha = 0, beta = 0, roll = 90.

Figure 44. SSLV Mach 4.96, alpha = 0, beta = 0, roll = 0.

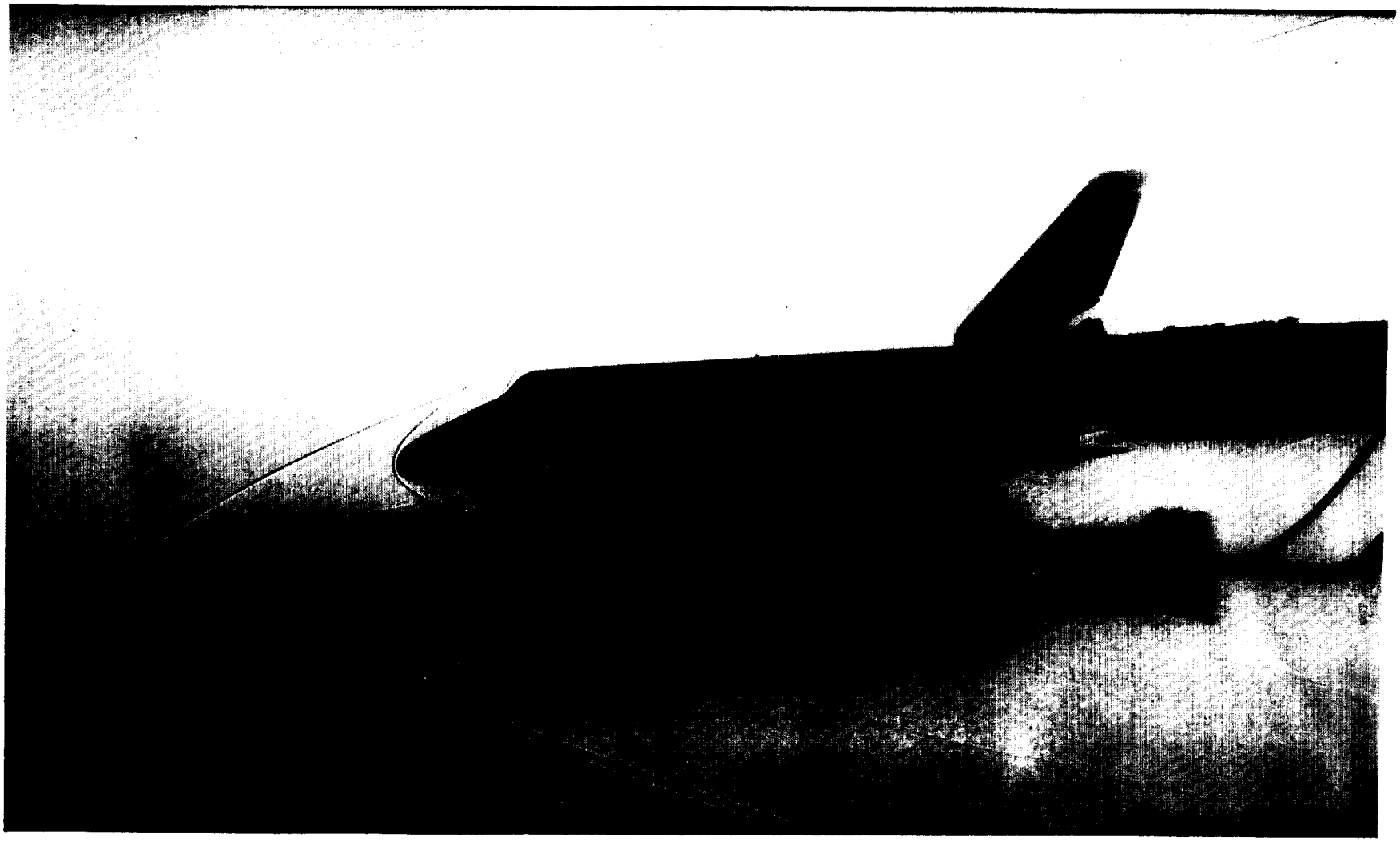

Figure 45. SSLV Mach 4.96, alpha = –4, beta = 0, roll = 0.

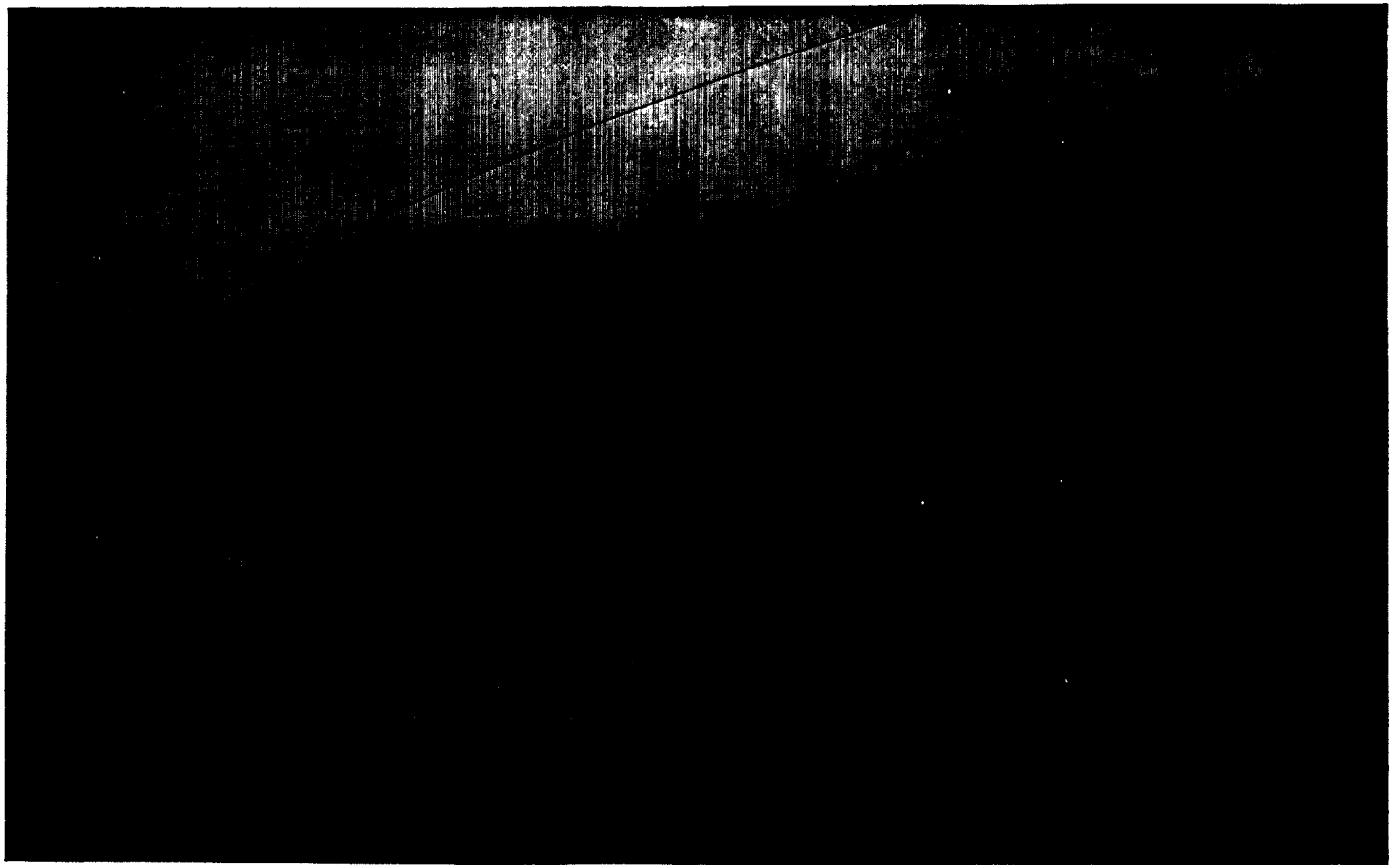

Figure 46. SSLV Mach 4.96, alpha = 0, beta = 0, roll = 90.

APPENDIX A

ORBITER

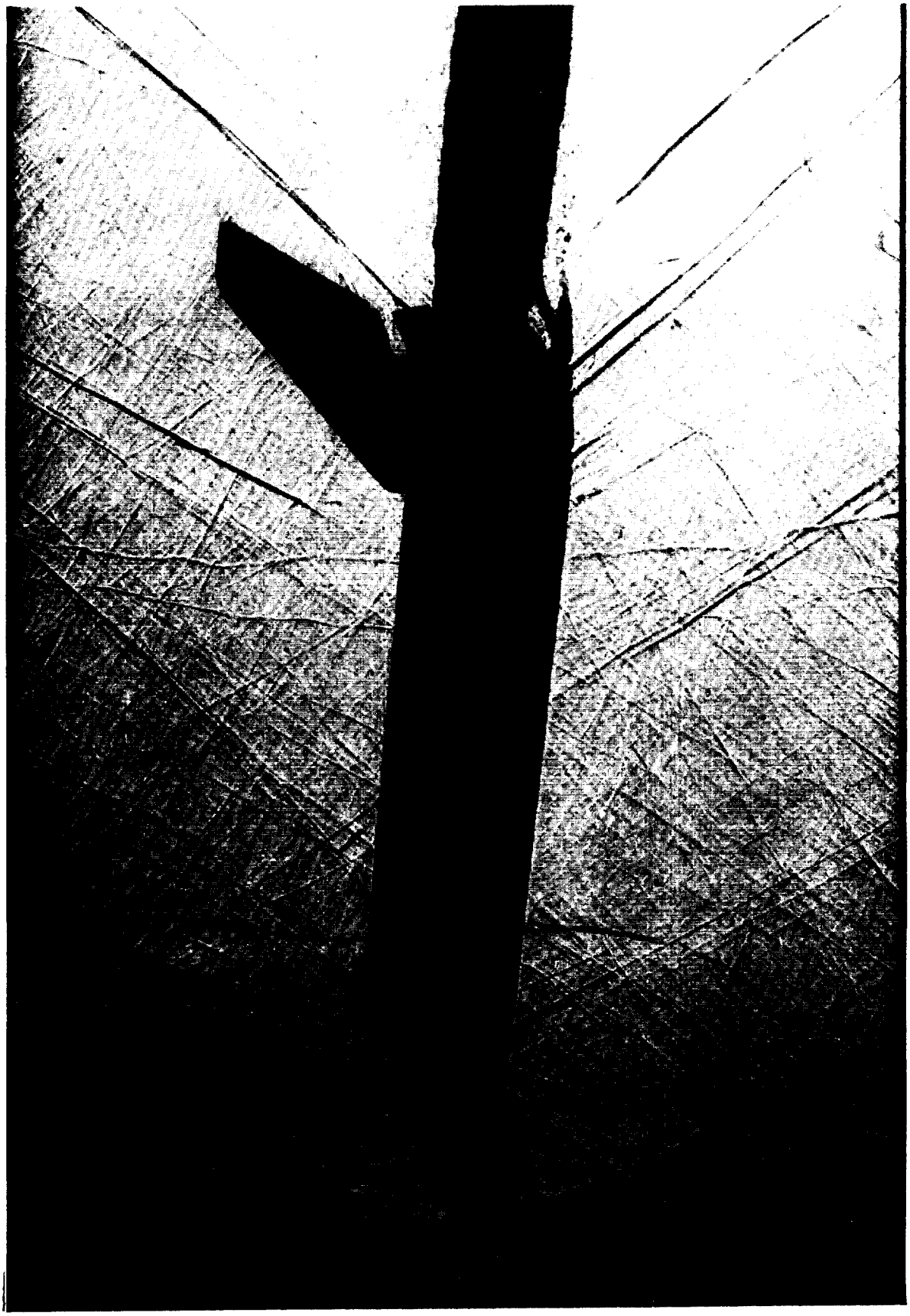

Figure A-1. SSLV ORB Mach 1.25, alpha = 2, beta = 0, roll = 0.

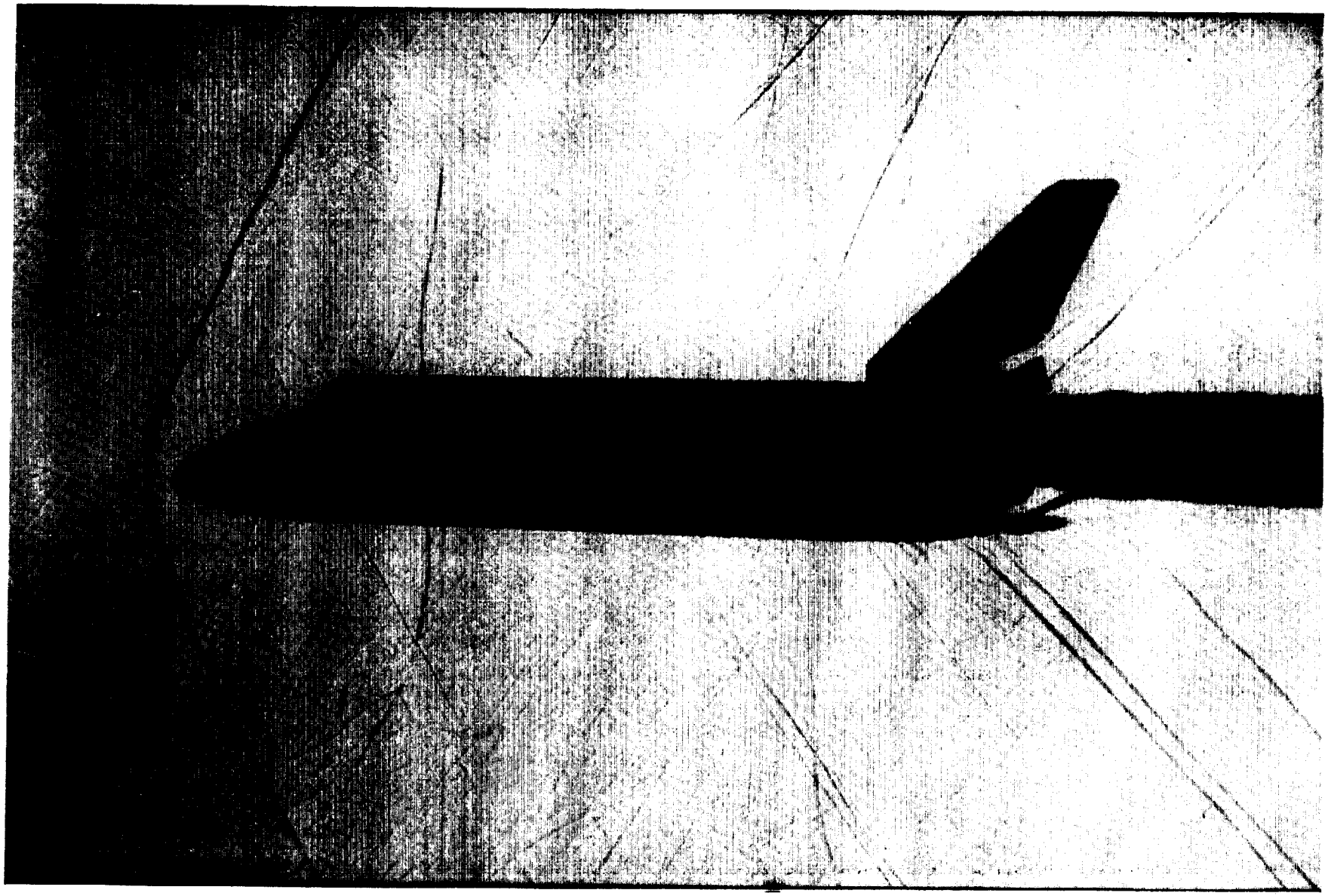

Figure A-2. SSLV ORB Mach 1.25, alpha = 0, beta = 0, roll = 0.

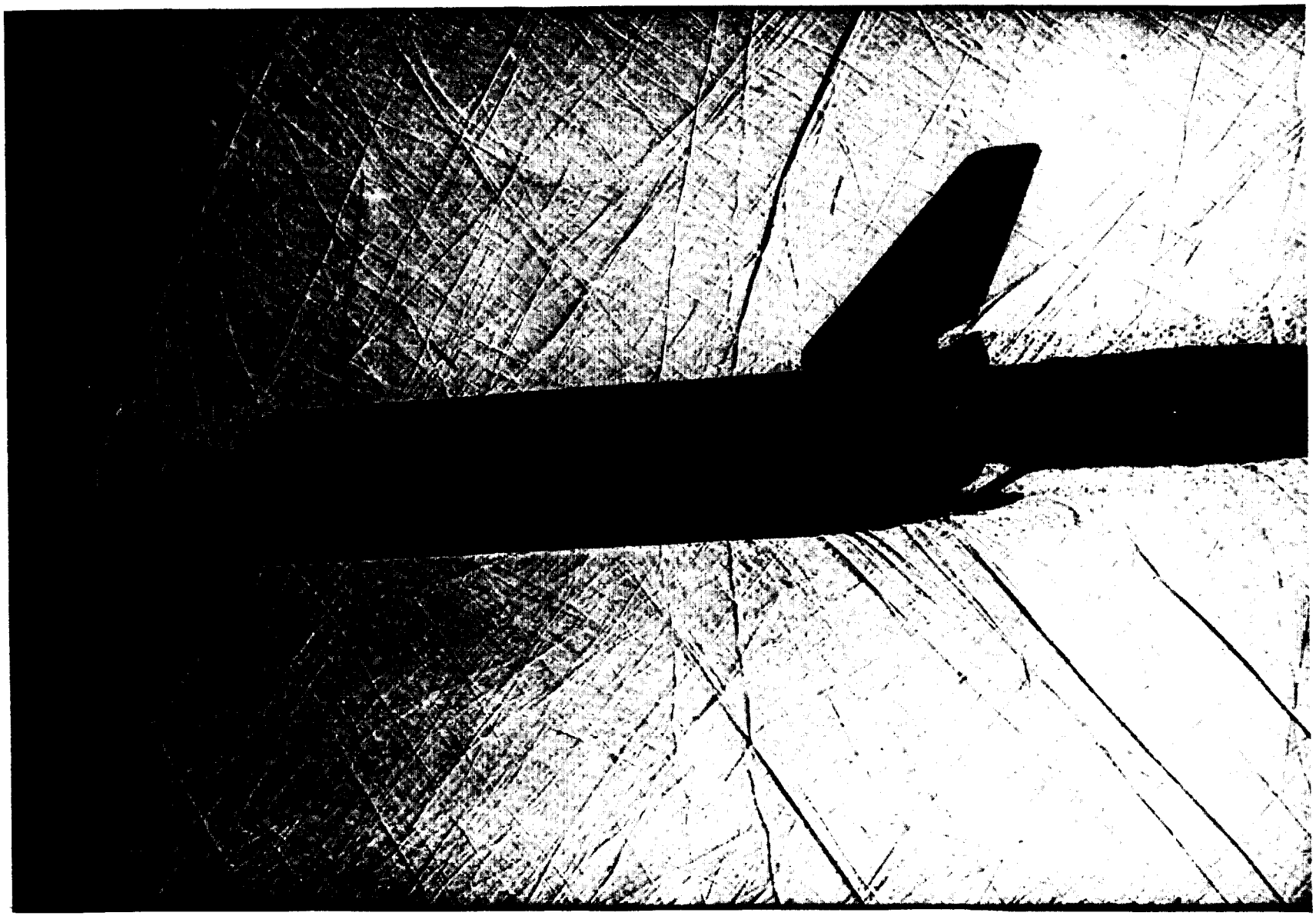

Figure A-3. SSLV ORB Mach 1.25, alpha = –2, beta = 0, roll = 0.

Figure A-4. SSLV ORB Mach 1.46, alpha = 2, beta = 0, roll = 0.

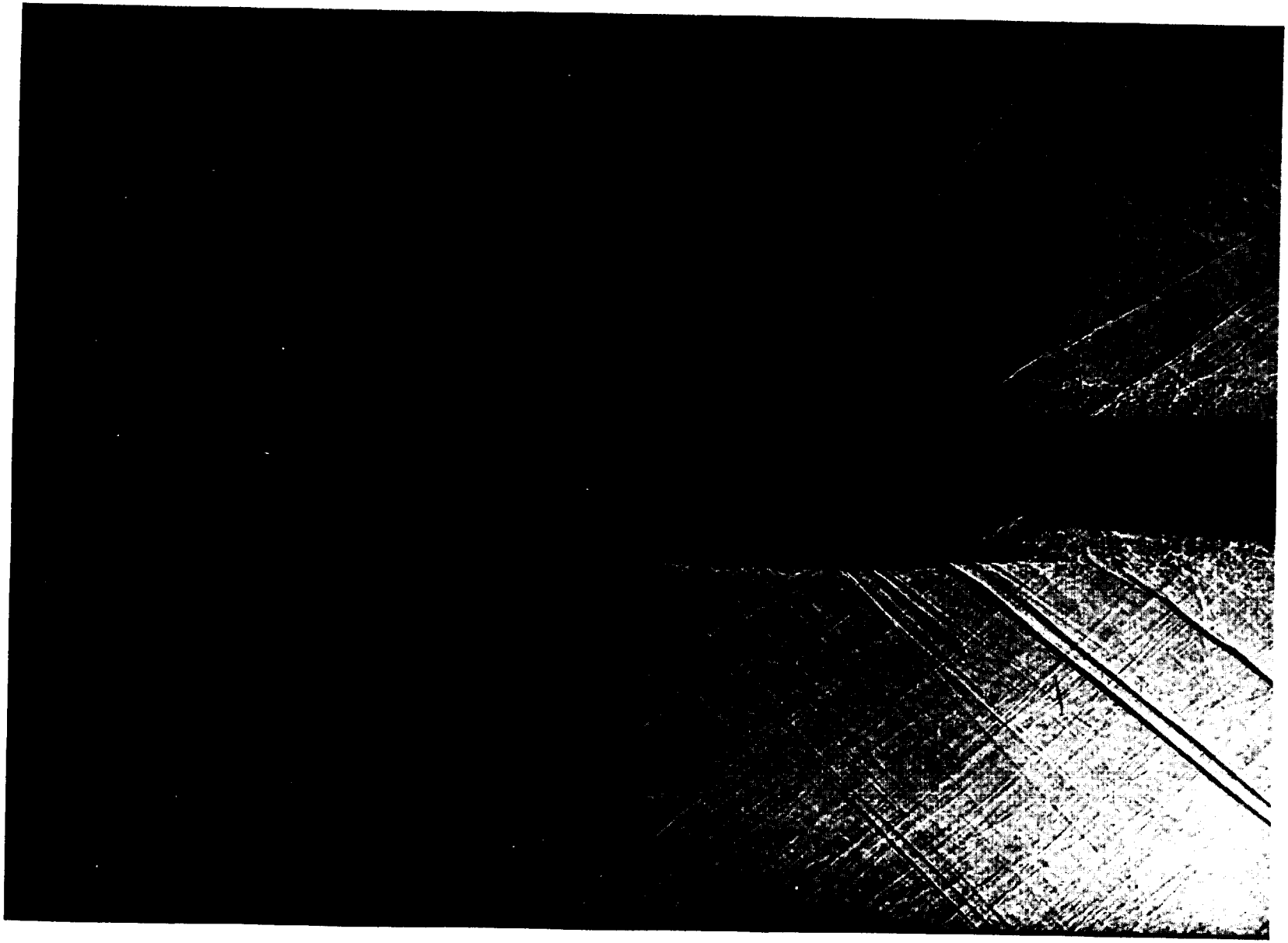

Figure A-5. SSLV ORB Mach 1.46, alpha = 0, beta = 0, roll = 0.

Figure A-6. SSLV ORB Mach 1.46, alpha = –2, beta = 0, roll = 0.

Figure A-7. SSLV ORB Mach 1.96, alpha = 2, beta = 0, roll = 0.

Figure A-8. SSLV ORB Mach 1.96, alpha = 0, beta = 0, roll = 0.

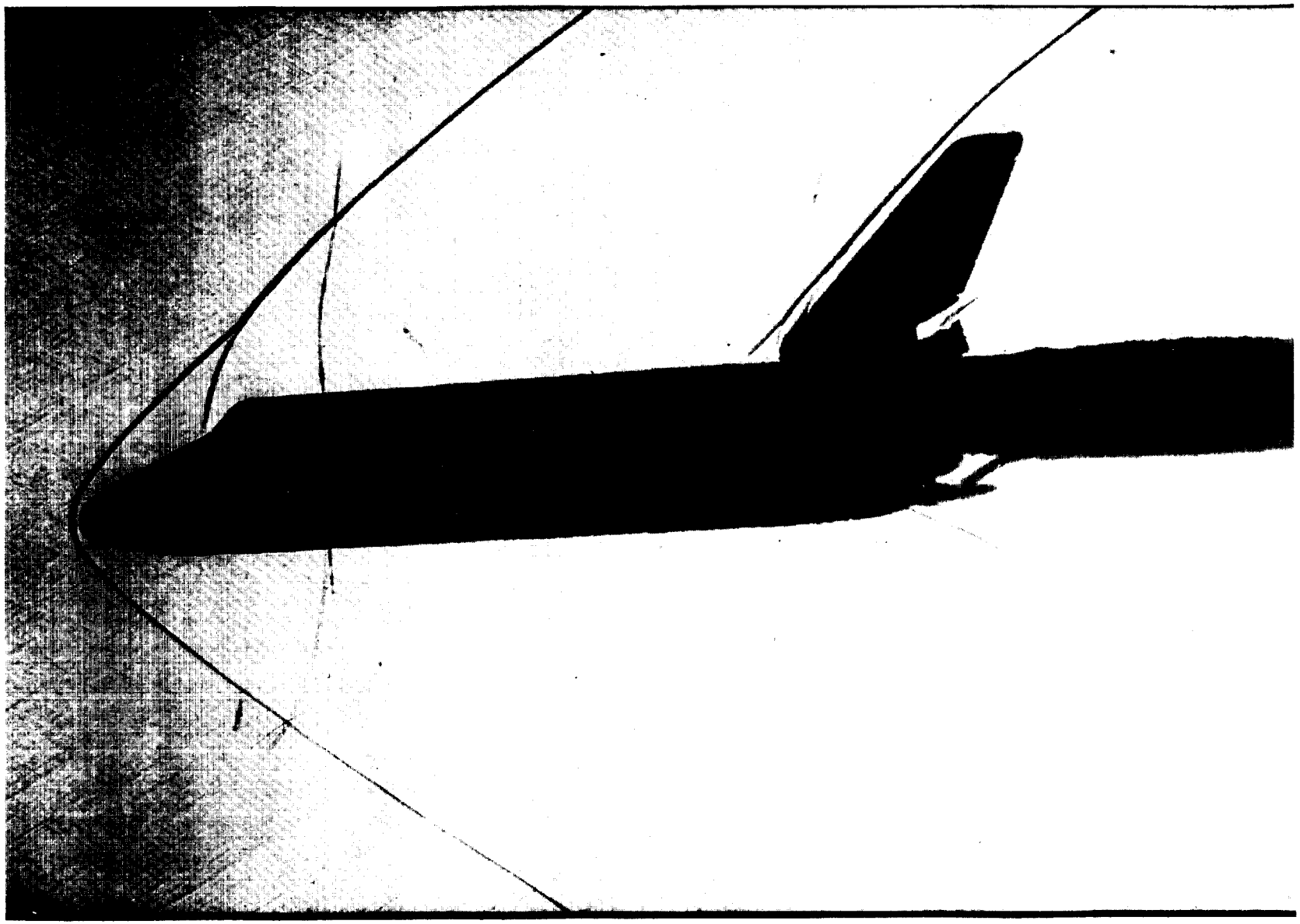

Figure A-9. SSLV ORB Mach 1.96, alpha = –2, beta = 0, roll = 0.

APPENDIX B

SSLV LOWER STACK

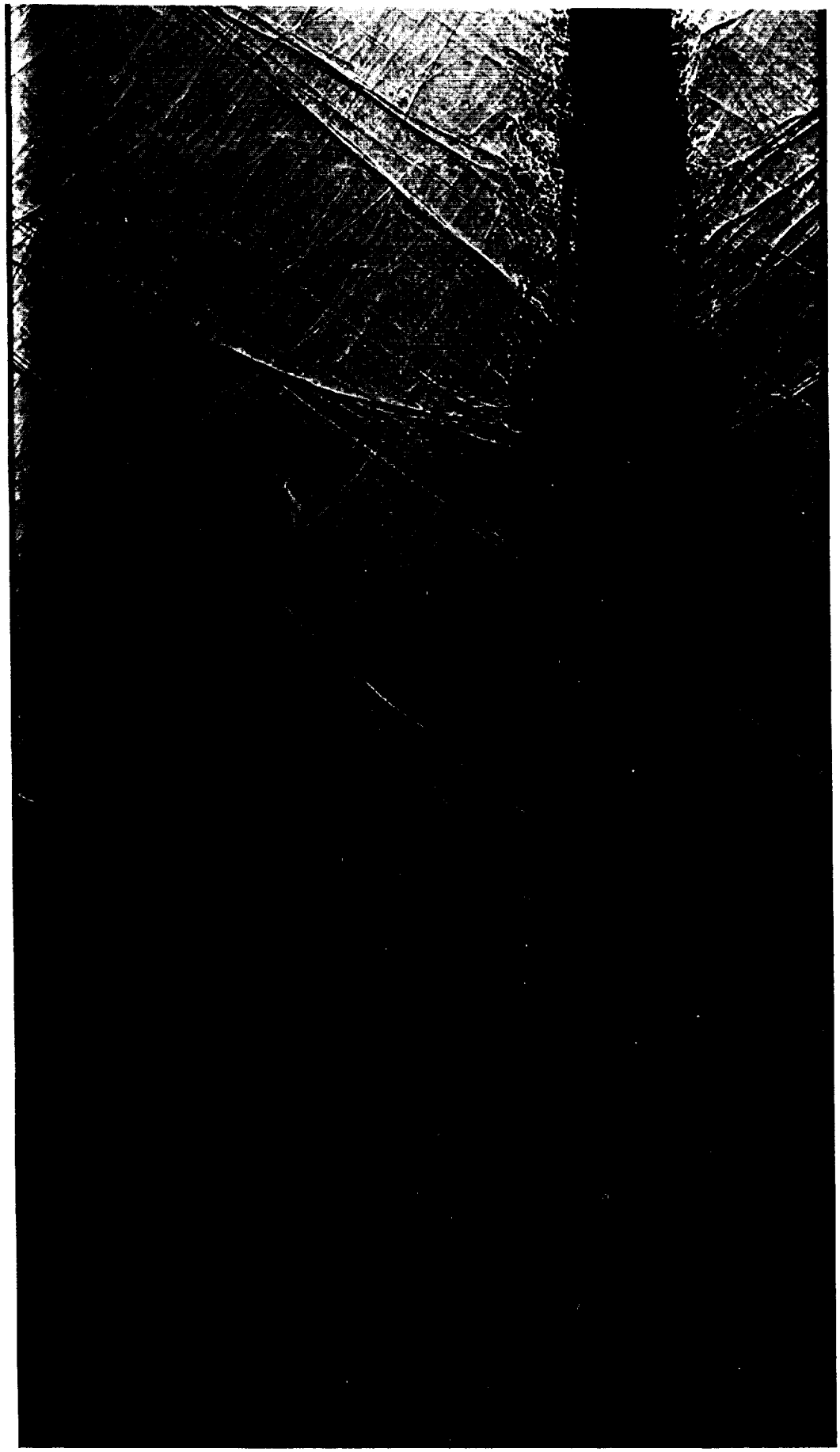

Figure B-1. SSLV lower stack Mach 1.25, alpha = 0, beta = 0, roll = 0.

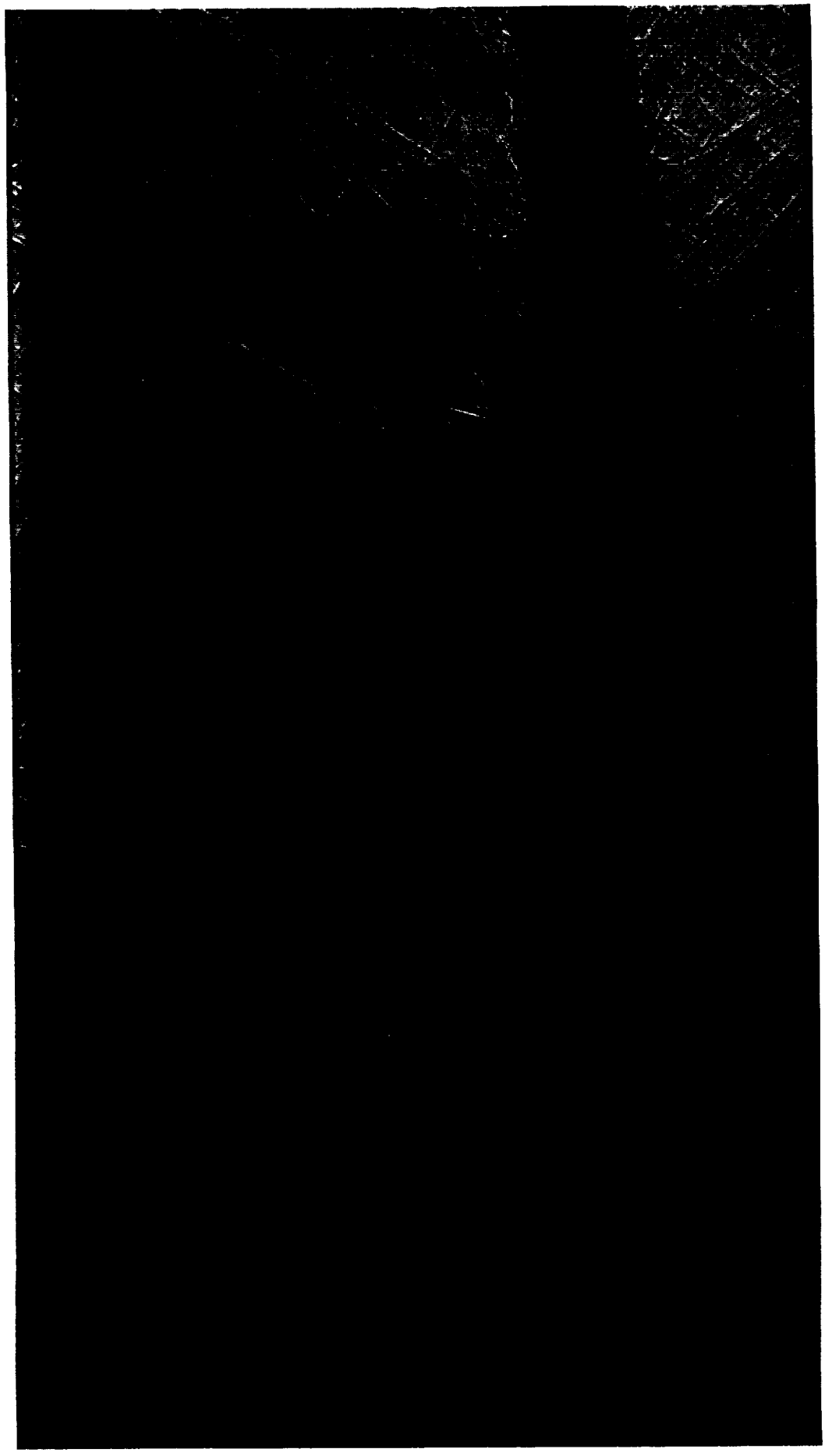

Figure B-2. SSLV lower stack Mach 1.25, alpha = –2, beta = 0, roll = 0.

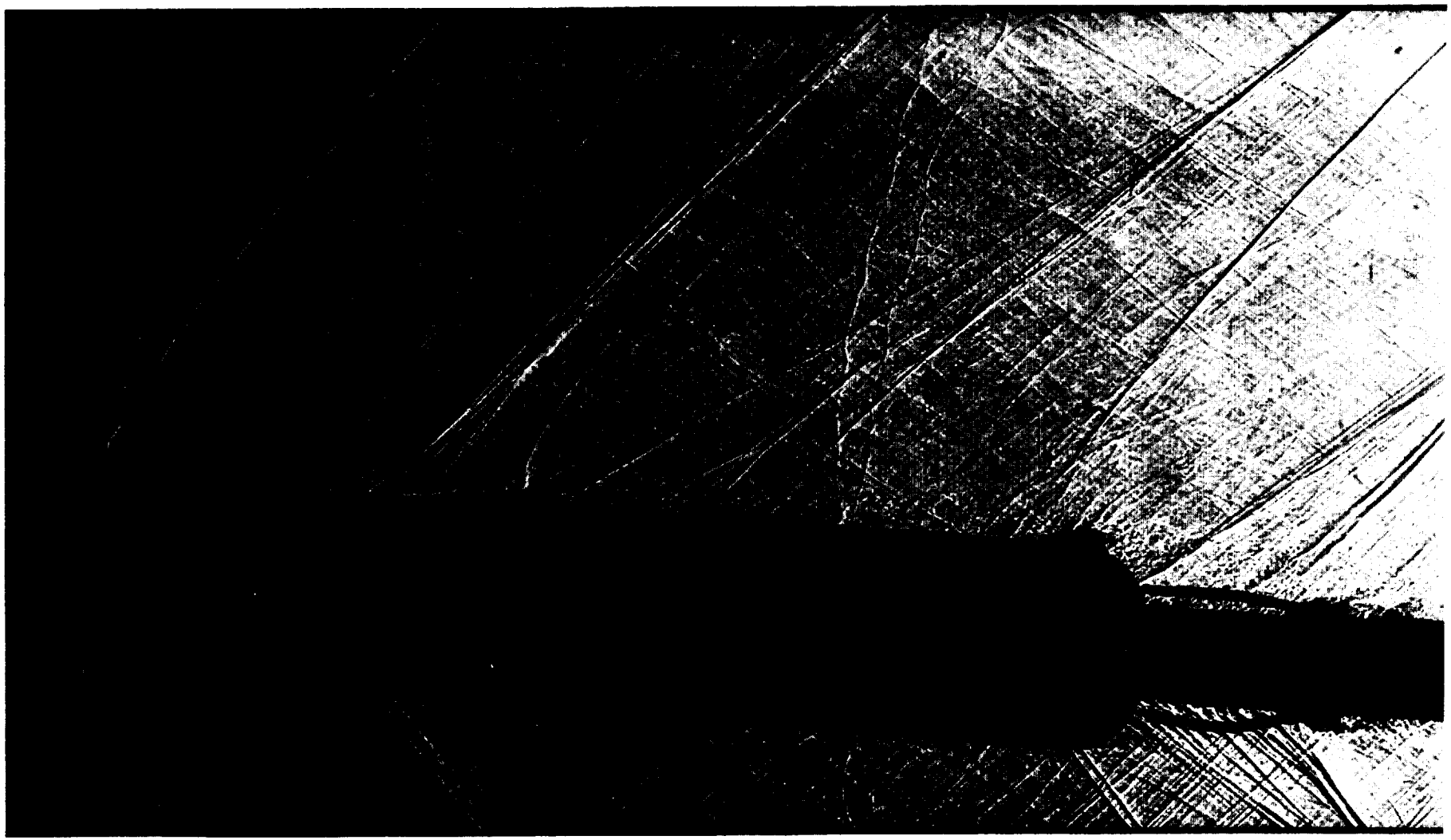

Figure B-3. SSLV lower stack Mach 1.46, alpha = 2, beta = 0, roll = 0.

Figure B-4. SSLV lower stack Mach 1.46, alpha = 0, beta = 0, roll = 0.

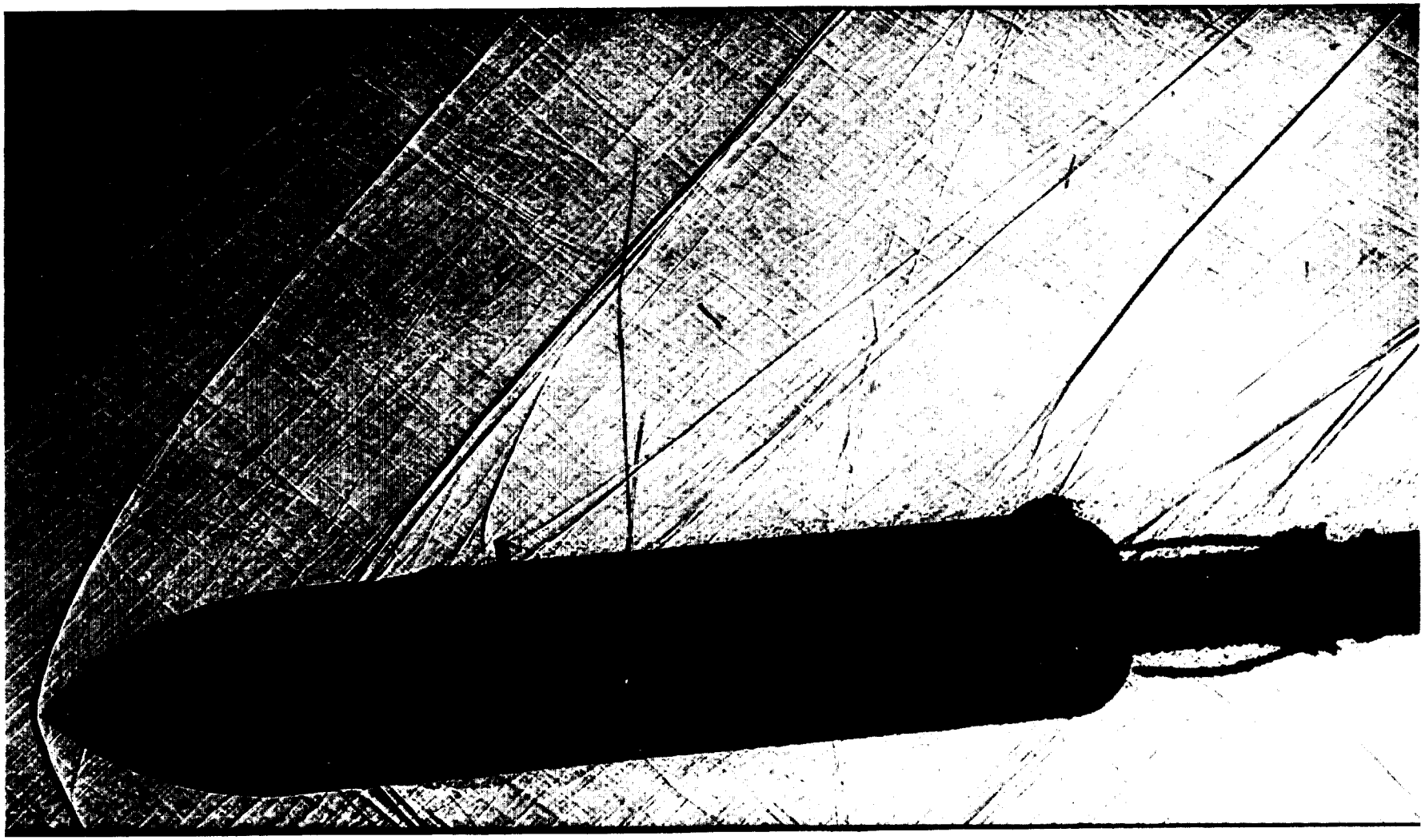

Figure B-5. SSLV lower stack Mach 1.46, alpha = –2, beta = 0, roll = 0.

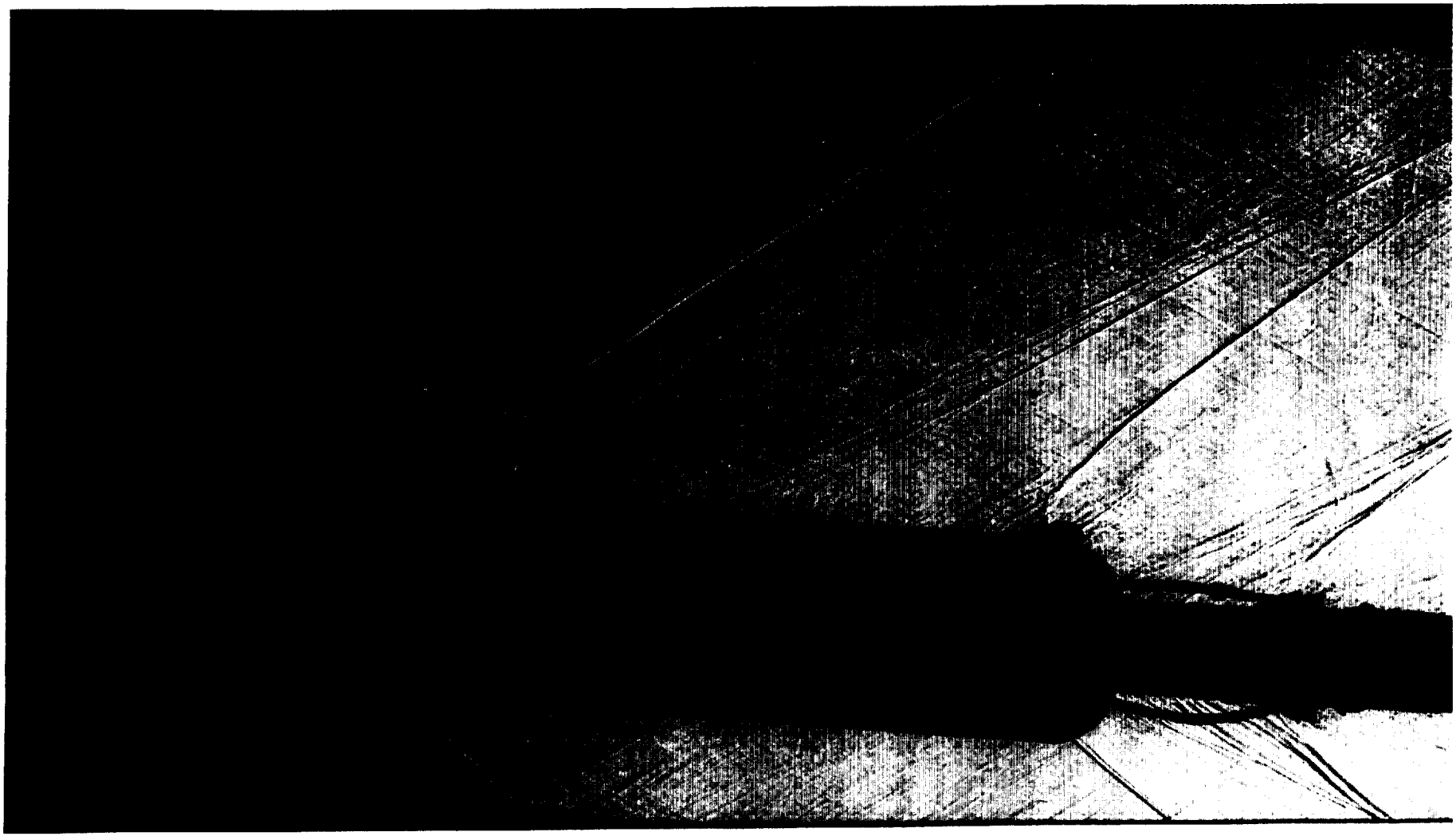

Figure B-6. SSLV lower stack Mach 1.96, alpha = 2, beta = 0, roll = 0.

Figure B-7. SSLV lower stack Mach 1.96, alpha = 0, beta = 0, roll = 0.

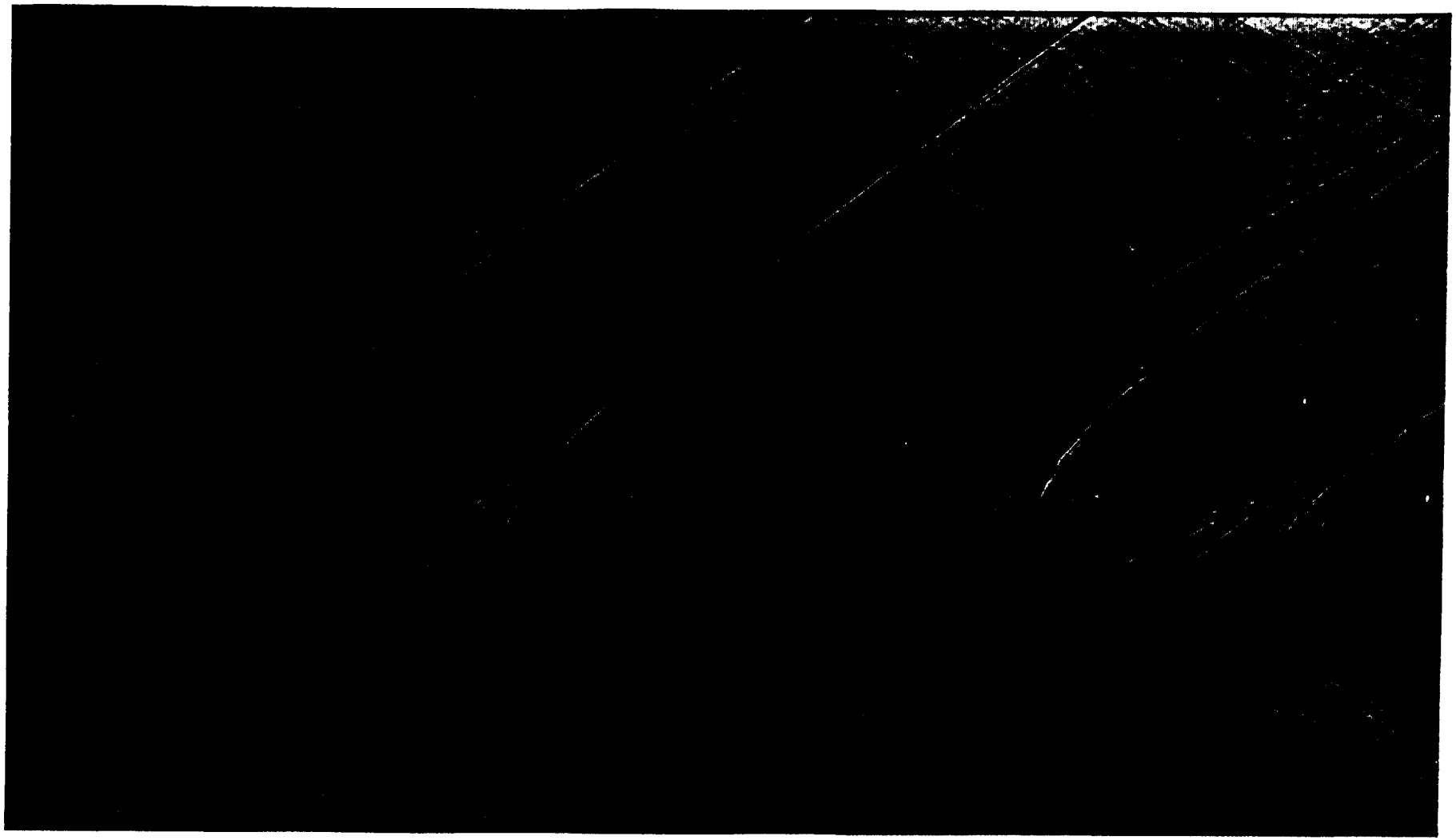

Figure B-8. SSLV lower stack Mach 1.96, alpha = –2, beta = 0, roll = 0.

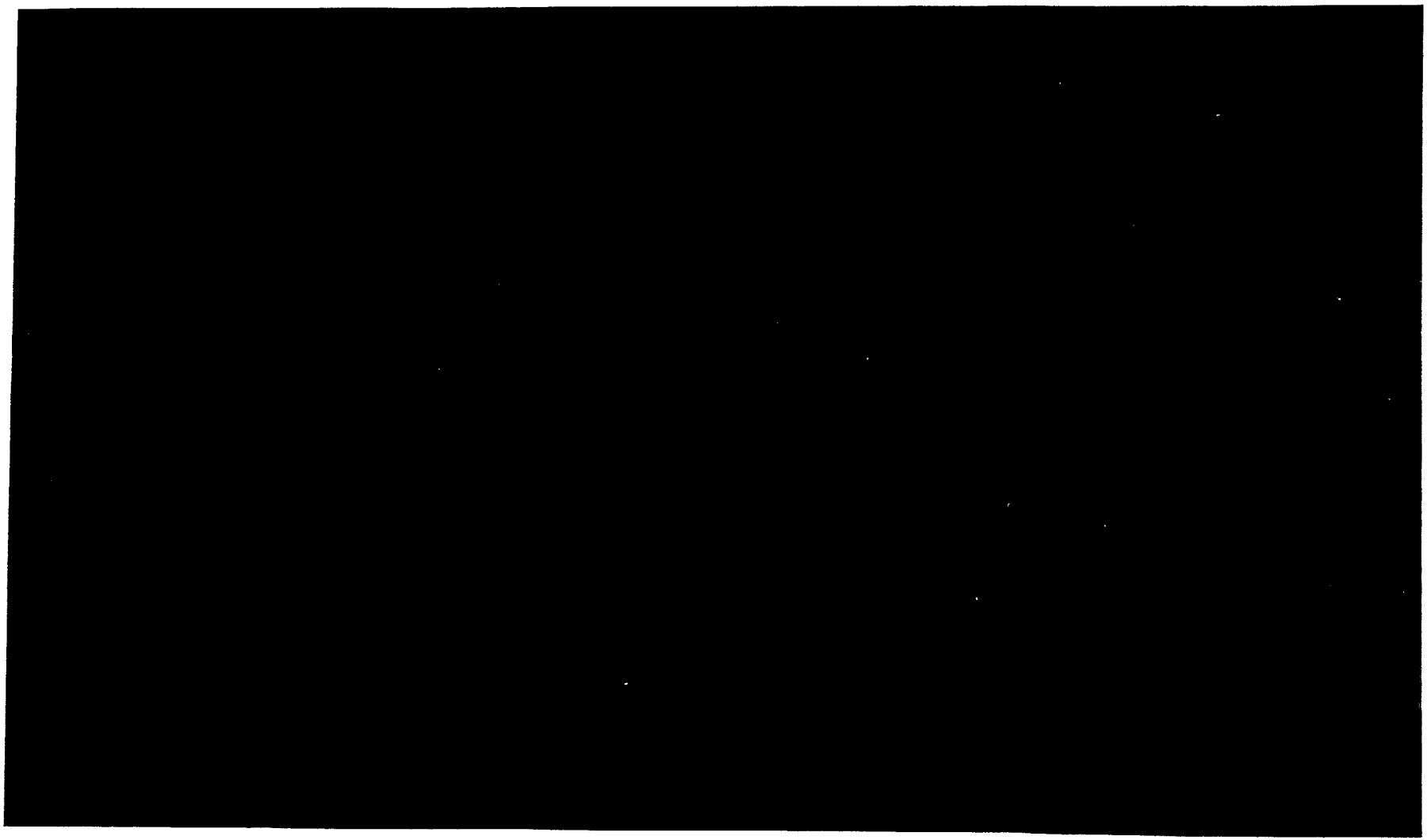

Figure B-9. SSLV lower stack Mach 2.74, alpha = 2, beta = 0, roll = 0.

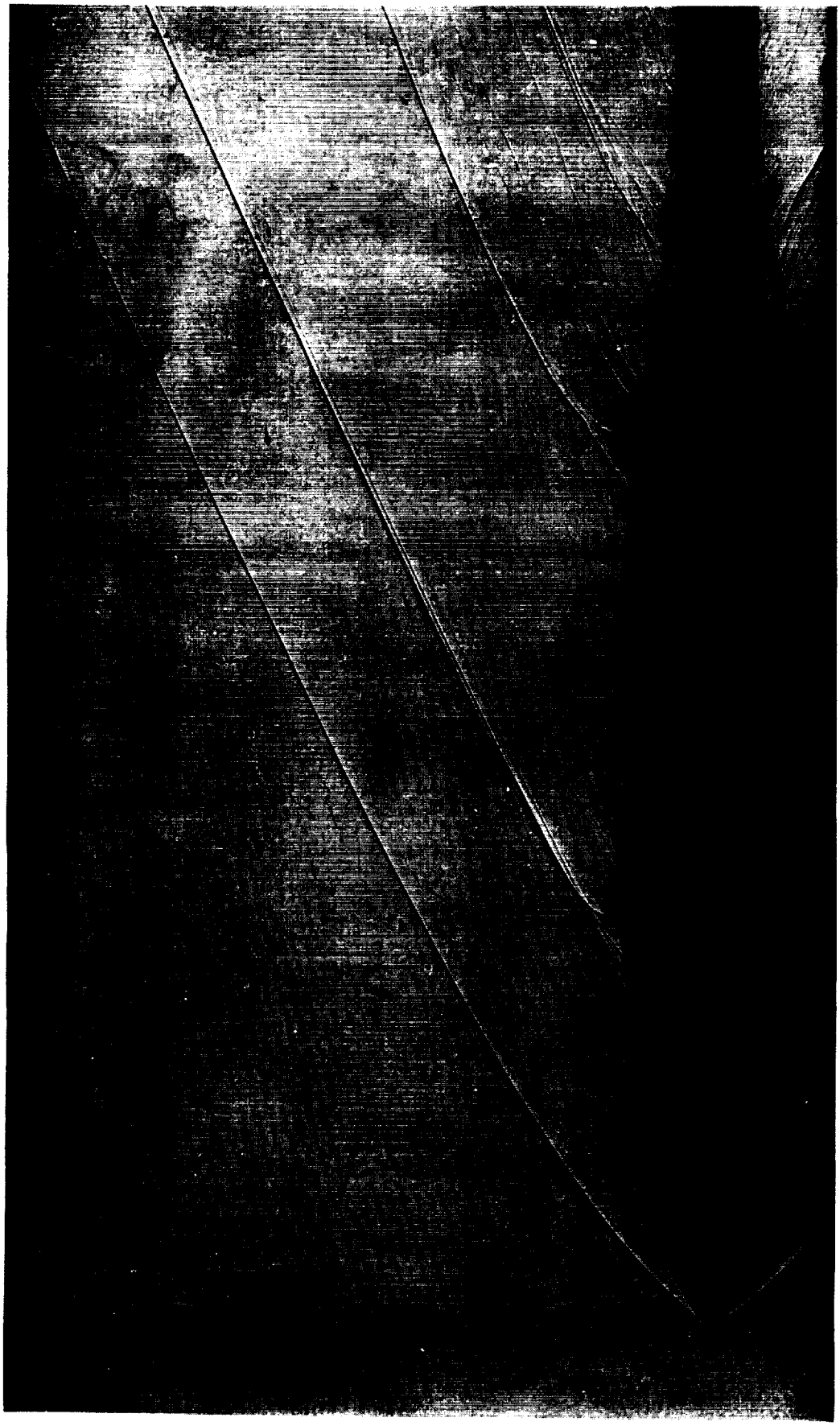

Figure B-10. SSLV lower stack Mach 2.74, alpha = 0, beta = 0, roll = 0.

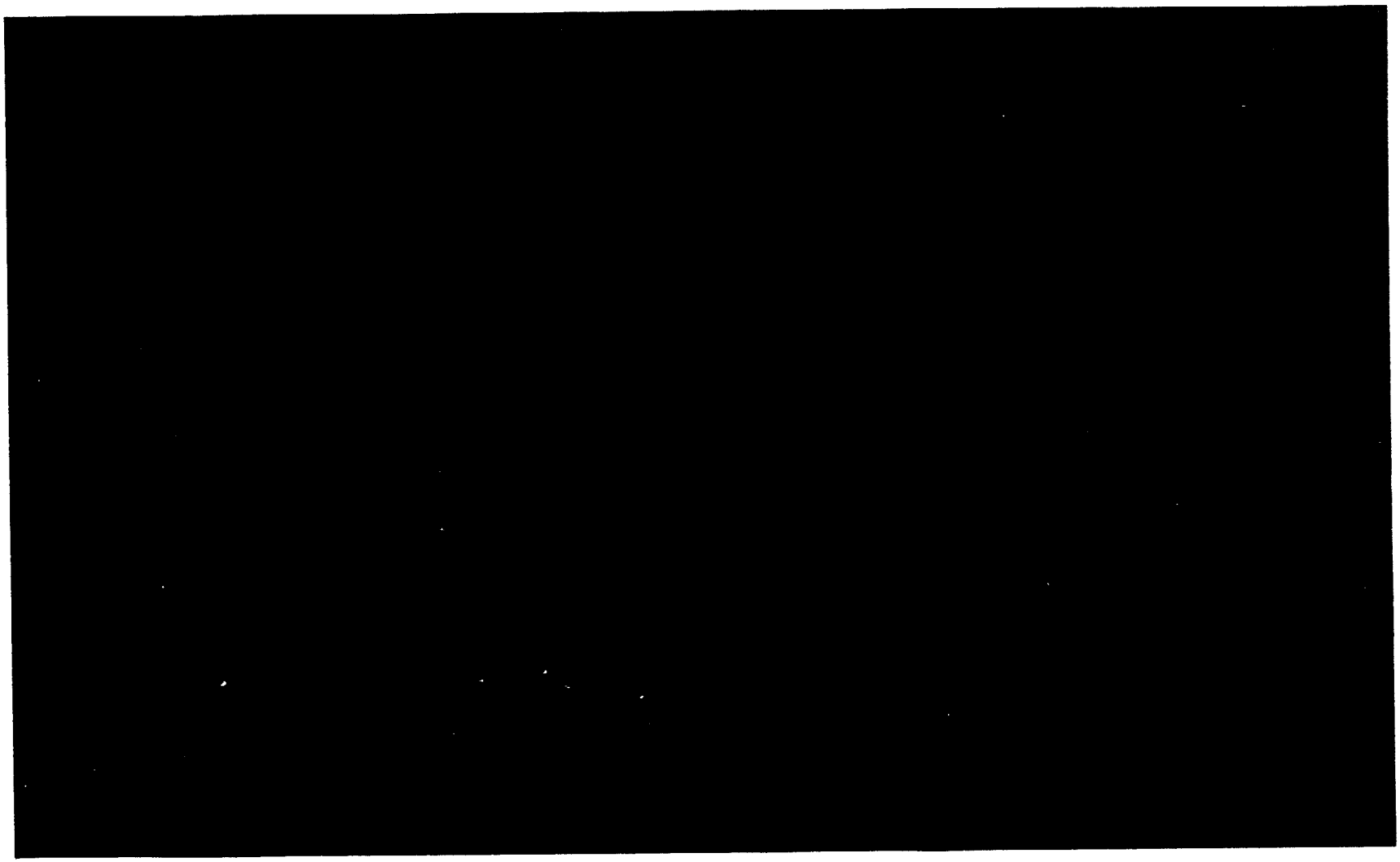

Figure B-11. SSLV lower stack Mach 3.48, alpha = 2, beta = 0, roll = 0.

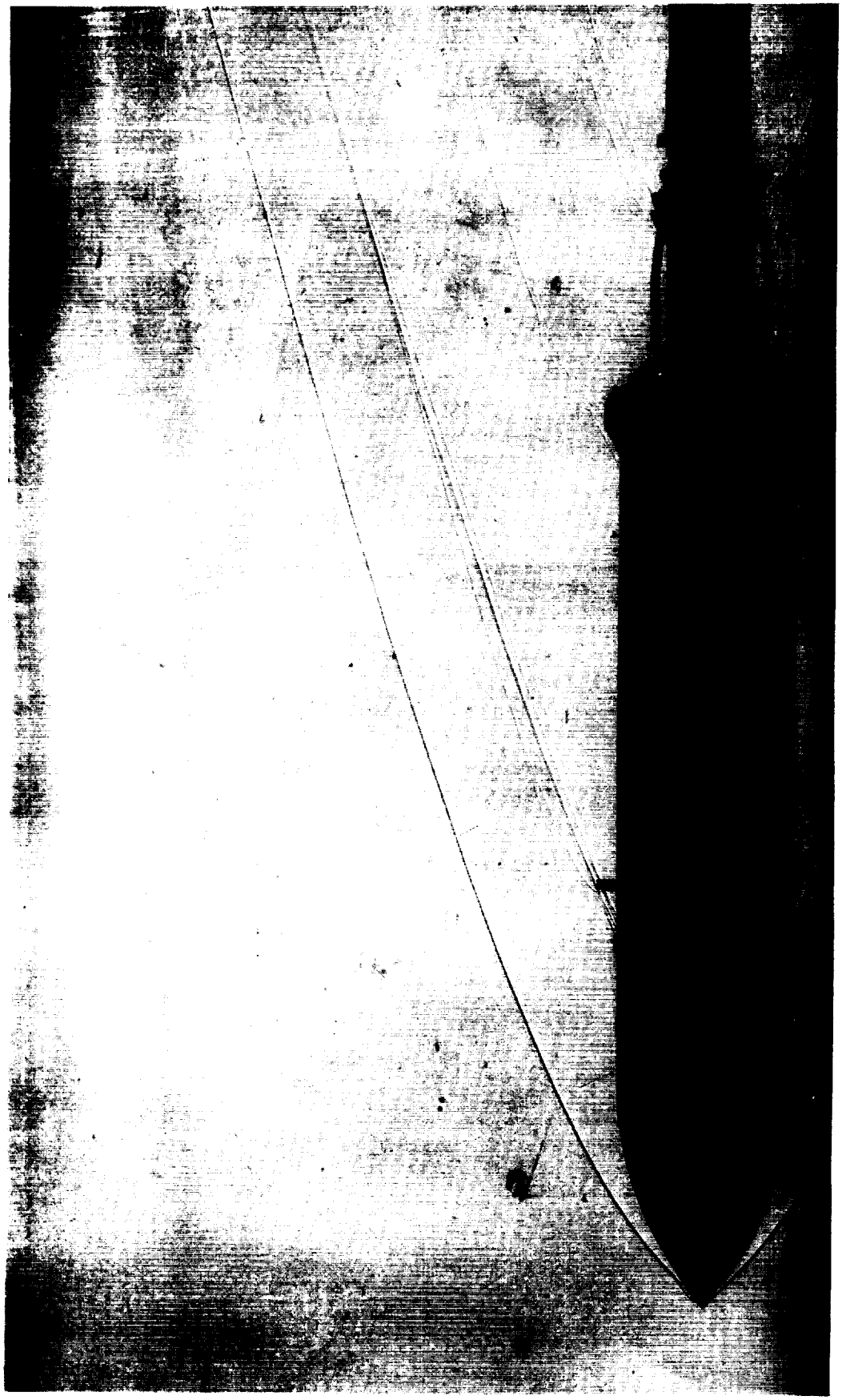

Figure B-12. SSLV lower stack Mach 3.48, alpha = 0, beta = 0, roll = 0.

APPENDIX C

ET NOSE STUDY

Figure C-1. Noses tested during the ET nose study.

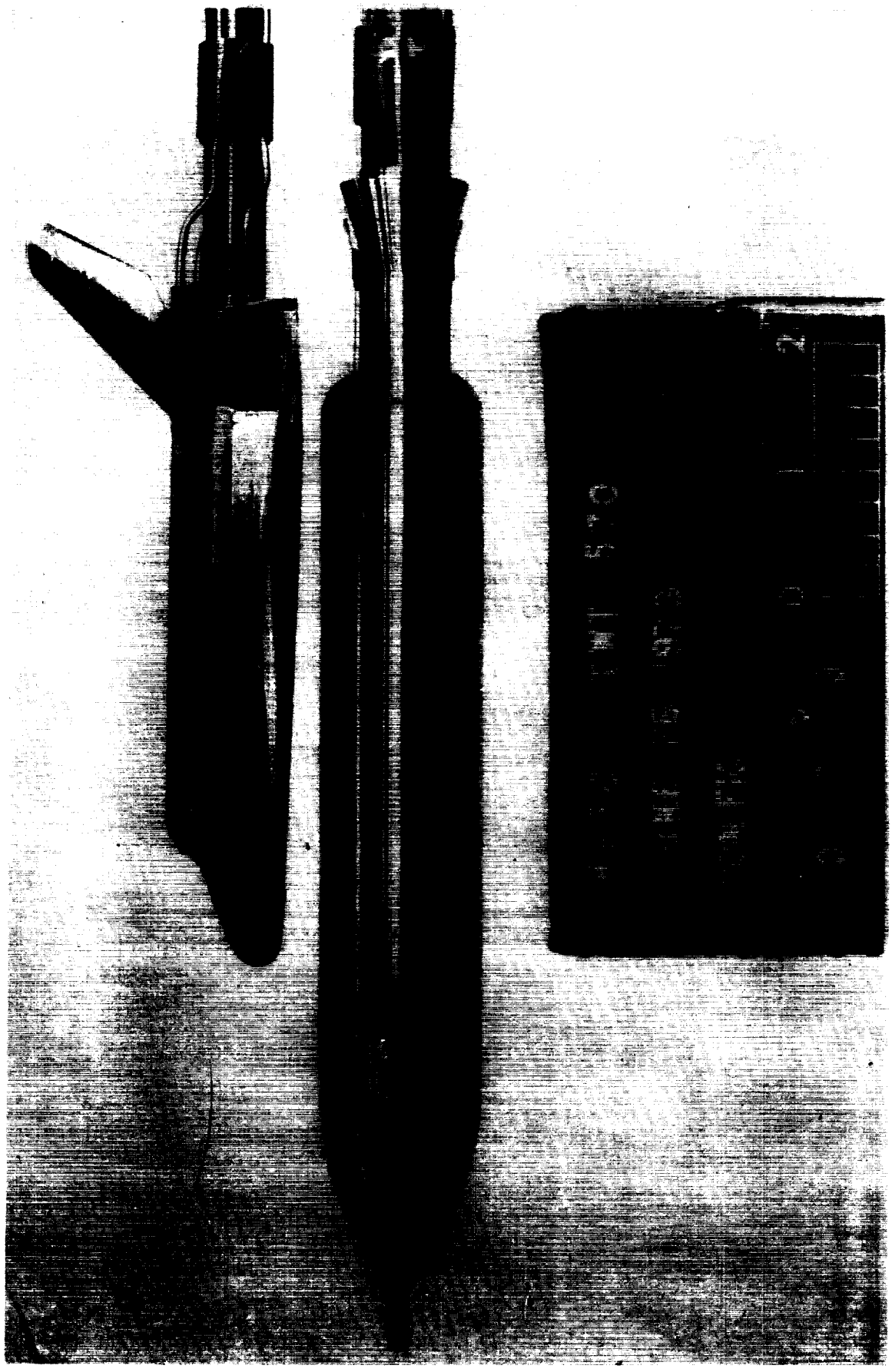

Figure C-2. SSLV with nose T7.

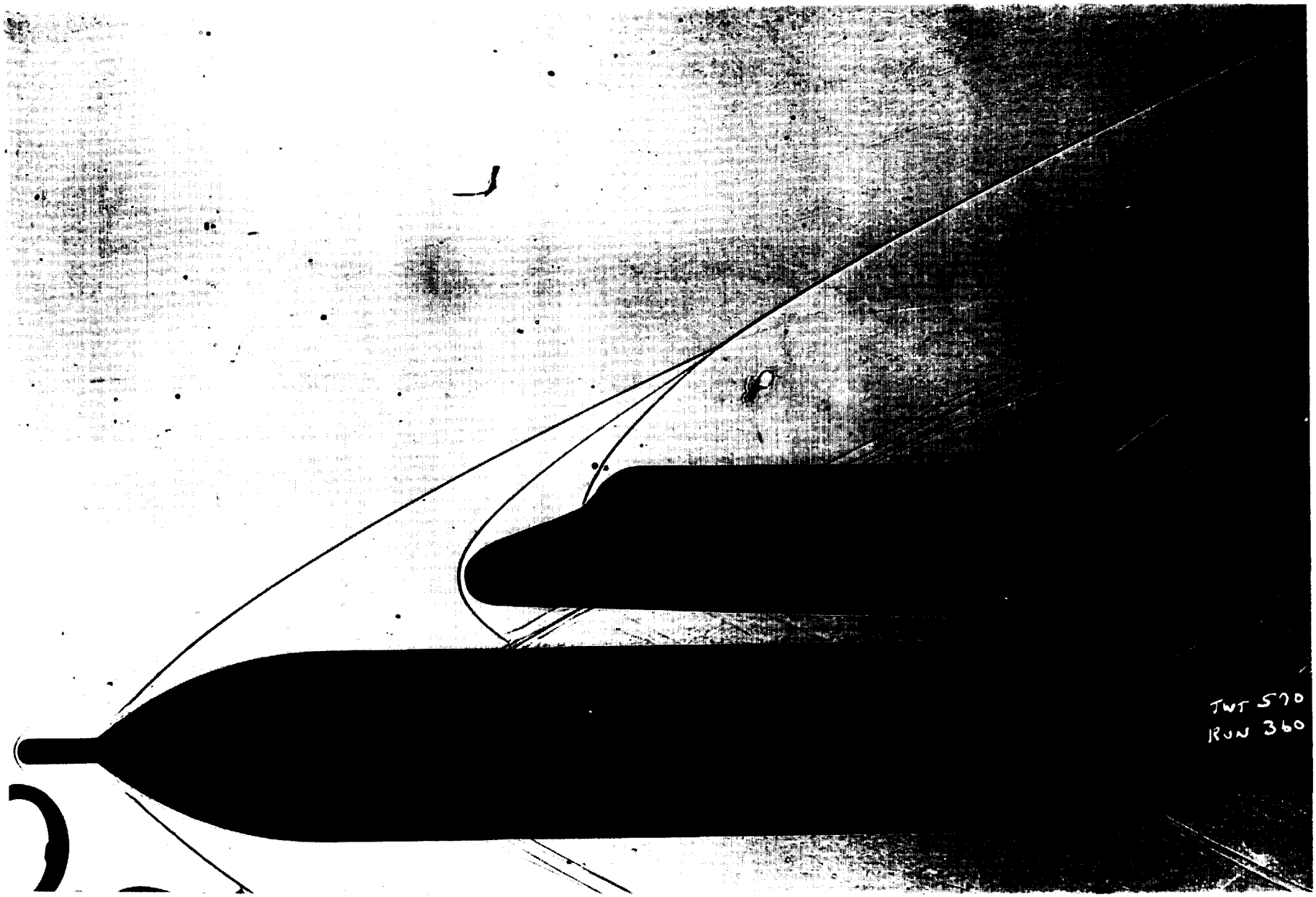

Figure C-3. SSLV with nose T7, Mach 3.48, alpha = 0, beta = 0, roll = 0.

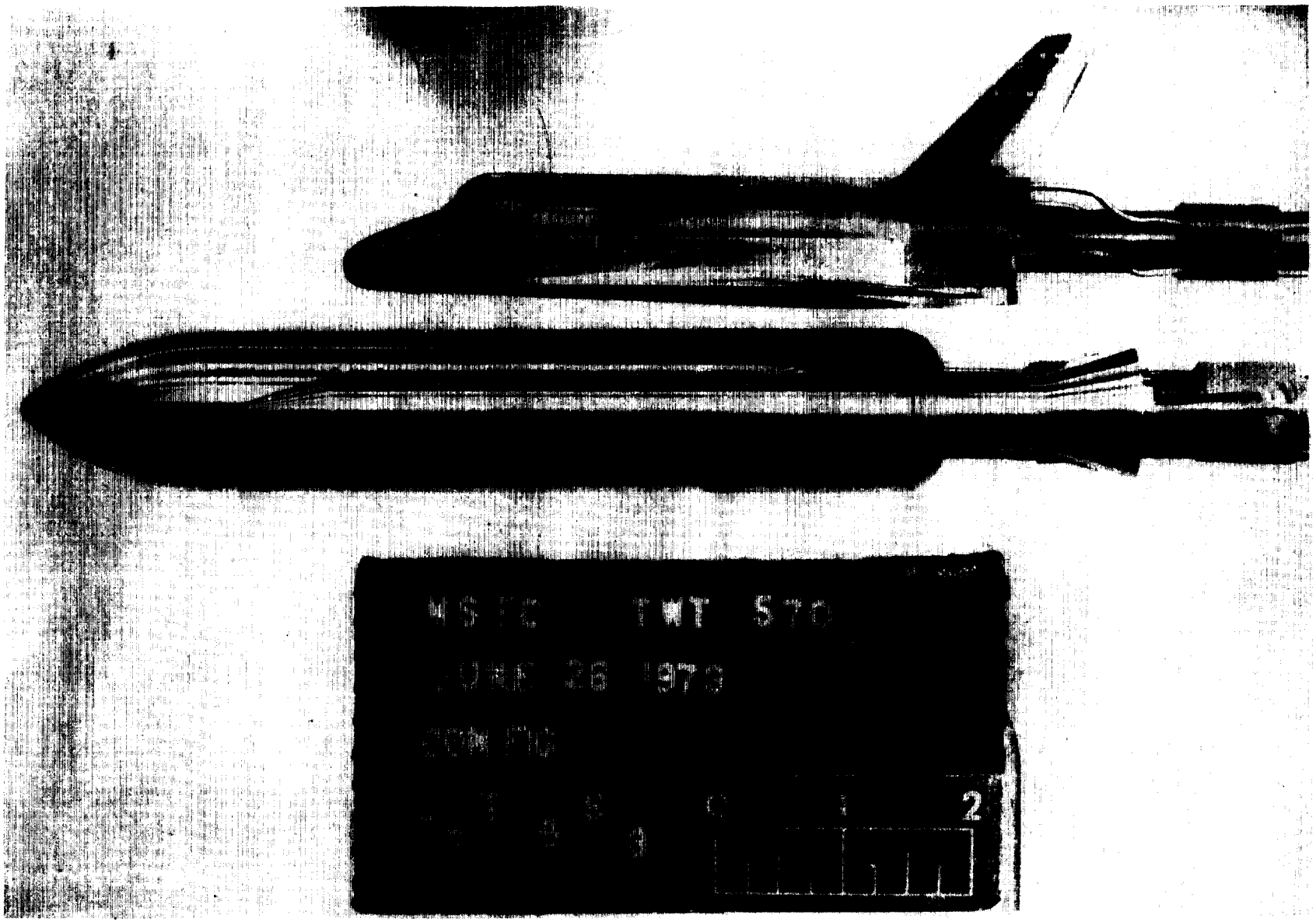

Figure C-4. SSLV with nose T9.

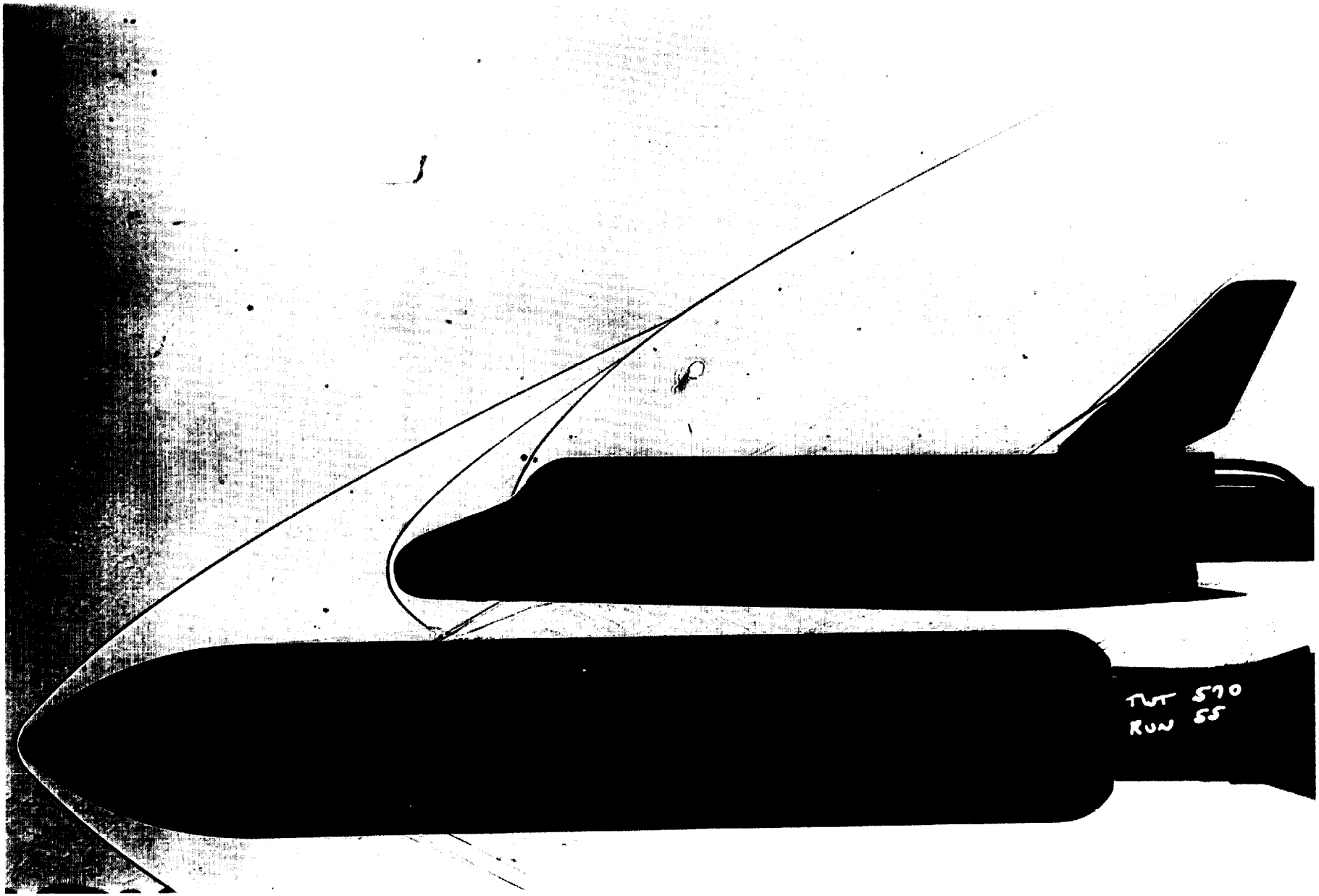

Figure C-5. SSLV with nose T9, Mach 3.48, alpha = 0, beta = 0, roll = 0.

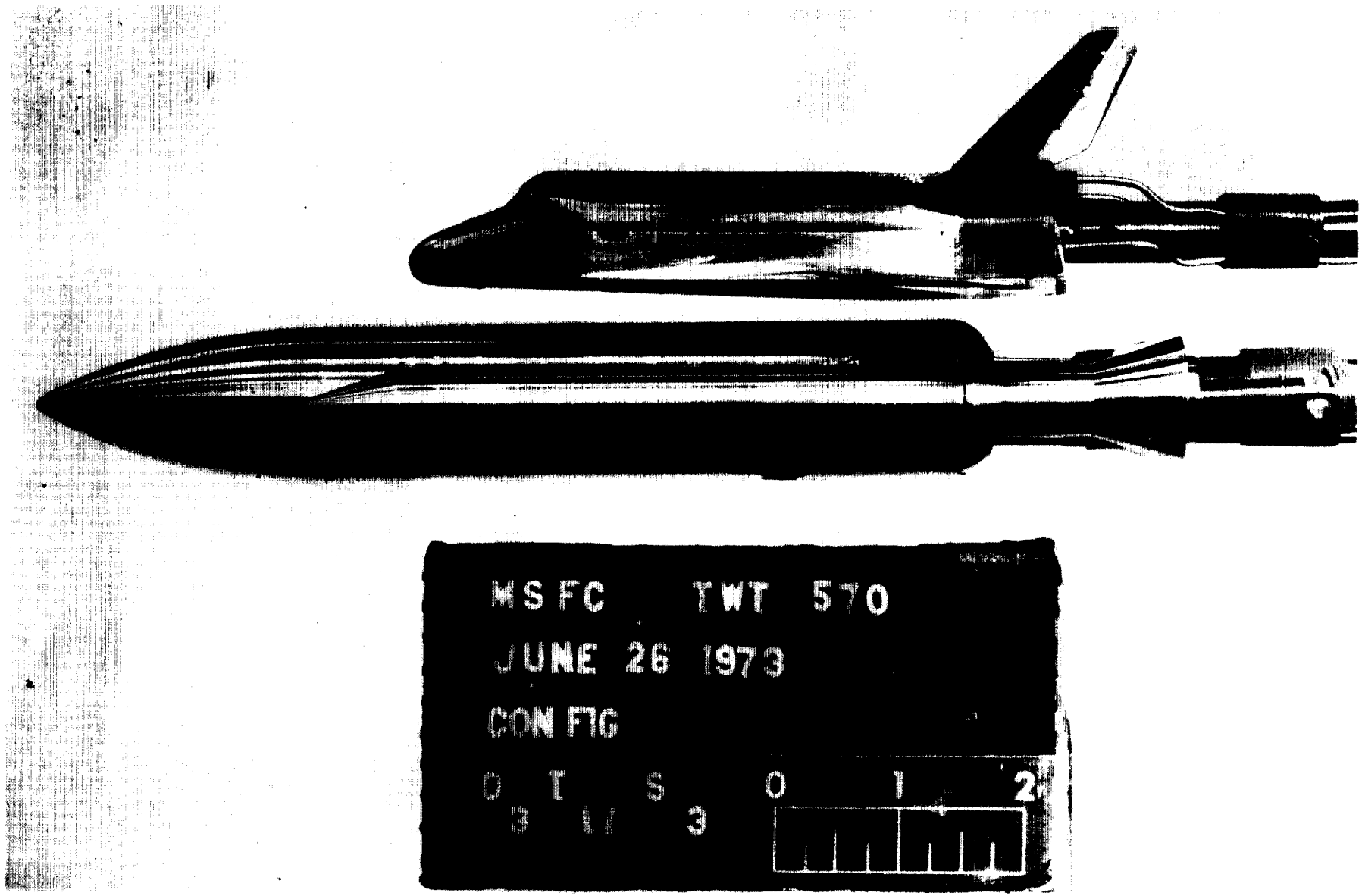

Figure C-6. SSLV with nose T11.

Figure C-7. SSLV with nose T11, Mach 3.48, alpha = 0, beta = 0, roll = 0.

Figure C-8. SSLV with nose T12.

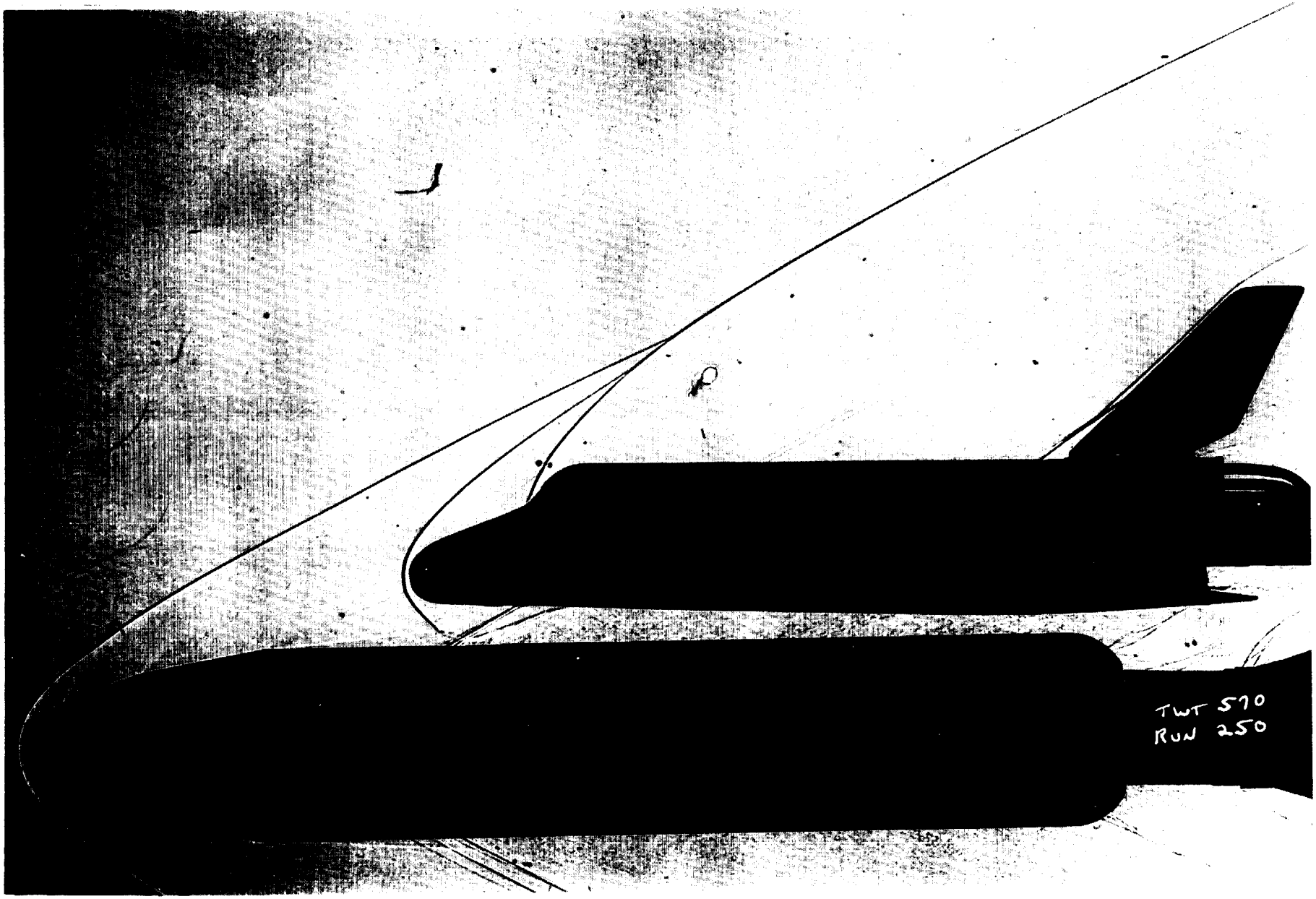

Figure C-9. SSLV with nose T12, Mach 3.48, alpha = 0, beta = 0, roll = 0.

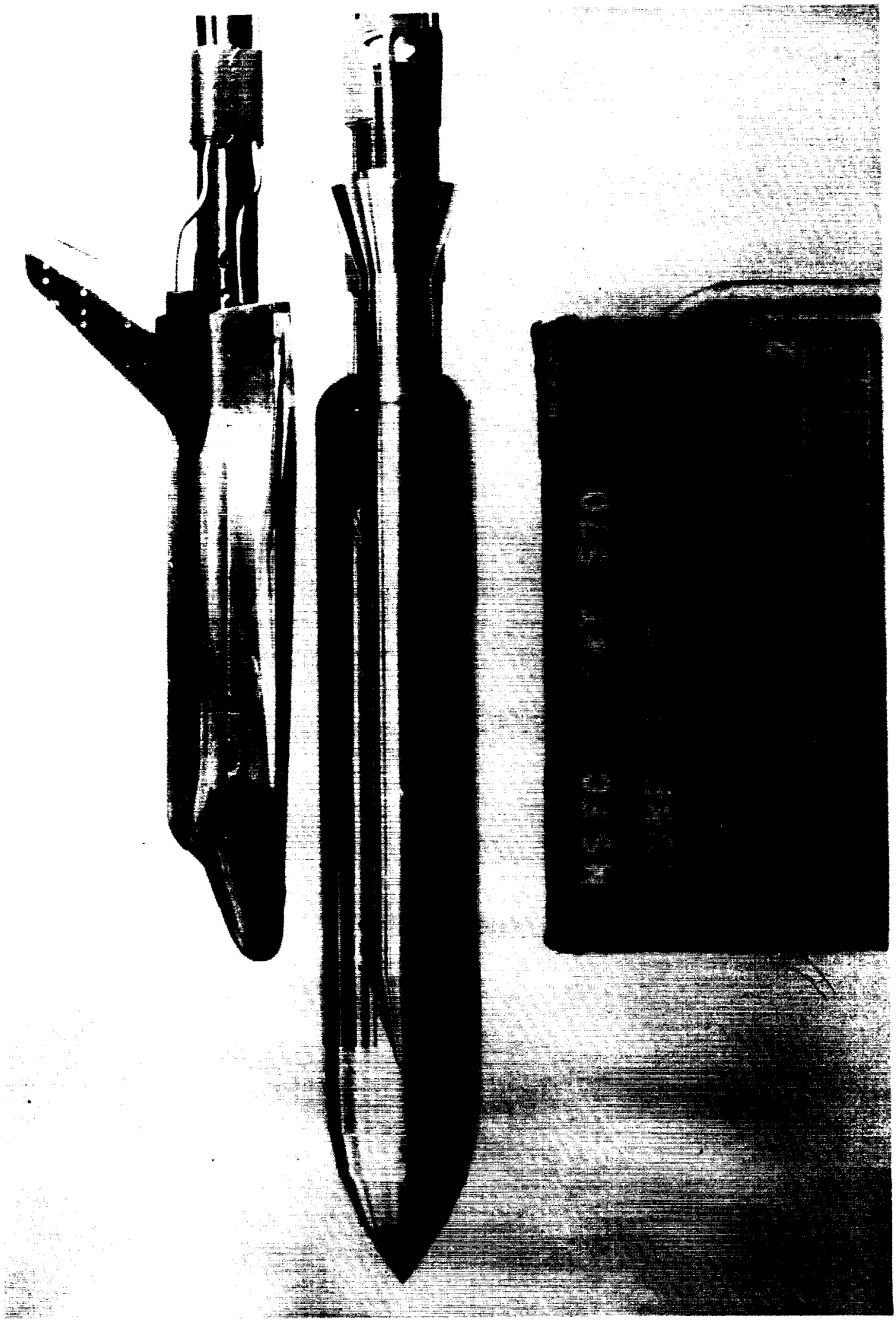

Figure C-10. SSLV with nose T13.

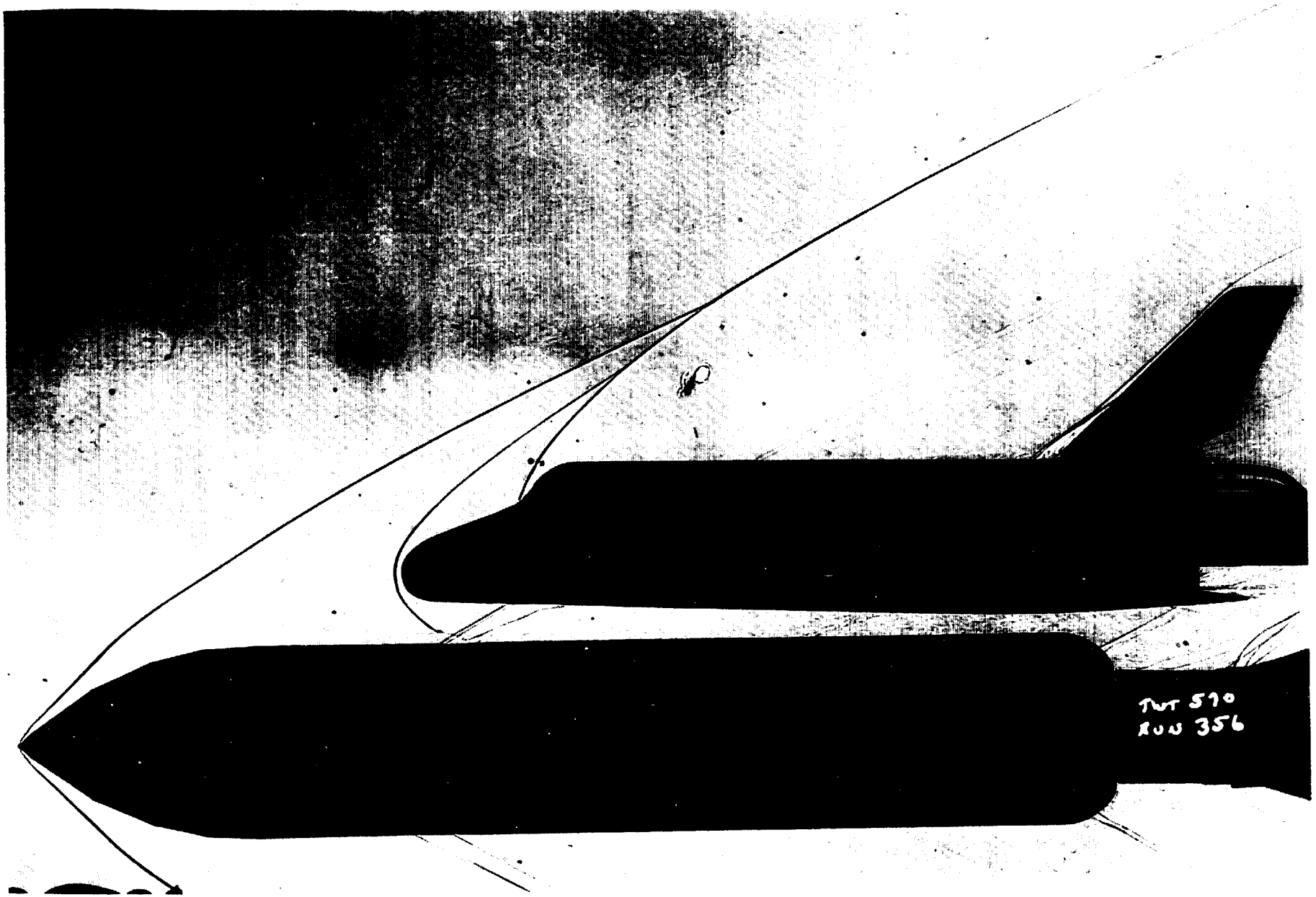

Figure C-11. SSLV with nose T13, Mach = 3.48, alpha = 0, beta = 0, roll = 0.

REPORT DOCUMENTATION PAGE

Form Approved
OMB No. 0704-0188

1. AGENCY USE ONLY (Leave blank)	2. REPORT DATE	3. REPORT TYPE AND DATES COVERED
	June 1994	Reference Publication

4. TITLE AND SUBTITLE

A Shadowgraph Study of Space Transportation System (STS); The Space Shuttle Launch Vehicle (SSLV)

5. FUNDING NUMBERS

6. AUTHOR(S)

A.M. Springer

7. PERFORMING ORGANIZATION NAME(S) AND ADDRESS(ES)

George C. Marshall Space Flight Center
Marshall Space Flight Center, Alabama 35812

8. PERFORMING ORGANIZATION REPORT NUMBER

M-752

9. SPONSORING/MONITORING AGENCY NAME(S) AND ADDRESS(ES)

National Aeronautics and Space Administration
Washington, DC 20546

10. SPONSORING/MONITORING AGENCY REPORT NUMBER

NASA RP - 1341

11. SUPPLEMENTARY NOTES

Prepared by Structures and Dynamics Laboratory, Science and Engineering Directorate

12a. DISTRIBUTION/AVAILABILITY STATEMENT

Unclassified—Unlimited

Subject Category: 02

12b. DISTRIBUTION CODE

13. ABSTRACT *(Maximum 200 words)*

A shadowgraph study of the space transportation system (STS), the space shuttle launch vehicle, is presented. The shadowgraphs presented in this study were obtained over the past 10 years from wind tunnel tests performed in the NASA Marshall Space Flight Center's 14-Inch Trisonic Wind Tunnel during the space shuttle development program. Shadowgraphs of the STS at various angles-of-attack and roll angles are shown for the Mach range of 0.6 to 4.96. The major flow field phenomena over the mated vehicle configuration are shown in these shadowgraphs. Shadowgraphs are also presented for the orbiter without the lower stack (reentry configuration) and the lower stack without the orbiter. A short study of external tank nose geometry effects on the mated vehicles flow field is presented. These shadowgraphs are used in the aerothermodynamic analysis of the external flow conditions the launch vehicle encounters during the ascent stage of flight.

14. SUBJECT TERMS	15. NUMBER OF PAGES
STS, shadowgraph, space transportation system, space shuttle, wind tunnel testing, flow visualization, launch vehicle	98
	16. PRICE CODE: A05

17. SECURITY CLASSIFICATION OF REPORT	18. SECURITY CLASSIFICATION OF THIS PAGE	19. SECURITY CLASSIFICATION OF ABSTRACT	20. LIMITATION OF ABSTRACT
Unclassified	Unclassified	Unclassified	Unlimited